Light and x-ray scattering studies of the mesophase of main-chain thermotropic polymeric liquid crystals/

LIGHT AND X-RAY SCATTERING STUDIES OF THE MESOPHASE OF MAIN-CHAIN THERMOTROPIC POLYMERIC LIQUID CRYSTALS

A Dissertation Presented

by

PAULA ELAINE HAHN

Submitted to the Graduate School of the
University of Massachusetts in partial fulfillment
of the requirements for the degree of

DOCTOR OF PHILOSOPHY

May 1987

Polymer Science and Engineering

National Science Foundation
Grant Numbers: DMR78 24151
DMR81 19510
DMR82 02482
DMR83 17949
DMR84 18068
DMR85 11724

LIGHT AND X-RAY SCATTERING STUDIES OF THE MESOPHASE OF MAIN-CHAIN THERMOTROPIC POLYMERIC LIQUID CRYSTALS

A Dissertation Presented

by

PAULA ELAINE HAHN

Approved as to style and content by:

Robert W. Lenz

Robert W. Lenz, Co-chairperson of Committee

Richard S. Stein

Richard S. Stein, Co-chairperson of Committee

M. Muthukumar

Murugappan Muthukumar, Member

Edwin L. Thomas

Edwin L. Thomas
Department Head
Polymer Science & Engineering

For my parents,

for believing.

ACKNOWLEDGEMENTS

I wish to express sincere gratitude to my coadvisors, Professor Robert W. Lenz and Professor Richard S. Stein, first, for suggesting this interesting joint project and, then, for providing guidance and unfailing support during its progress. Much appreciation is due Professor Murugappan Muthukumar for being on the committee and for his insightful commentary concerning the interpretation of the results. I would like to acknowledge the financial support of the National Science Foundation, both directly and via the Materials Research Laboratory of the University of Massachusetts.

Of the many benefits to being associated with two research groups, first to mind comes the gracious hospitality of both Mrs. Lenz and Mrs. Stein who have made Amherst a warm and friendly place in my memory. I have had the good fortune to become acquainted and work alongside student and post-doctoral colleagues in both the Lenz and Stein groups; I value their comradship and assistance over the years. Of this group I must single out Dr. Cameron T. Murray for his close friendship and tutoring on the topic of computer programming. Much appreciation goes to Drs. Juric Majnusz, Paolo Nieri, Christopher K. Ober, C. Rami Reddy, and Wang Xiayu, associates who provided me with scientific

insight on this project and/or homologous series of complete, well-characterized polymeric liquid crystals without which this project would not have been possible.

I would like to thank the secretarial and technical staffs of the Polymer Science and Engineering Department, especially Mr. William McCarthy, for their assistance and my fellow students in the Polymer Science, Chemistry, and Chemical Engineering Departments for making my residence at the University pleasant; this endeavor has been greatly enriched by my social and scientific association with Yachin Cohen. I appreciate the faculty of the Polymer Science department for providing a stimulating research environment and attracting seminar speakers and scientists in residence who shared their expertise and greatly supplemented the teachings of the Department. Highlights were most enlightening discussions with Drs. Stamatoff and Vonk and Professors Atkins, Azároff, Ballauff, Blackwell, Hosemann, Noël, Ruland and Windle. Most special thanks go to my classmate, Ravi Saraf, for his friendship, encouragement and tutelage.

Above all, this dissertation is possible because of the steadfast love, support and emotional sustenance of my parents, Helen Cichoski Hahn and James Arthur Hahn.

ABSTRACT

LIGHT AND X-RAY SCATTERING STUDIES OF THE MESOPHASE OF MAIN-CHAIN THERMOTROPIC POLYMERIC LIQUID CRYSTALS

(May, 1987)

Paula Elaine Hahn, B.S., College of William & Mary

M.S., Ph.D., University of Massachusetts

Directed by: Professors Robert W. Lenz & Richard S. Stein

The morphological transitions of two classes of thermotropic main-chain polymeric liquid crystals was investigated using the techniques of small angle light scattering and x-ray scattering, supplemented by mesophase textural observation by polarized light optical microscopy and differential thermal analysis. Homologous series belonging to the categories of alternating mesogen/flexible spacer and the rigid all-aromatic backbones were studied.

Initial morphology was controlled and utilized to approach the intermediate state of order of the mesophase from both the more ordered semi-crystalline state and from the less ordered isotropic state. Super-structural morphologies and crystal structures peculiar to solvent crystallization were identified and compared with those from melt crystallization.

The uniaxial mesophase of the rigid polymers was found to undergo a transition to a biaxial nematic structure on

cooling. The distance between the aromatic cores is dependent upon the length of the appended substituents and was confirmed by diffraction of oriented specimens.

The random orientation approximation was found to apply to the light scattering of the mesophase of certain polymeric liquid crystals. The orientation correlation function with correlation distance of 1 to 2 μm serves as a statistical measure of the persistence of parallel orientational ordering of mesogens in the liquid crystalline state. The "pseudo-Gaussian" decay in orientation correlation with separation of two mesogens was modeled using a domain description for the mesophase morphology which considers both intra-domain and inter-domain (i.e., between domain directors) correlations.

TABLE OF CONTENTS

LIST OF ABBREVIATIONS

Structures

LC, LCs	liquid crystal(s)
SMLC, SMLCs	small molecule liquid crystal(s)
PLC, PLCs	polymeric liquid crystal(s)
LCnP, LCnPs	liquid crystalline polymer(s)

States of Matter

LCn	liquid crystalline	
	uniaxial nematic	N
	biaxial nematic	B
	smectic	S
XLn	semi-crystalline	
	crystal	XL

Transitions

$T_{A\longrightarrow B}$, $T_{B<\!\!-A}$	transition from state A to B

specifically:

T_m	melting transition temperature
T_c, T_i	clearing or isotropization temperature
T_d	deisotropization temperature
T_g	glass transition temperature
	of amorphous glass $T_{g\text{-}am}$
	of LCn glass $T_{g\text{-}lc}$
T^*	critical temperature

Experimental Techniques

DSC	differential thermal calorimetry
TGA	thermal gravimetric analysis
PLOM	polarized light optical microscopy
WAXS	wide angle x-ray scattering
SAXS	small angle x-ray scattering
SALS	small angle light scattering

LIST OF TABLES

Table

LIST OF FIGURES

C H A P T E R I

INTRODUCTION

Description of Small Molecule and Polymeric Liquid Crystals

Liquid crystalline (LCn) materials are those that exhibit a degree of long-range order intermediate between that of an isotropic liquid, melt, or solution and a three-dimensionally ordered crystal. The terms, mesomorphic or mesophasic, have been applied by Friedel [1] to this state of matter to correct the apparent contradiction in the original terminology. The distinction between lyotropic and thermotropic liquid crystallinity is that this spontaneous ordering occurs at a critical concentration in the former and at a specific temperature upon cooling from the isotropic melt in the latter.

Reinitzer [2] is credited with the discovery of the LCn phase of cholesteryl benzoate in 1888 from its anomalous melting behavior. Lehmann [3] dubbed these materials above their melting temperature, T_m, and below their clearing or isotropization temperature, T_c or T_i, "flussige" or "fliessende krystall" (fluid or flowing) to simultaneously describe their liquid-like rheology and optical anisotropy.

Interest in liquid crystals (LCs) has been sporadic and topical. Early emphasis centered about cataloging structures which would produce a mesophase and describing the thermodynamic properties and appearance or "texture" under the polarizing microscope. The structural criteria necessary for liquid crystallinity was recognized by Vörlander [4] to be rigid and elongated units, termed mesogens, with a length/width ratio greater than two. Rod- or lath-like molecular structures, as found in multiple para-substituted benzene groups with or without bridging units (as in the classic liquid crystal, p-azoxy anisole, PAA) fit this requirement. Thus, parallel alignment of the aromatic units and a linear structure are preserved. Permanent dipolar groups with a high anisotropy of polarizability enhance mesomorphic ordering.

Two basic types of LCs have been identified (Figure 1-1). The nematic have at least orientational order of the molecular axis along a preferred director axis, $\hat{n}$, while the center of gravity of each unit is positioned with no long-range order, as in a fluid. The more ordered, lower energy smectics have a well-defined layered structure, positionally ordered in at least one dimension. The various smectic structures, A through H, differ by tilt angle of the molecular axis from the layer normal and by amount of positional ordering of the centers of gravity within the

layers. Because within an individual layer there may or may not be a great deal of long-range positional order, yet that information is not be transmitted to the adjacent layer, smectics are considered to be two-dimensional liquids and solids. (They are variously designated normal/tilted and with/without order.) Cholesteric order is a twisted variation of the nematic induced by an asymmetric center in the molecule or by mixing a nematic material with a chiral solvent. In this case, the director rotates continuously about a perpendicular axis with a pitch of $p = \lambda/\bar{n}$, where $\bar{n}$ is the average refractive index and λ is the wavelength of the reflected light. X-ray diffraction to differentiate the various smectic mesophases from nematic and cholesteric became a tool in the early part of this century [6a-c].

Although numerous biological substances which exhibit liquid crystallinity (where rigidity is due to helical secondary super-structures) are high molecular weight and/or polymeric, most research had centered on small molecule liquid crystals (SMLCs) until recently. Interest in polymeric liquid crystals (PLCs) or liquid crystalline polymers (LCnPs) was sparked in 1956 with the publication of Flory's lattice theory [7] which predicted spontaneous parallel ordering of rod-like structures at some critical concentration. In order to visualize the structure of PLCs, the mesogens in Figure 1-1 should be made infinitely long or should be connected with flexible spacers.

The historical development of PLCs is industrially related. Commercial interest of the main-chain type of PLCs, where the mesogen is incorporated in the polymer backbone, lies, for the most part, in these materials for fiber use and for their thermal and dimensional stability. It was reasoned that the fiber strength in a perfectly oriented specimen becomes ultimately a function of chemical bond strength and bond length and bond angle deformation constants. The orientationally ordered fluid phase that PLCs display allows for the formation of high degrees of orientation in fibers or films in the coagulated or quenched state and their consequent high modulus. (This is in contrast the the side-chain or comb-like PLCs, being studied for their use as electronic display devices in deference to the much faster response time exhibited in an orienting field.)

Pioneering industrial development on synthetic PLCs was begun in the mid-1960's. The first example was demonstrated in the 1971 patent issued on the lyotropic aramid (i.e., all aromatic polyamide) materials to Kwolek of du Pont. Numerous thermotropic PLCs have since been patented to take advantage of the potential ease and economy of processing relative to lyotropic PLCs. Thus, PLCs offer a shortcut to high modulus, high strength fibers by being pre-oriented and by having a conformation of a relatively stiff worm or stiff

rod (as in the polyheterocyclic ladder and semi-ladder structures of the Air Force Materials Laboratory).

The strong hydrogen bonding in the polyamides requires very polar solvents for dissociation and gives rise to melting transition temperatures higher than the decomposition temperature of the polymer. This is avoided in the thermotropic PLCs which are generally polyesters or polyethers. Industrial and academic "tricks" of molecular design to inhibit crystallinity by reducing symmetry and linearity include [1] synthesizing random copolymer sequences, incorporating [2] short flexible spacers, [3] swivel units, [4] aromatic ring substituents and [5] bent, yet rigid, units (i.e., meta-substituted benzene rings and 2,6-naphthyl derivatives) which result in a parallel offset or crankshaft structure. These, or a combination of these techniques, serve to increase the entropy of the solid (usually semi-crystalline) state with respect to the mesophase and, thereby, reduce T_m. This is illustrated in Tables 1 and 2. Extensive and thorough studies of the effect of chemical structural changes on transition temperatures, mesophase stability and mesophase type enable the chemist to custom design a PLC with specific properties. Several excellent reviews have been published [15, 16, 17].

The mesophase of main-chain PLCs exhibit rheological behavior very different from that of the isotropic state.

Table 1

Some early and commercial polymeric liquid crystals

ALL AROMATIC HOMO- AND CO-POLYMERS

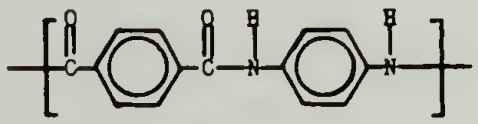

du Pont Kevlar ® [8]
(lyotropic)

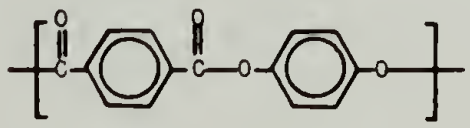

poly(p-phenylene terephthalate) [9]
(infusible)

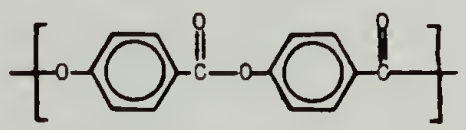

poly(p-hydroxybenzoic acid) [10]
(infusible)

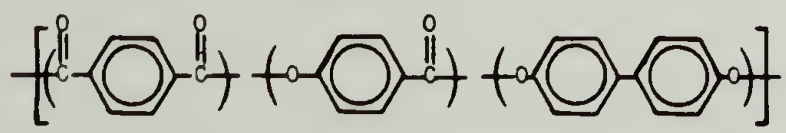

Carborundum Ekkcell I-2000 ® [11]

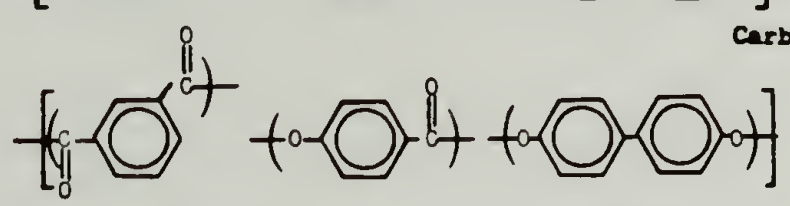

-replace (1) 1,4-phenyl with 2,6-naphthyl below:

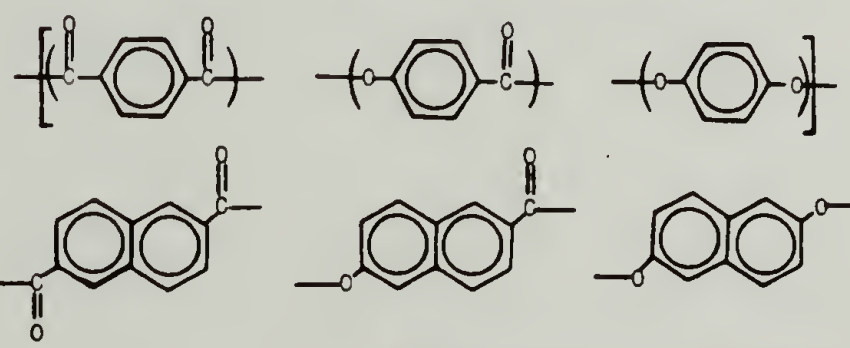

Celanese Vectra ® [12]

ALIPHATIC/AROMATIC CO-POLYMERS

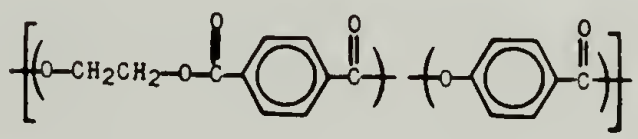

Eastman Kodak X7G ® [13]

40 - 70%

LINKAGELESS POLYMERS

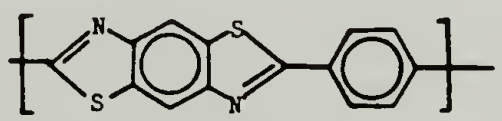

poly(p-phenylene benzobisthiazole) [14]

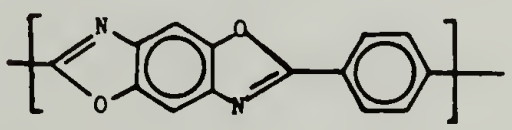

poly(p-phenylene benzobisoxazole) [14]

Table 2

Structural design features commonly used reduce transition temperatures in polymeric liquid crystals

RANDOM COPOLYMER

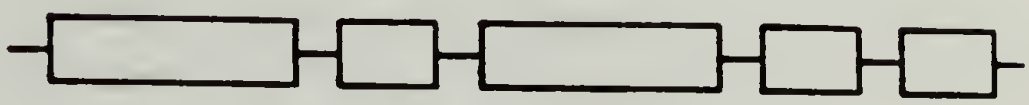

FLEXIBLE SPACERS

SWIVEL UNITS

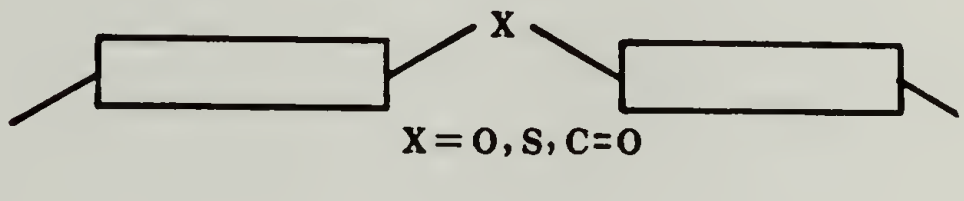

SUBSTITUENTS

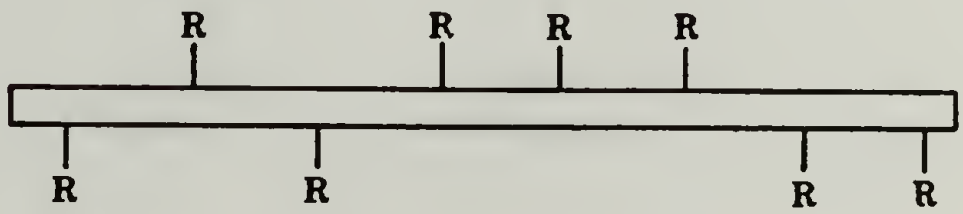

PARALLEL OFFSET

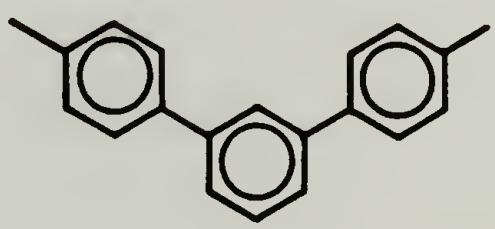

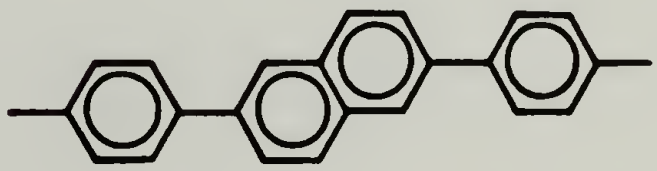

Typical viscosity dependence as a function of polymer concentration and temperature are shown in Figures 1-2 and 1-3. The abrupt decrease in viscosity is evidence of the phase transition to the biphasic regime or the LCn melt, respectively.

Products fashioned from the oriented mesophase display a "woody" texture and anisotropic properties: excellent strength along the deformation axis yet poor transverse properties and poor properties in compression [20, 21]. As in the case of metals, the observed strength falls short of theoretical estimates. The concept of various types of defects and grain boundaries, in other words, non-equilibrium structures, have been invoked to account for this deviation from ideality in metals [22]. Similarly, small- and large-scale morphological structures and the extent of correlation of orientation are important in understanding the mechanical and rheological behavior of PLCs.

Scope of the Dissertation

The premise of this dissertation is the quantitative characterization of the state of order of the mesophase of thermotropic, main-chain polyesters. Various scattering techniques provided three dimensional levels of study:

[1] lattice parameters (0 to 20 A by wide angle x-ray scattering, WAXS), [2] smectic layer widths (20 to 100 A by small angle x-ray scattering, SAXS) and [3] long-range orientational super-structures or "domains" (0.5 to 20 μm by small angle light scattering, SALS). Whenever possible, the PLCs were studied in the mesophase state, that is, at elevated temperatures so that secondary effects of the quenching procedure, such as crystallization, would not complicate the situation.

By performing these experiments as a function of temperature and by correlating the results with differential scanning calorimetry (DSC) and optical microscopic findings under condititions of polarized light (PLOM), a complete picture of the step-wise disordering of matter may be obtained. The mesophase, of an intermediate state of order, was approached from both directions - by the disordering of the three-dimensionally ordered crystalline lattice and by the ordering of the isotropic melt.

The PLCs studied fell into two categories: the type where there are alternating rigid and flexible sequences along the polymeric backbone and the more rigid type without spacers.

Format of the Dissertation

Having established in this chapter the basic terminology, concepts of liquid crystallinity and thrust of this project, with an emphasis on main-chain liquid crystalline polymers, Chapter II expands upon the various theories of the mesophase relevant to the research presented herein. A review of the existing literature on biaxial nematics is included.

Chapter III begins with a survey of the synthetic efforts of the Lenz group at the University of Massachusetts. A consistent system for the abbreviated designations of the specific PLCs which were studied is established. Further sample treatment to tailor the initial morphology is discussed. Details of the experimental techniques which were used to characterize the polymers at their sub- and super-structural levels as a function of temperature are described.

Chapter IV contains a discussion of the unique structural transitions (semi-crystalline<—>biaxial nematic<—>uniaxial nematic<—>isotropic) observed in the alkyl-substituted poly(p-phenylene terephthalate) series as determined largely by correlation of thermal analysis with x-ray scattering.

Chapter V illustrates how the tailoring of initial morphology and the use of the complementary techniques of WAXS, SALS, PLOM and DSC can be employed to describe morphological changes in the complex systems of PLCs with flexible spacers.

Chapter VI lays the groundwork for the SALS analysis by introducing theoretical arguments in which refractive index and orientation correlation functions are the dominant factors to be considered in LCn systems. The random orientation approximation and its relevance to this study is discussed. Other light scattering studies on LCs are reviewed.

In Chapter VII a two-parameter model which considers correlation in orientation within a "domain" and correlation between the directors of "domains" is proposed to account for the SALS results. This model is general enough to account for behavior ranging from sharp-boundaried discrete domains to continuously changing mesogen orientation.

Chapter VIII is a synopsis of the general conclusions of the dissertation concerning the structure of the mesophase of the various PLCs studied as determined by scattering techniques in conjunction with more standard methods of characterization. Suggestions are made for further experiments, in particular the formation and study of polymeric single liquid crystals by melting solution cast single crystals.

The Appendices contain the following: mathematical derivations pertaining to the analysis of correlation functions from the SALS experiments and the program FORINV - a sine fast Fourier transform program.

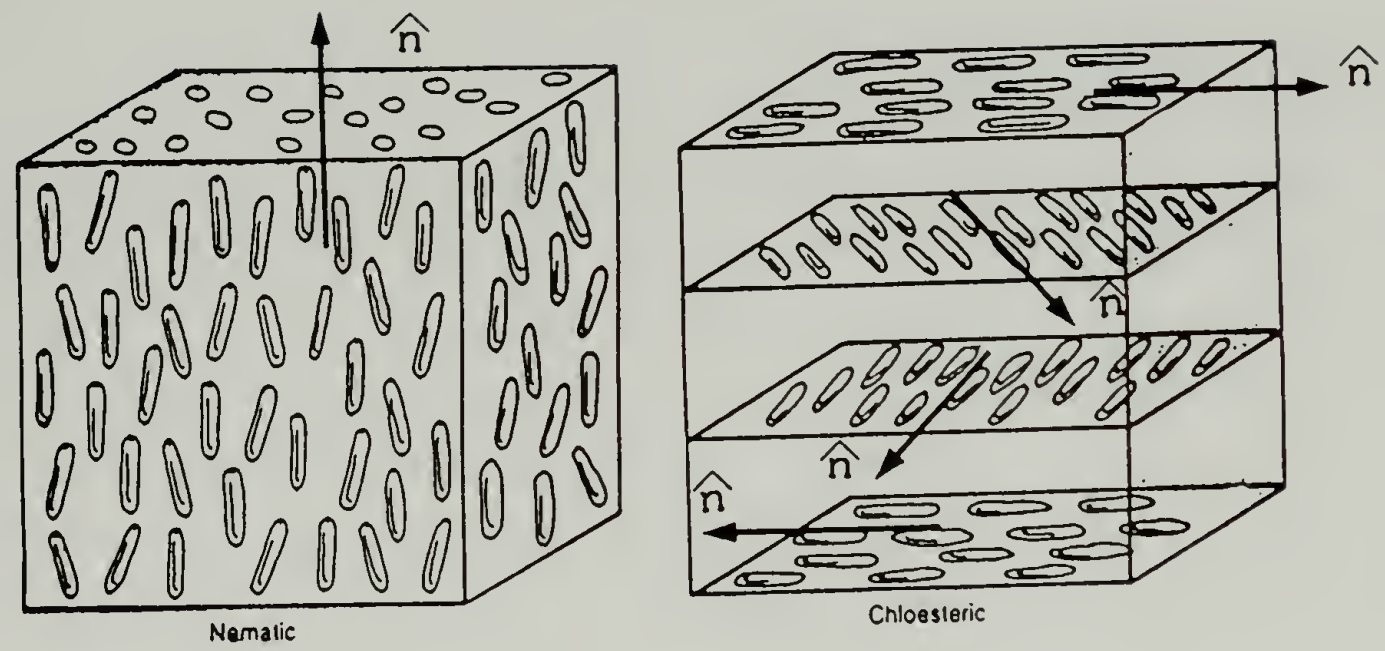

pitch ~ λ_{light}

$\omega = \cos^{-1}(d/l)$

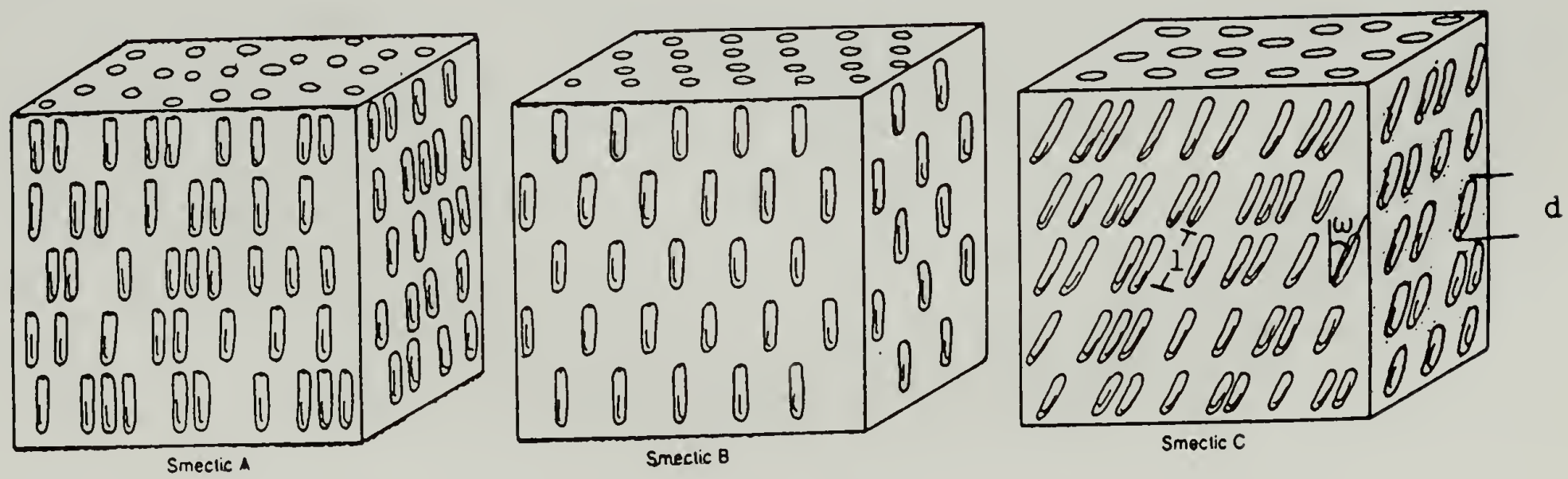

Figure 1-1. Schematic diagram of the nematic, cholesteric and various smectic mesophases of small molecule mesogens [5].

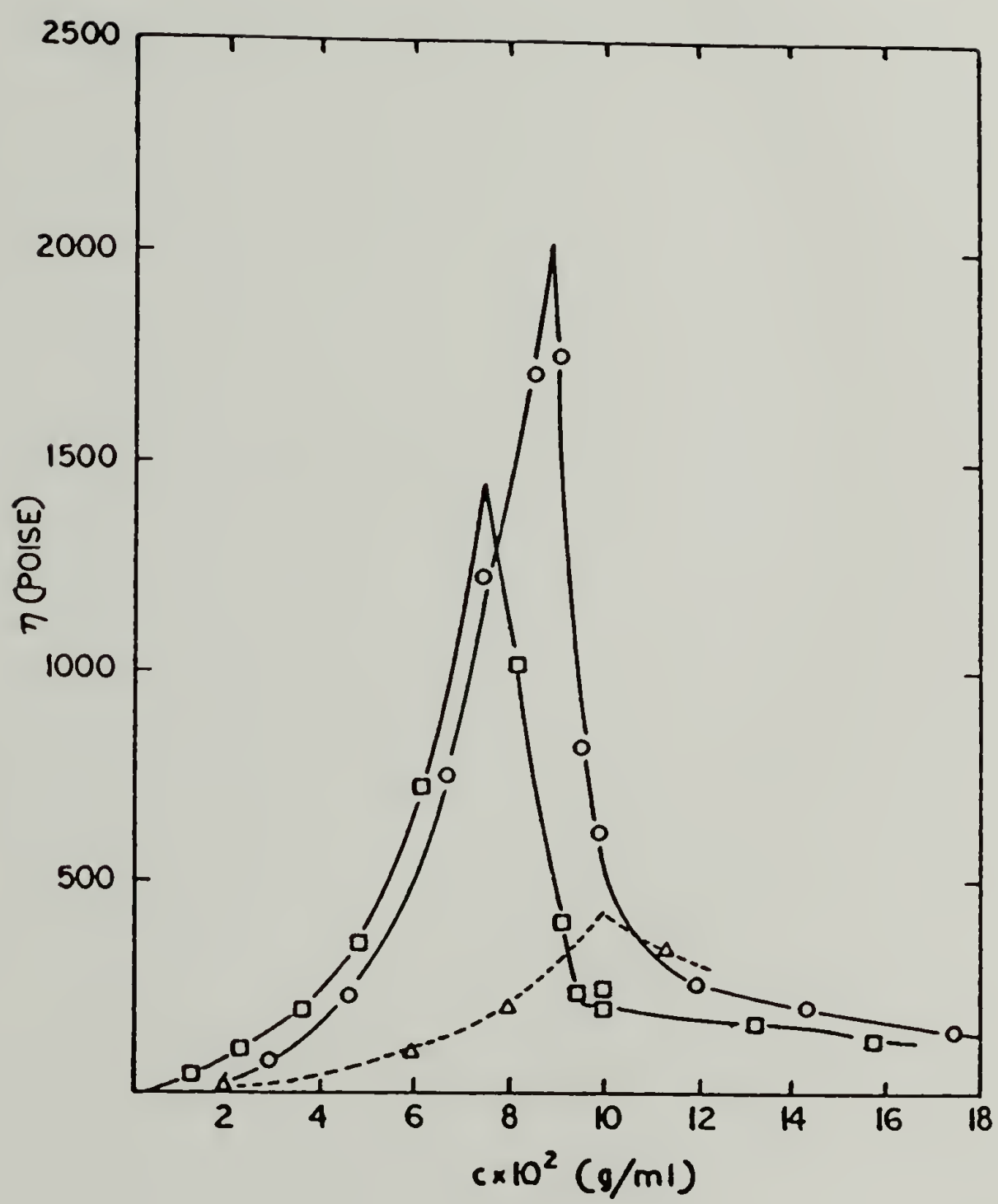

Figure 1-2. Concentration dependence of viscosity of a lyotropic polymeric liquid crystal [18].

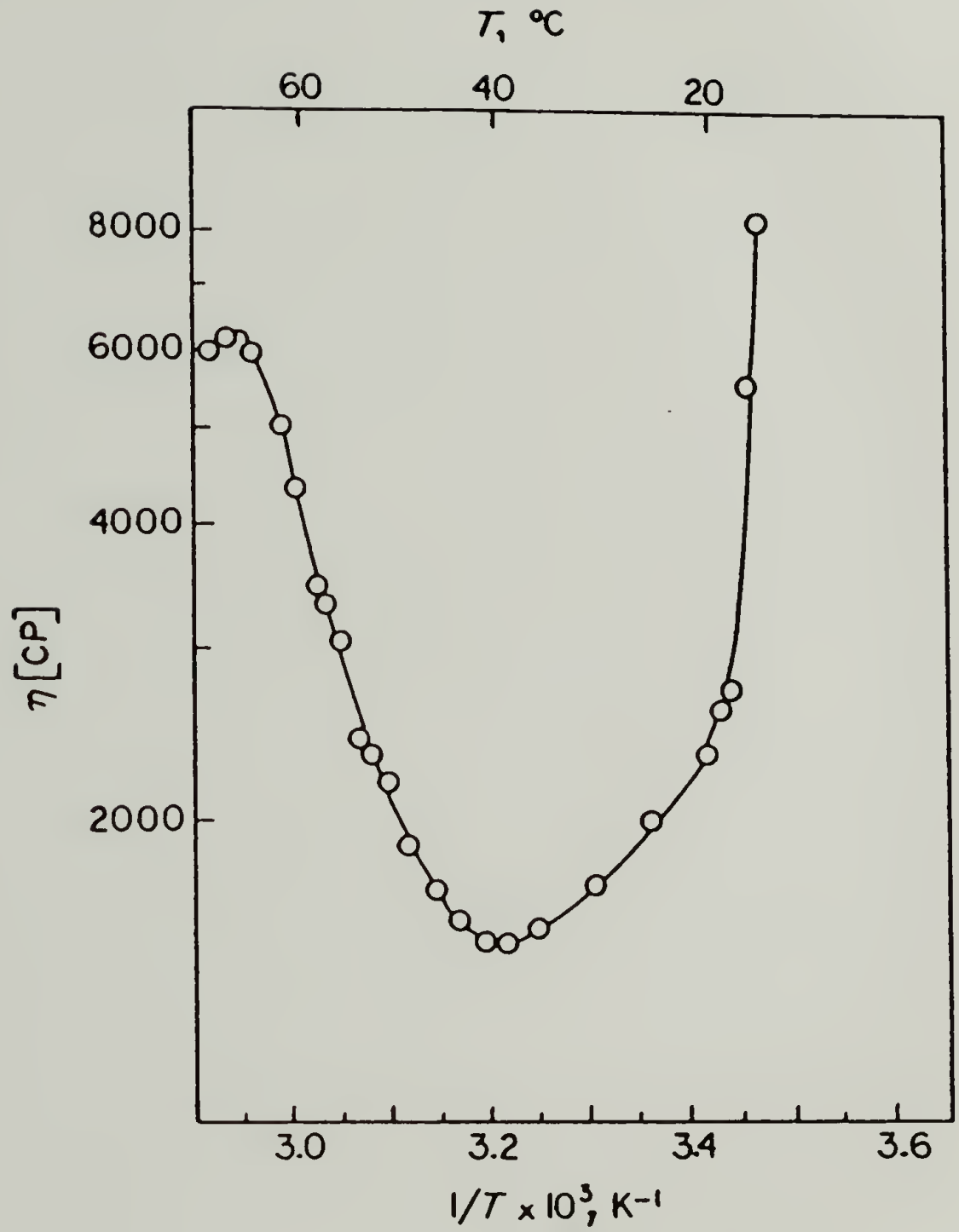

Figure 1-3. Temperature dependence of viscosity of a lyotropic polymeric liquid crystal [19].

C H A P T E R II

BACKGROUND

Intoduction

The contents of this chapter constitute a condensed review of the various theoretical approaches used to describe the liquid crystalline state, mainly the thermotropic state. This background chapter will serve as a basis for understanding the disordering and ordering processes which were studied in this dissertation. The format is fashioned after reviews in [23, 24, 25, 26 and 27]. To date, most theoretical analyses have dealt with the uniaxial nematic state of infinitely long rods (i.e., cylindrically symmetric structures) for the most part. Specific treatments of SMLCs [28], PLCs, the role of flexible tails [29] and spacers [30], the smectic state [31] and biaxiality [32, 33 and 34] have also appeared.

The theories can be classified in two major categories: the molecular approach, which has lead to a concept of "swarms", and the continuum approach which describes the flow behavior of the mesophase. The molecular theories relate the molecular structure to thermodynamic, macroscopic properties. In the continuum theories constitutive

equations relating the stress developed by the strain field are derived.

A valid molecular theory predicts and explains the increase in the extent of long-range orientational ordering which occurs at the I ⇒ N transition and the change in the extent of positional ordering at the N ⇒ XL transition; these are the unique distinguishing features of these transitions for the simplest cases. The molecular theories are statistical mechanical models that invoke an appropriate intermolecular pair potential to correctly account for the molecular characteristics which are esssential to the existence of the two phases and the intervening transition. The prediction of thermodynamic properties (free energy, entropy, enthalpy of transition and transition temperatures) should be of the correct magnitude and the order of the derivative of the free energy with respect to temperature, according to the Ehrenfest scheme, should reflect reality.

The I ⇒ N (i.e., disorder ⇒ order) phase transition has been found experimentally to be "weakly first order." This means that there is a discontinuous change in the entropy, S, given by the first derivative of the Helmholtz free energy, A, with respect to temperature, T, at constant volume, V:

$$A = E - TS$$

$$-S = (\partial A/\partial T)_V$$

where E is the internal energy. For that reason there is a latent heat, $T\Delta S$. Since the value of the latent heat is small, the transition is said to be "weak". For higher order transitions S would change in a continuous fashion. The lower entropy nematic state becomes stable when the lower intermolecular potential of the aligned configuration dominates. Even though the total entropy is decreased, due predominantly to the decreased ideal gas entropy of mixing, the translational component of entropy increases as there are more ways to pack aligned anisotropic particles. At high density this entropy effect serves to stabilize the mesophase. Structural biaxiality and the presence of flexible segments have been shown to reduce the "strength" of the first order transition for hard rods [27, 35 and 36].

The Molecular Approach

Distribution Functions and Order Parameters

Consider a system of N rigid particles [26], which have their spatial positions specified by $r = r_x$, r_y and r_z and orientation specified by the three Euler angles $\Omega = \alpha$, β and γ (Figure 2-1), the equilibrium configurational partition function is given as

$$Q_N = \frac{1}{N!} \int \{d\chi^N\} \quad \exp\left[\frac{-U(\{\chi^N\})}{kT}\right]. \qquad (2\text{-}1)$$

where $U(\{\chi^N\})$ is the total potential energy of the N-particle system, $Q_N = Z_N/N!$, k is the Boltzmann constant, $\{\ \}$ indicates collectively N variables, χ specifies both position and orientation,

$$d\chi = dr\ d\Omega = dr_x dr_y dr_z\ d\alpha\ \sin\beta\ d\beta\ d\gamma,$$

$0 \leq \alpha \leq 2\pi$, $0 \leq \beta \leq \pi$, $0 \leq \gamma \leq 2\pi$ and

$$\{\chi^N\} = \{\chi_1^N\} = (\chi_1, \chi_2, \ldots, \chi_N).$$

Frequently $U(\{\chi^N\})$ is expressed as a sum of pairwise interactions

$$U(\{\chi^N\}) = \sum_{1<i<j<N} U(\chi_1, \chi_2). \qquad (2\text{-}2)$$

The n-particle distribution (i.e., the probability density of finding n out of N particles in the range $\chi_1 + d\chi_1$, $\chi_2 + d\chi_2$, ..., $\chi_n + d\chi_n$) is

$$P^{(n)}(\{\chi^n\}) = \frac{N!}{(N-n)!Z} \int \{d\chi_{n+1}^N\} \exp\left[\frac{-U(\{\chi^N\})}{kT}\right].$$

The above equation describes the general n-particle distribution function. Of these the one- and two-particle distributions, commonly called the singlet and pair distributions, are the easiest to deal with, the most important and are given, respectively, as

$$P^{(1)}(r_1, \Omega_1) = \frac{N}{Z_N} \int \{dr_2^N\}\{d\Omega_2^N\} \exp\left[\frac{-U(\{r^N, \Omega^N\})}{kT}\right] \text{ and}$$

$$P^{(2)}(r_1, \Omega_1; r_2, \Omega_2) = \frac{N(N-1)}{Z_N} \int \{dr_3^N\}\{d\Omega_3^N\} \exp\left[\frac{-U(\{r^N, \Omega^N\})}{kT}\right].$$

At low density, where inter-particle distance is large and where inter-particle influences are negligible, the probabilities of finding particles in their respective volume elements become statistically independent. Thus, the n-particle distribution becomes the product of n one-particle distributions:

$$P^{(n)}(\chi_1,\chi_2,\ldots,\chi_n) = \frac{N!}{(N-n)!N^n} P^{(1)}(\chi_1)P^{(1)}(\chi_2)\ldots P^{(1)}(\chi_n).$$

The reduced (or normalized) n-particle distribution or correlation function is defined as

$$g^n(\{\chi^n\}) = \frac{P^n(\{\chi^n\})}{\prod_{i=1}^{n} P^{(1)}(\chi_i)}.$$

This function approaches one, signifying no correlation, when inter-particle distances approach infinity or, in practice, become much larger than intermolecular distances. Thus, the pair correlation function is given as

$$g^{(2)}(\chi_1,\chi_2) = \frac{P^{(2)}(\chi_1,\chi_2)}{P^{(1)}(\chi_1)\,P^{(1)}(\chi_2)}. \qquad (2\text{-}3)$$

In uniform systems, such as the isotropic and nematic states, which exhibit translational invariance, absolute positions are replaced with relative positions (the vectors, $r_{ij} = r_j - r_i$, connecting particles i and j) and distances (the magnitude, r_{ij}) and $g^{(2)}(\chi_1,\chi_2)$ becomes $g^{(2)}(r_{12},\Omega_1,\Omega_2)$. (For spherical particles, $g^{(2)}(\chi_1,\chi_2)$ is a function of inter-particle distance only. This is also

referred to as the radial distribution function, $g^{(2)}(r_{12})$ which describes the number of pairs of molecules separated by r_{12}.)

The order parameter has been cleverly chosen to be a statistical quantity, which may be experimentally determined, that undergoes a marked change at the phase transition and distinguishes the phases under consideration. The singlet distribution function may be factored into:

1) positional (important for N ⇒ XL transition),

2) orientational (important for I ⇒ N transition) and

3) composite positional/orientational distribution functions. The separate distribution functions may be expanded as series, the coefficients of which are called order parameters.

The singlet distribution function for a translationally invariant system is given as

$$P^{(1)}(r_1,\Omega_1) = P^{(1)}(\Omega_1) = \rho\, f(\Omega_1) \qquad (2\text{-}4)$$

where the number density is

$$\rho = \frac{N}{\int dr} = \frac{N}{V} .$$

Upon rearrangement and elimination of subscripts $f(\Omega)$, the singlet orientation distribution function, is given as

$$f(\Omega) = \frac{P^{(1)}(\Omega)}{\rho} .$$

By substituting eq. 2-4 in eq. 2-3 and rearranging, $P^{(2)}$ may be written as

$$P^{(2)}(r_1,\Omega_1;r_2,\Omega_2) = P^{(1)}(r_1,\Omega_1)\, P^{(1)}(r_2,\Omega_2)\, g(r_{12},\Omega_1,\Omega_2)$$
$$= \rho^2 f(\Omega_1)\, f(\Omega_2)\, g(r_{12},\Omega_1,\Omega_2). \quad (2\text{-}5)$$

$f(\Omega)$ may be generally expanded in a Wigner series. For the simple case (Figure 2-2) where the molecules may be considered cylinders and give rise to a mesophase with uniaxial symmetry about the z axis (taken as coincident to the director, $\hat{n}$), $f(\Omega)$ is a function only of the angle β, which shall be redesignated θ, between the director and the cylinder axis and

$$f(\Omega) = 4\pi^2 f(\beta) = 4\pi^2 f(\theta).$$

The Wigner series expansion reduces to the Legendre series expansion in this case and the familiar order parameters, $\overline{P}_2(\cos\theta)$ and $\overline{P}_4(\cos\theta)$, are averages of the even Legendre polynomials.

The many smectic mesophases are not translationally invariant. Even more complicated, analysis of the smectic A (still cylindrically symmetric molecules and a uniaxial mesophase) is possible but positional as well as orientational distribution functions must be considered. Other mesophase symmetries and the question of biaxiality demand further refinements to the functions.

The Mean Field Approximation: Attraction

Once the arrangement in space has been described, the molecular interactions to account for the energetics of the system are considered. The statistical independence of particles in a low density system was shown in the previous section. When considering dense systems, especially those with obvious long-range order such as nematic LCs, the molecular field or mean field approximation is an often used simplification. The essence of the approximation is that a particle experiences an average orienting field due to its interactions with all other particles in the system. Because the field is an average field, the interaction of one particle is independent of the coordinates of all the other N-1 particles. Therefore, it is not sensitive to short-range ordering via local correlations with its neighbors. Mathematically, $U(\{\chi^N\})$ is expressed as a sum of pair potentials as in eq. 2-2, which are integrated over all orientations of the intermolecular vector, r_{ij}, all intermolecular separations, r_{ij}, and all orientations of the second molecule. Eq. 2-5 reduces to

$$P^{(2)}(r_1,\Omega_1;r_2,\Omega_2) = \rho^2 f(\Omega_1)\, f(\Omega_2)\, g(r_{12}) \ .$$

In 1916 [37] Born developed a theory of the nematic mesophase based on the long-range interaction of a pair of electric dipoles. It has since been shown that electric

dipoles are not a requirement. In the late 1950's, the very successful mean field theory of Maier and Saupe [38a-c], borrowed substantially from the Weiss theory of ferromagnetism [39], was introduced. The premise taken was that the induced dipole-induced dipole part of the anisotropic London dispersion forces of attraction [40, 41, 42 and 43] is responsible for the existence of the mesophase. The pair potential is separated into scalar and anisotropic components. The scalar part, related to the spatial distribution, is assumed to be the same for both the nematic and isotropic phases. The anisotropic part, U_a, is directly related to the order parameter, s or $\overline{P}_2(\cos\theta)$,

$$U_a \sim [\, 1/2\ (3\cos\theta_i^{\,2} - 1)]\ [\, 1/2\ \langle 3\cos^2\theta - 1\rangle]$$

$$\sim [\, 1/2\ (3\cos\theta_i^{\,2} - 1)]\ \ s$$

where θ_i is the angle which the long molecular axis makes with the director axis, $\hat{n}$ (Figure 2-2). Having this relationship between the potential and s, other thermodynamic properties can be calculated. s can be related directly to experimental quantities, namely diamagnetic susceptibility, birefringence and linear dichroism.

By plotting the Helmholtz free energy, A = E - TS, versus s at different temperatures, one can see that at $T = T_{N->I}$ there are two equal minima corresponding to the nematic and isotropic states (Figure 2-3a). The transition

occurs with no change in volume but an abrupt change in s or $\overline{P}_2(\cos\theta)$ from 0.0 to a universal value of $\simeq$0.44 and in $\overline{P}_4(\cos\theta)$ from 0.0 to $\simeq$0.12. (See Figure 2-4.) This corresponds well with experimental values for SMLCs: in general, the experimental values are higher in PLCs [44]. In real systems there is a volume change but it is very small.

Hard Rod Fluids: Repulsion

In hard particle theories of nematics, only short-range steric repulsions of mutually excluded volumes or co-volumes are considered [40, 41, 42 and 43]. The intermolecular pair potential to represent this is:

$$U_{ij} = U^{\star}(r_{ij},\Omega_i,\Omega_j) = \begin{cases} \infty & \text{when particles overlap} \\ 0 & \text{when particles are apart} \end{cases}$$

where, like eq. 2-2, $U_N = \sum_{1<i<j<N} \overset{\star}{U}(r_{ij},\Omega_i,\Omega_j)$.

Similar to eq. 2-1, the equilibrium configurational partition function with a normalization factor is given as:

$$Q_N = \frac{1}{N!\ (8\pi^2)^N} \int dr^N \int d\Omega^N \exp\left[\frac{-U_N}{kT}\right].$$

which must be summed over all possible orientational distributions. The goal is to derive the excess free energy function of an n-component system each with a given orientation, $\phi_N(N_1,N_2,\ldots,N_n)$, from which thermodynamic

parameters and orientation functions may be obtained. Two approaches to arriving at an expression of ϕ_N are [1] the cluster or virial expansion and [2] the scaled particle methods. In method 1, the series can be truncated after the virial coeficient representing two-particle interactions if the density is low. The pair distribution function is not necessary for method 2; instead, the reversible work required to form a cavity in the fluid into which a particle can be fit is calculated.

Mesogens have been simulated by rigid spherocylinders, cylinders of length L and radius a, capped by hemispheres. The length to width ratio, $x = 1+L/2a$, is an important consideration. Onsager [45], using the cluster expansion approach, obtained the best agreement for very long rods ($x > 100$) but real nematogens (SMLCs and PLC mesogenic units between flexible spacers) have x values between 3 and 10. The value of .784 predicted for $\overline{P}_2(\cos\theta)$ at the $I \Rightarrow N$ transition is higher than experimentally observed.

The scaled particle approach predicts trends correctly for shorter mesogens but the calculated thermodynamic values differ considerably from the experimental. For example, a small relative density discontinuity, $\Delta\rho/\rho_{nem}$, of <1% is observed. The theory predicts values of $\Delta\rho/\rho$ and $\overline{P}_2(\cos\theta)$ which are too large and $\overline{P}_2(\cos\theta)$ which is independent of temperature, contrary to experiment. Hard rod theories, including the lattice treatments which will not be covered

here, fail due to the neglect of long-range intermolecular attractions, repulsions represented unrealistically by exclusion and the neglect of flexibility in the rod. The generalized van der Waals approach is an attempt to overcome these deficiences by taking both angle-dependent intermolecular attractions and anisotropic hard core repulsions into account.

Short-Range Order and Pretransition Effects

The theories outlined above neglect short-range orientational order. The importance of short-range order is demonstrated experimentally, however. Theoretical calculations for the heat of transition from the nematic to isotropic states are 2 to 3 times larger than those observed experimentally. Such a discrepancy can be accounted for by the persistence of clusters of 2 or 3 molecules into the isotropic state [38]. A second example is the 100-fold increase in magnetic birefringence of a thermotropic SMLC as the sample is cooled from the isotropic state to just above T_c. The birefringence shows a $(T - T^*)^{-1}$ dependence which is directly analogous to phase transition behavior observed in ferromagnetic systems. In ferromagnets T^* is identified as the Curie or critical temperature. In the LC case, T^* corresponds to the temperature below which the isotropic state becomes unstable.

Such pretransitional behavior, which occurs in LCn systems prior to the first order transition to the nematic state, has been treated by de Gennes [46] using the Landau [43 and 47] theory of continuous or second order phase transitions near a critical point. If the excess free energy of an ordered system is expanded in powers of the order parameter,

$$A = A_0 + (1/2)A_2s^2 - (1/3)A_3s^3 + (1/4)A_4s^4 + \ldots.$$

a discontinuous transition is predicted for $A_3>0$ and $A_4>0$. A continuous transition is predicted for $A_3=0$ where A_2 is given as

$$A_2(T) = a(T - T^*)^\gamma$$

where the exponent γ is 1 for the mean field approximation. If A_3 is small and positive, T^* will occur at a slightly lower temperature than T_c. (See Figure 2-3b.)

Anisotropic molecular polarizability coupled to fluctuations in molecular orientation gives rise to fluctuations in optical anisotropy and the scattering of light. Litster and Stinson [48a-d] used light scattering to study thermal fluctuations in the degree and orientation of molecular alignment above the clearing temperature in p-methoxy benzylidene-p-n-butylaniline (MBBA). They verified the de Gennes predictions and found a $(T_c - T^*)$ of less than 1 K. Chu et al. [49] found a coherence length of 120 to 150 A (Figure 2-5) from a comparison of polarized and depolarized light scattered intensities.

The Cotton-Mouton and Kerr effects observed for SMLCs validate the Landau-de Gennes treatment of the phase transition. In the former experiment, Δn, the birefringence or difference in refractive indices parallel and perpendicular to an applied magnetic field, H, can be shown to exhibit the following proportionalities:

$$\Delta n = n_{\parallel} - n_{\perp} \sim \frac{\chi H^2}{A_2(T)} \sim \frac{H^2}{a(T - T^*)} \sim s$$

where χ is the magnetic susceptibility. T^* is obtained as the intercept of a straight line plot of $H^2/\Delta n$ versus T. Thus, the second order phase transition, which was predicted and pretransitional effects experimentally observed, would occur were it not for the first order $I \Rightarrow N$ transition which intervenes. The utility of light scattering in measuring the associated fluctuations has been demonstrated for very pure SMLCs.

The Continuum Approach

In the 1920's Oseen [50] and Zocher [51] proposed the first treatment of the nematic mesophase as a continuum, a treatment which was firmly based in molecular statistics, however. The more recent formalism of Ericksen [52] and Leslie [53] are in common usage. Frank [54] has related the curvature elasticity constants of twist, splay, and bend

illustrated in Figure 2-6 to defects observed in the textures of LCs.

The mesophase is considered to be an incompressible anisotropic fluid in which the director, $\hat{n}$, indicates the direction of preferred orientation of the medium; the direction of individual mesogens is entirely neglected. Molecular interactions which give rise to long-range orientational order are assumed much greater than the deformation field. The free energy density for deformation is given as

$$A = \frac{1}{2} k_{11}(\Delta.n)^2 + \frac{1}{2} k_{22}(n.\Delta Xn)^2 + \frac{1}{2} k_{33}(nX\Delta Xn)^2$$

where k_{11}, k_{22} and k_{33} are the moduli of infinitesimal, isothermal splay, twist and bend components of deformation, respectively. The experimentally determined ratio of $k_{11}:k_{22}:k_{33}$ values for PAA at 120^{o}C are 1.6:1:3.2 (magnitude is of the order 1 X 10^{-}6 dynes) [23]. The elastic twist constant is the smallest which accounts for the ease of formation of cholesterics and twisted nematics; bend deformation is unfavorable for rods. The elastic constants may be determined in a straightforward manner by obtaining the threshold or critical magnetic field, H_c, required for deformation under conditions of specific mesophase alignment and sample and field geometries. Equivalent electric field experiments have some drawbacks. Field nonuniformities

above E_c (Williams domains) and conduction induced instabilities due to impurities are problematic.

The multiple dark brush features in the schlieren texture of thin (10μm) LCs samples observed by PLOM are regions where the optic axis is either parallel or perpendicular to the direction of polarization of the incident beam. The sample at these locations does not change the state of polarization and is extinguished by the analyzer oriented at 90^{o}. The term disinclination, shortened to disclination (analogous to dislocations in crystals) represents the line singularities at the center of the brushes (Figure 2-7). The strength of the disclination is defined as the number of brushes/4 and the sign convention is based on the direction of rotation relative to the rotation of the crossed polars. Texture is dynamic; disclinations of the same sign may add while those of equal and opposite sign may coalesce, thus approaching the minimum energy of distortion which would be achieved in a monodomain. In a macroscopic sample the sum of the strengths is zero.

Biaxial Nematics

Gray [26] has pointed out that the structural profile of many nematogens is more lath-like (rectangular or ellipsoidal in cross-section) than rod-like (circular in

cross-section) with coplanar aromatic rings and double bond character of the linkages which serve to hinder free rotation. Freiser [33a-b] has generalized the Maier-Saupe treatment to include an orientation distribution function which is dependent upon the rotational angle of the molecules about their long axes, that is, a multiaxial structure. This should not be confused with optical biaxiality which could arise from tilt within smectic layers as well as from an inherently biaxial molecular structure. In the second case only, primary structure and property are related [55].

A ground state which is not uniaxial and a transition to the lower symmetry, biaxial nematic state which may proceed directly from the isotropic state or via a second order phase transition from the uniaxial nematic state are predicted by this theory. Alben [34] has determined the entire phase diagram for prolate uniaxial (rod-like LCs - long axes parallel), oblate uniaxial (discotic LCs - flat faces parallel), biaxial (both long axes and flat faces parallel) and isotropic states (all orientations equally likely). Figure 2-8 gives the phase diagram of a fluid of biaxial particles of a length to width ratio of 2.6; the reduced effective asymmetry versus the reduced pressure is plotted. By proceeding along lines 1 or 2 from the isotropic state, there is a first order phase transition to a uniaxial state followed by a second order phase transition

to a biaxial state. The biaxial state can be arrived at directly by taking the path along line 3.

Summary

The state of order of some model PLCs was probed by the techniques of x-ray scattering and small angle light scattering during the course of this dissertation. For that reason, in this chapter theories which attempt to account for the existence of the mesophase and correctly describe mesophase behavior and state of order were reviewed. The disorder ⇒ order transition was highlighted. At the other extreme, the intermediate state of order of the mesophase is also arrived at by an order ⇒ disorder melting transition of the three-dimensionally ordered crystalline state. Pople and Karasz [56] modified the Lennard-Jones and Devonshire [57] description of melting to include anisotropic molecules where disorder in orientation as well as position becomes important. Molecular diffusion to an interstitial vacancy site is favored if there is misorientation between neighboring particles. The question of the existence and recognition of a biaxial nematic mesophase is of importance for the more lath-like nematogens. Careful thermodynamic measurements must be made to distinguish a second order phase transition. It is likely that transition to a smectic

mesophase or crystallization may intervene and prevent the observation of the biaxial nematic state. The non-equilibrium nature of polymers in general and polymeric liquid crystal in particular may permit one to quench in the biaxial nematic morphology for study.

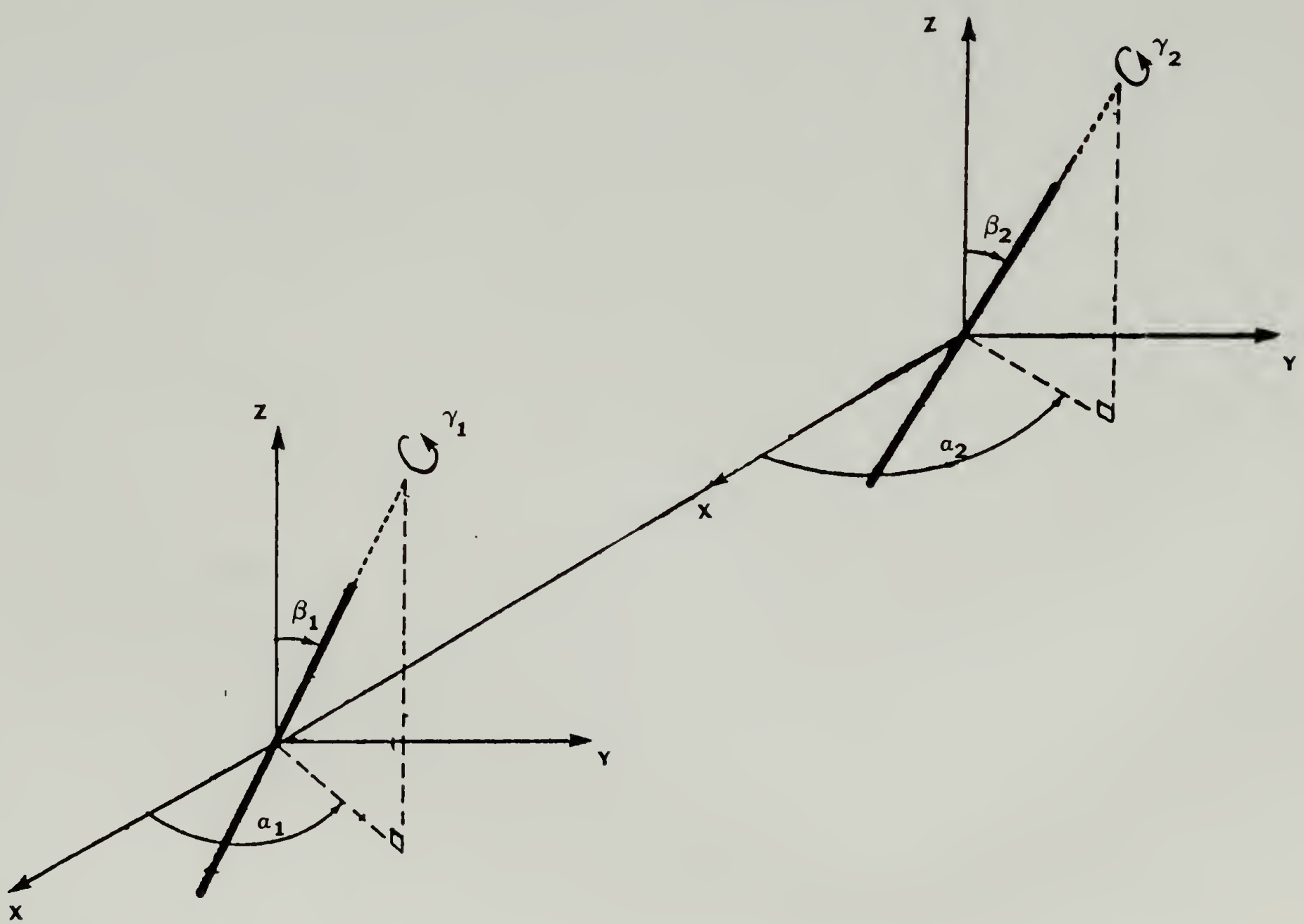

Figure 2-1. Orientation of two rods.

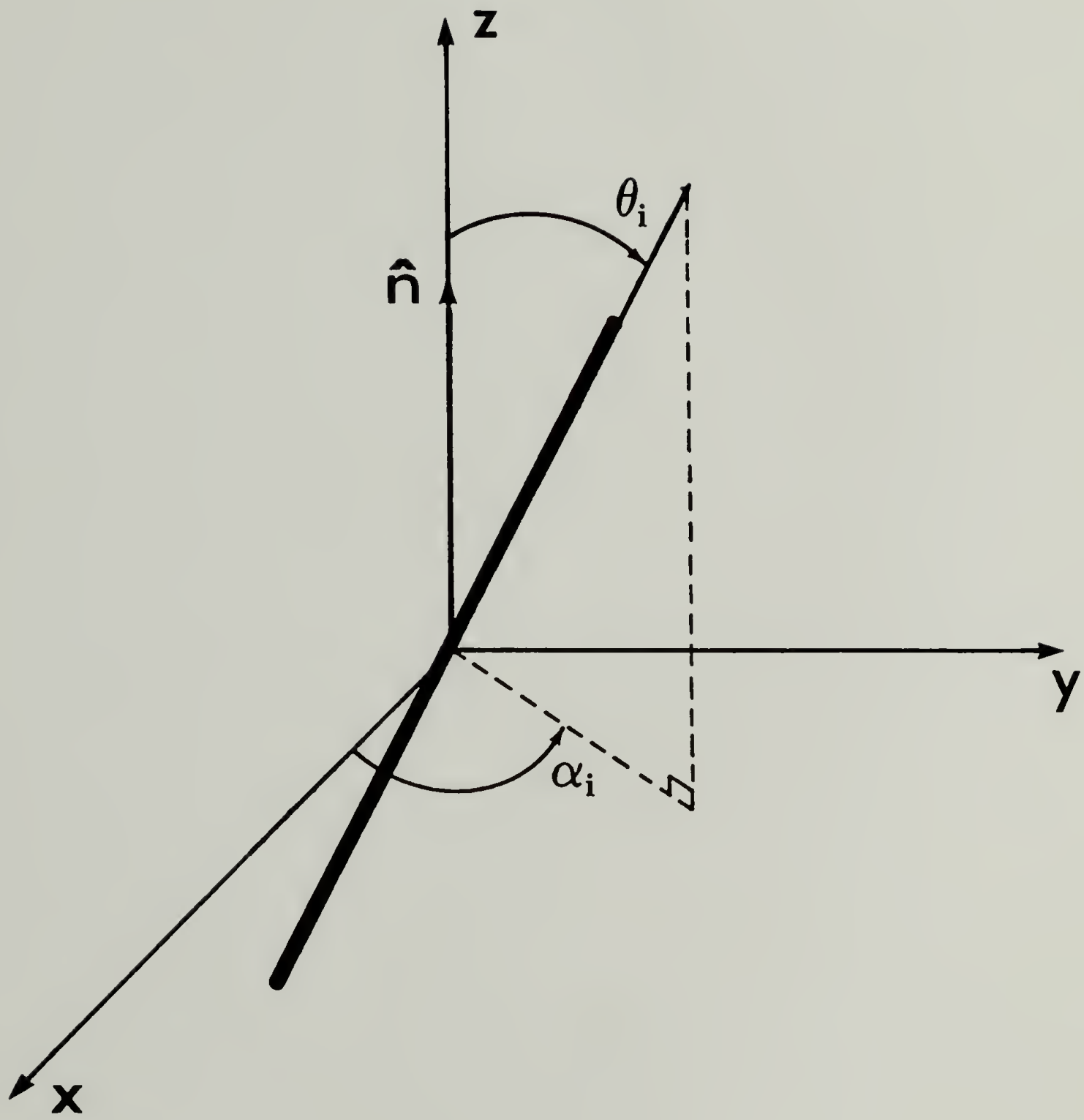

Figure 2-2. Orientation of one rod with respect to the local director.

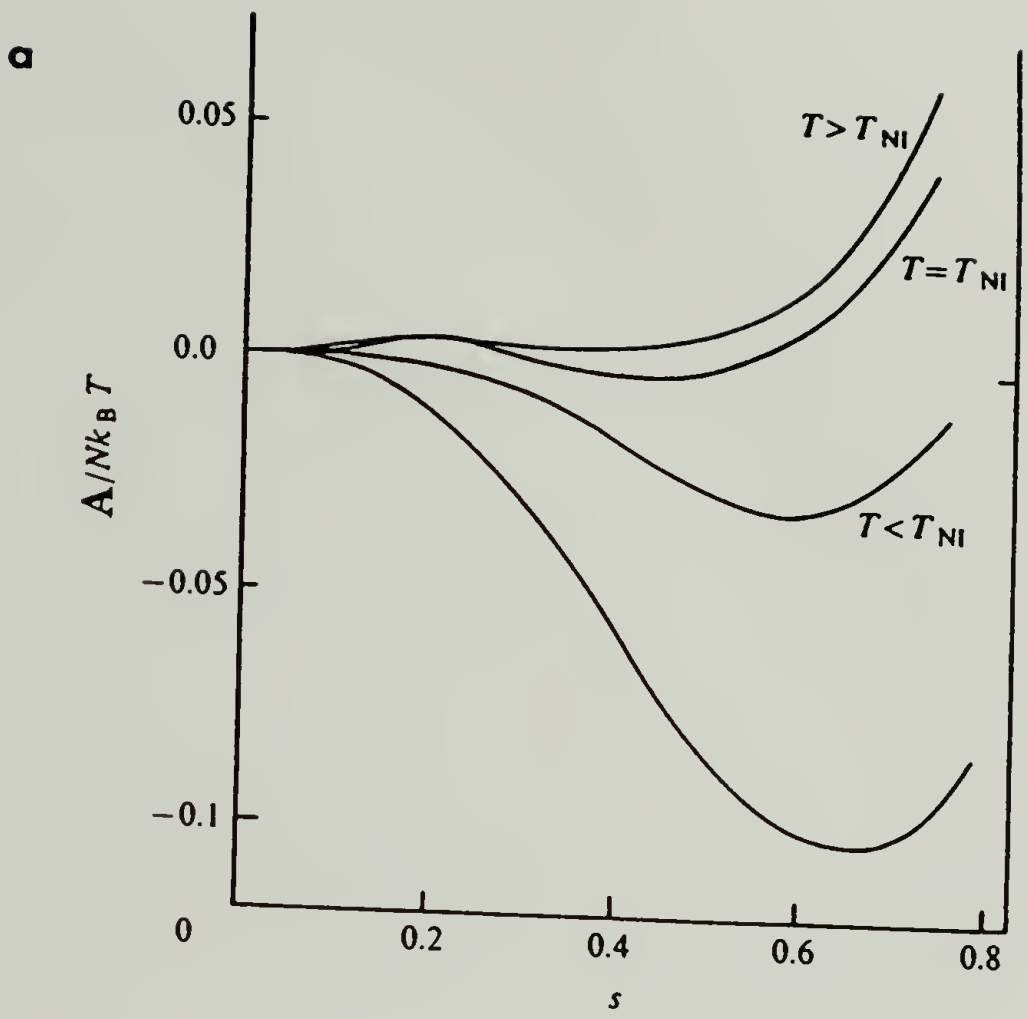

Figure 2-3. Helmholtz free energy as a function of order parameter: calculated for a) the Maier-Saupe mean field treatment [25] and b) for the Landau-de Gennes consideration of critical phenomena [23].

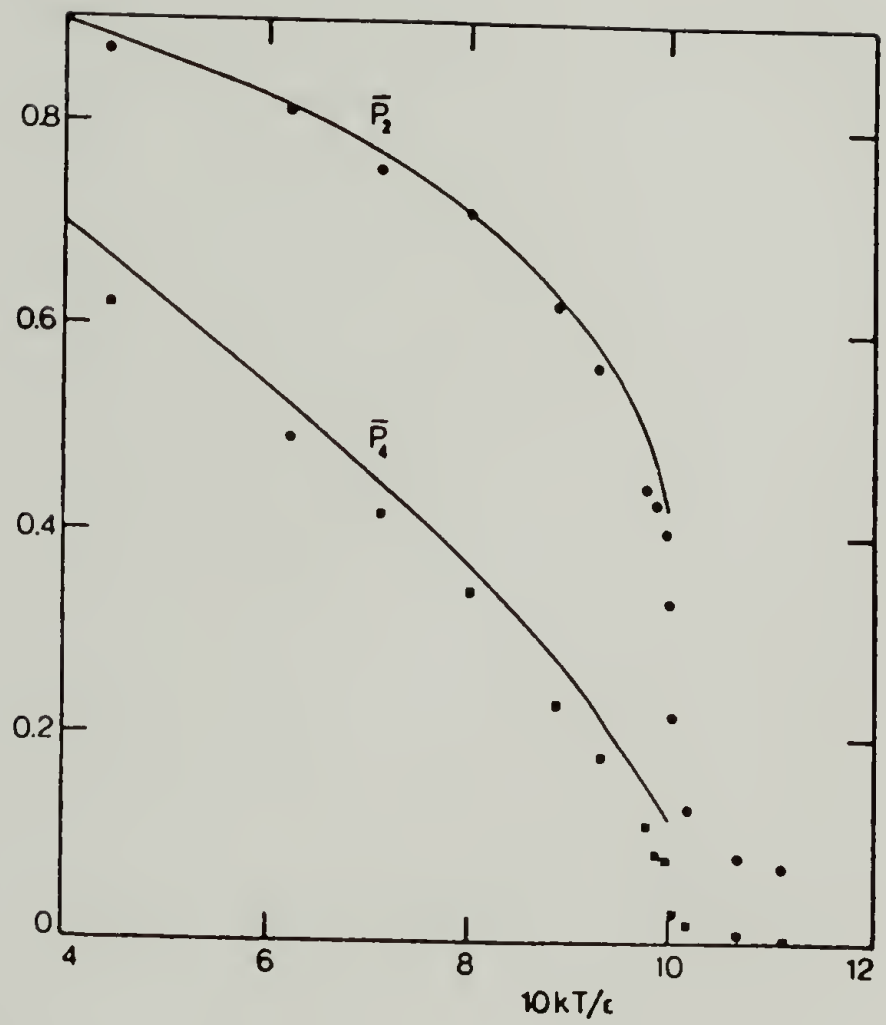

Figure 2-4. The dependence of the order parameters upon reduced temperature (———for Maier-Saupe theory, ...for Monte Carlo simulation) [26].

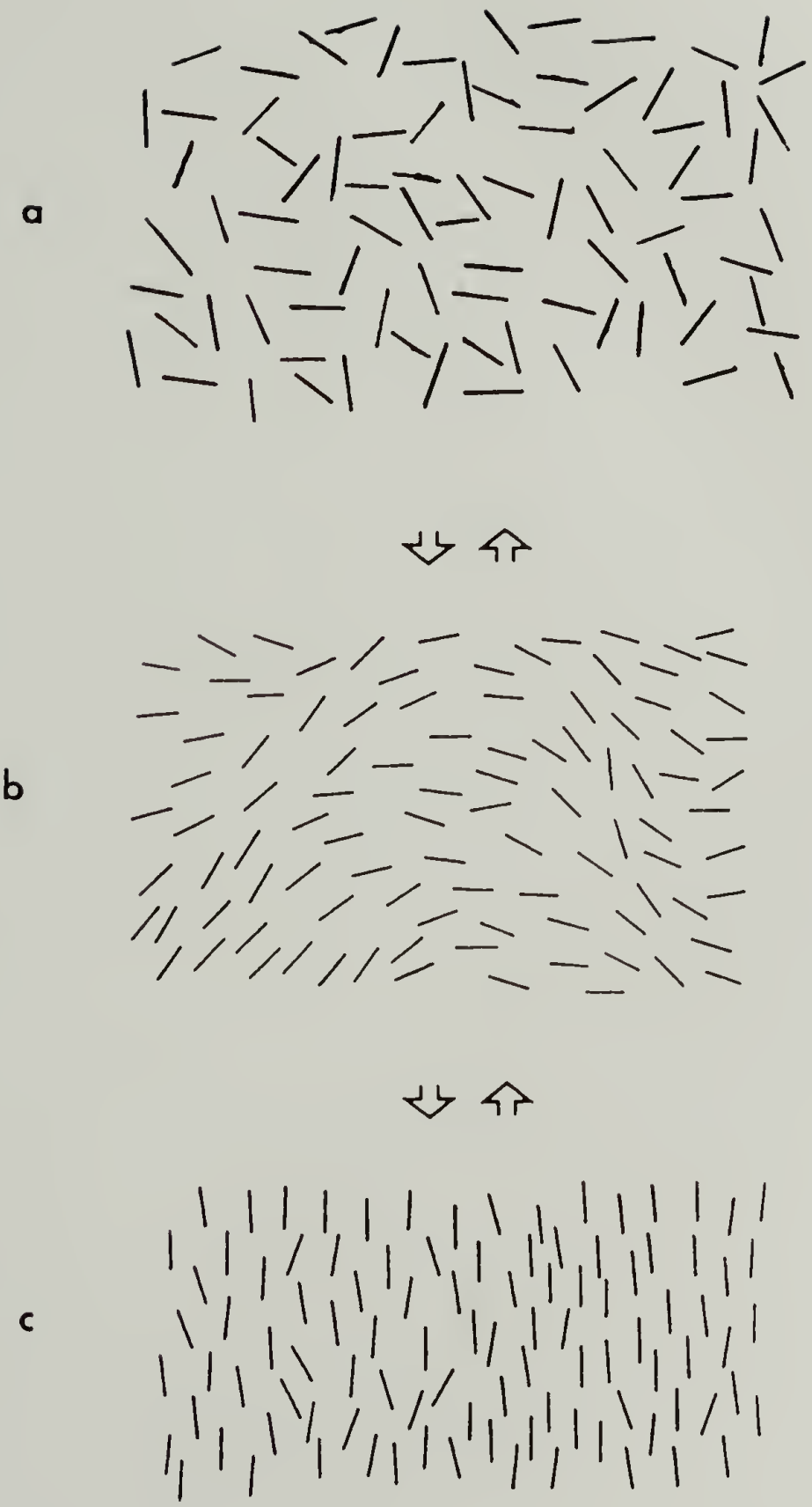

Figure 2-5. Illustration of the sequential transitions from isotropic state to pretransitional state (showing onset of short-range order) to mesophase.

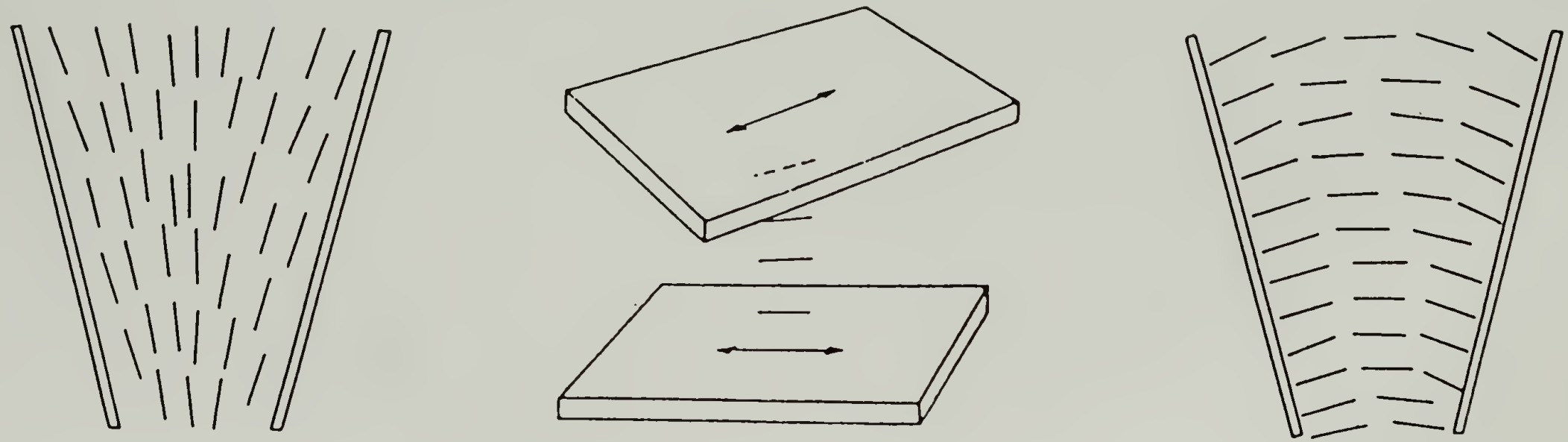

Figure 2-6. Three types of deformation in liquid crystals [from 23 and 25].

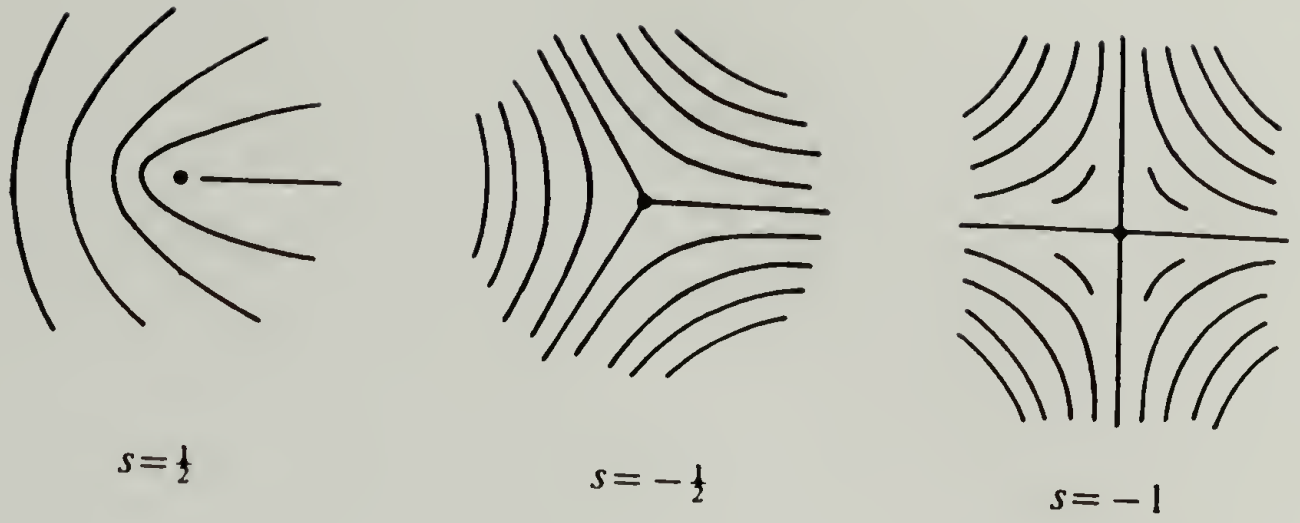

Figure 2-7. Director orientation near a disclination [from 25]. (c is an additive constant in angular distribution of director.)

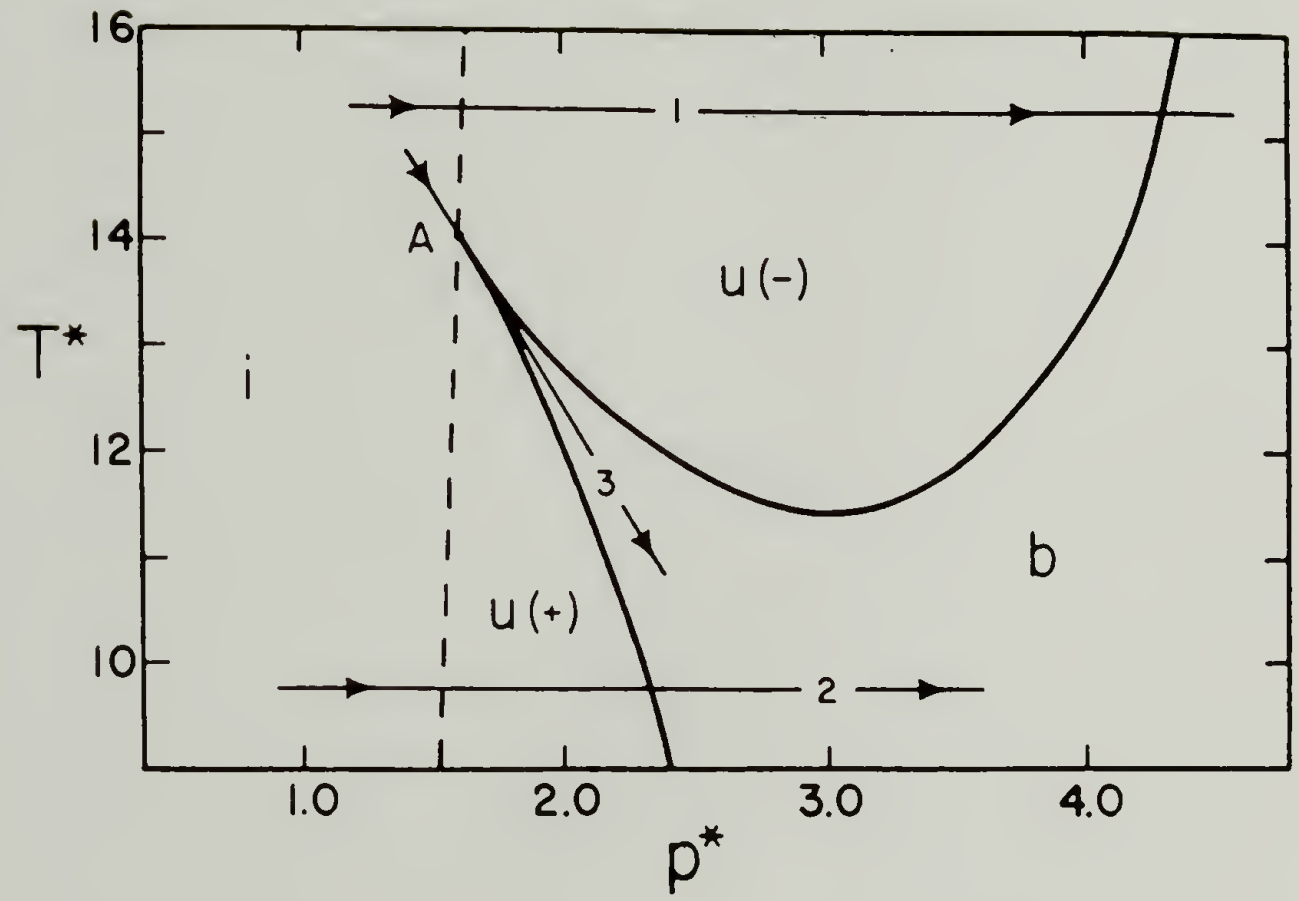

Figure 2-8. Phase diagram showing the uniaxial<-->biaxial nematic phase transition [34].

C H A P T E R III

EXPERIMENTAL

Polymer Samples Used and Notation

Introduction

Two general classes of main-chain thermotropic liquid crystalline polymers were used in this study: 1) the all aromatic backbone with alkyl substituents

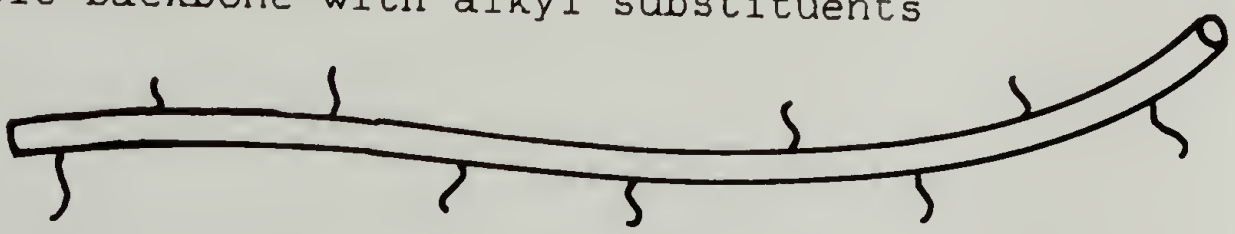

which shall be referred to as the rod- or lath-like class (although there is some flexibility to the backbone) and 2) the class in which the mesogen and flexible spacer alternate in a regular fashion

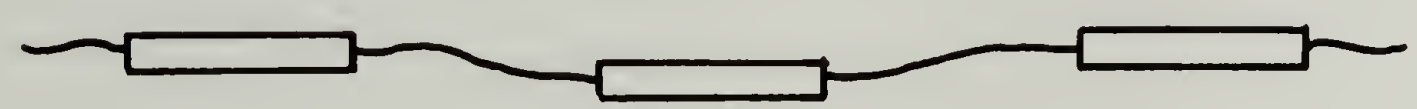

The mesogen may or may not have appended substituents to further reduce transition temperatures.

The PLCs were prepared by Drs. Qi-Feng Zhou, Christopher K. Ober, Paolo Nieri and C. Rami Reddy over a span of approximately eight years. A brief outline of the polymer syntheses and post-reaction workup procedure is included as it pertains to the characterization and morphology of the as-obtained material. The morphology, in many cases, was

found to be very different when the polymer was variously subjected to solution and melt casting procedures. The morphology was also highly dependent upon the rate of casting. These observations bear a direct relationship to anomalous results obtained in first heating DSC scans and in subsequent scans after the cooling rate is changed from a gradual cooling to a quench.

The morphology thus considered is composed of both sub-structural (crystalline, liquid crystalline or amorphous) and super-structural (spherulites, fringed-micelle formation or domains) features. Thus, the morphology of the solution precipitated polymer may be very different from that obtained from a melt polycondensation if no reprecipitation was done during workup. Two different samples will become morphologically equivalent after being heated to the isotropic state. It is unclear if heating only as far as the mesophase is sufficient to erase memory of the solid state morphology. Unfortunately, due to the different solubility properties of the different PLCs (even within a homologous series) no consistent final workup was possible.

However, the different morphologies obtained by solution and melt casting made it possible to tailor the initial morphology to some extent. This was taken advantage of in order to correlate structural changes at different dimensional levels with thermal events which were evident by DSC.

Rod-Like Polymers

The original preparation of the homologous series, alkyl substituted poly(phenylene terephthalates), where R spans the entire range from ethyl to dodecamethyl including selected branched alkyls, has been described before [58, 59]. Only the materials obtained by the condensation reaction of terephthaloyl chloride and alkyl hydroquinone in methylene chloride were used in this study (Method B [59]). Although resulting in polymer of low degree of polymerization, this was the "cleanest" of the synthetic routes described in [59]. The final preparative procedures, after the polymer precipitated from the reaction mixture probably in a semi-crystalline state, were ethanol and acetone washes which visibly swelled the polymer [60] and might have disrupted any crystal packing present. The powdered product was used without further treatment for DSC and WAXS studies. The inherent viscosities of these materials were in the 0.25 to 2.10 range with most approximately 0.50 dl/g.

It was found in study [59] that there was a steady decrease in transition temperatures (and, therefore, in estimated processing temperature) up to the heptyl homolog, beyond which the temperatures remained fairly constant. Thus, the octyl homolog was chosen as the polymer which would be synthesized in larger quantities and higher degree

of polymerization for more extensive study. A greatly improved synthetic procedure, the melt polycondensation of octyl hydroquinone and diphenyl terephthalate, resulted in polymer of greater purity and thermal stability and is described in [61]. By this method two batches of high polymer with inherent viscosities of 2.5 dl/g were obtained in clean reactions. After solid state post-polymerization, the inherent viscosity of the first batch increased to 3.2 dl/g. These materials were ground up after being removed from the melt polycondensation flask. They were used without washing and the concomitant swelling. It is likely that some monomer was still present (see DSC and TGA results).

The polymers will be designated PPT-R-S and PPT-R-M to differentiate the various substituents (R) and solution (S) and melt (M) polymerization procedures, respectively. M-b and M-a stand for melt polycondensation, before and after solid state post-polymerization as described in [61]. R will represent the number of carbon atoms in the normal alkyl side chain and acronyms represent the branched alkyl side chains (for example, TB and DMB respectively represent tertiary-butyl and 3,3-dimethyl butyl). The sample designation, inherent viscosities and thermal data are summarized in Table 3.

Table 3

Rod-like PLCs studied and their physical data

POLYMER	[η](dl/g)	T_m(°C)	T_c(°C)	references
PPT-2-S		>370	---	[59, 60]
PPT-4-S		360	---	
PPT-6-S	0.59(a)	330	---	
PPT-8-S		305, 325	~385	
PPT-12-S		290	345	
PPT-TB-S		>370	---	
PPT-DMB-S		360	---	
PPT-8-M-B	2.5(a)	310,325	~385	[61]
PT-8-M-A	3.2(a)	312,328	~385	

a - measured in p-chloro phenol, 0.5 g/dl, 45°C

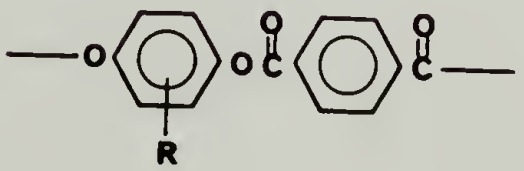

PPT - R

Polymers with Alternating Mesogenic and Flexible Units

Three sets of polymers of similar structures were investigated: [1] a series of unsubstituted triad mesogens with flexible spacers ranging from ethylene to dodecamethylene, [2] a series of centrally substituted triad mesogens with decamethylene spacers, and [3] one exactly alternating dyad mesogen with a decamethylene spacer.

In the polymer designation scheme which will be followed, the mesogen will be identified by two or three letters depending on if it is a dyad or triad, followed by a number to indicate the number of methylene units in the flexible spacer. H stand for hydroxy benzoic acid, T for terephthalic acid, and Q for hydroquinone. If there is a substituent on the central unit of the triad mesogen, the acronym for that substituent will appear in parentheses after the mesogen designation: Br for bromo-, Me for methyl- and Et for ethyl-. The polymer notations, inherent viscosities and thermal data are given in Table 4.

The HTH-R series were prepared by the condensation reaction of the appropriate α,ω-bis (p-hydroxybenzoyloxy) polymethylene and terephthaloyl chloride in 1,1,2,2-tetrachloroethane (TCE) with pyridine as an acid acceptor as described in [62, 63, 64 and 65]. The final purification step was washing of the polymer, which had precipitated from the reaction solution, with acetone or methanol.

Table 4

PLCs with flexible spacers studied and their physical data

POLYMER	[n](dl/g)	T_m(°C)	T_c(°C)	references
HTH-5	0.14(a)	---	267	[62, 65, 63, 64]
HTH-9	0.28(a)	174	233	
HTH-10	0.34(a)	220	267	
HTH-12	0.48(a)	212	245	
HTH(Cl)-10	0.31(a)	167	---	[65]
		114	137	
HT-10-TH-10	0.13(a)	124	---	[65, 63]
TQT(Br)-10	0.33(c)	140	196	[68]
HQH(H)-10	0.91(a)	253	294	[66, 62, 70]
HQH(Me)-10	0.57(b)	187	280	
HQH(Et)-10	0.51(b)	130	234	

a - measured in p-chloro phenol, 0.5 g/dl, 45°C
b - measured in chloroform, 0.5 g/dl, 25°C
c - measured in 1,1,2,2-tetrachloroethane, 0.5 g/dl, 40°C

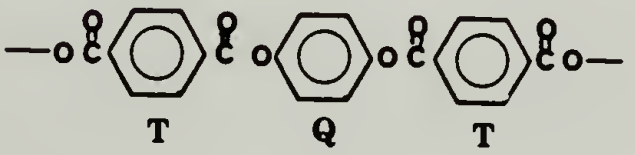

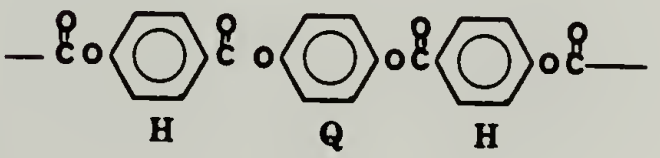

HQH(Me)-10, HQH(Et)-10 [66], TQT(Br)-10 [67, 68] and HT-10-TH-10 [63, 65, 69] were also synthesized by the method described above with the appropriate diacid chloride and diphenol. The unsubstituted HQH-10 [66, 70] was prepared by bulk polycondensation from the free diacid and the diacetate of the diol. HQH(Me)-10 and HQH(Et)-10 were dissolved in chloroform and reprecipitated with acetone whereas the less soluble HQH-10 was reprecipitated from p-chlorophenol solution with methanol. TQT(Br)-10 and HT-10-TH-10 were precipitated from the reaction mixture with acetone.

Treatments to Tailor Initial Morphology

Solution Cast Films

Thin films (10 to 20 μm measured by micrometer) were prepared by dropping a 2% to 3% (by weight) polymer solution, filtered through a Millipore filter, onto microscope cover glasses. The solvent was either p-chlorophenol, chloroform, 1,1,2,2-tetrachloroethane or 1,1,1,3,3,3-hexafluoroisopropanol (HFIP). p-chlorophenol was distilled under vacuum and sealed under a nitrogen atmosphere before using. The other solvents were used as received from Aldrich Chemical Company. When p-chlorophenol was the solvent it was necessary to pretreat the cover glasses in a controlled fashion by washing with a 5% aqueous

NaOH solution followed by extensive rinsing with distilled water and careful drying. This treatment altered the glass surface for optimum solution spreading and film formation.

The films prepared from p-chlorophenol were extensively dried at 50°C for 72 h under 5 torr vacuum until dry. Then the temperature was raised to 65°C.

Films cast slowly from p-chlorophenol solution tended to be more highly crystalline and were more likely to develop semi-crystalline super-structural details such as spherulites. At the other extreme, films cast from HFIP solution onto cover glasses, preheated to 40°C, were either amorphous or appeared to be in a frozen LCn state from the threaded microscopic texture.

Fiber Formation

Method 1: Disk-shaped pellets (1.3 cm diameter, 0.2 cm thick) of PPT-8-M-a were pressed in a nitrogen-flushed, evacuated press at 340°C. The pellets were loaded into a barrel with a motorized screw plunger. Fibers were extruded from the polymer sample in the mesophase state under nitrogen atmosphere at 340°C. Upon exiting the capillary (~ 50μm bore) the fibers were drawn and air quenched.

Method 2: For samples available in smaller quantities, namely the PPT-R-S series, fibers were obtained by pulling with tweezers from the mesophase. A pool of liquid

crystalline melt was formed under nitrogen atmosphere in a glove box by rapidly subjecting powdered sample, contained in a DSC pan, to the temperature of a heated block. The block was preheated to the temperature at which the mesophase would exist for the respective polymer sample as determined by DSC.

Identical degrees of orientation of three different PPT-8 samples, melt polycondensed before and after solid state post-polymerization and solution polycondensed, was obtained by Methods 1 and 2. This was determined by x-ray diffraction of thin segments (i.e., highly drawn) of the fibers.

General Characterization Techniques

Description of Hotstage

A Mettler FP-2 hotstage provided programmed heating and cooling rates of 0.2, 2.0, and 10.0^{o}C/min under a nitrogen atmosphere. This heater was used in microscopy and SALS experiments where the samples were films which had been either melt cast or solution cast onto microscope cover glasses. The hotstage was factory calibrated and modified (12/84) so that temperatures of 370^{o}C could be attained.

Differential Scanning Calorimetry

Differential scanning calorimetry (DSC) was done on a Perkin Elmer DSC 2 with thermal analysis data station (TADS) capability under dry nitrogen. Heating and cooling rates of $10^{o}C$/min and $20^{o}C$/min were typically used. One experiment on PPT-8-S was run over a wide spectrum of heating rates ($2.5^{o}C$/min to $160^{o}C$/min) to test observed transition peak separation as a function of heating rate.

Appropriate care was exercised to avoid sample decomposition by limiting the time that the sample was held at high temperature and to compare samples which had experienced equivalent thermal processing. Generally, a first heating scan was run on the as-obtained, virgin sample followed by a quench. A second heating scan after the quench, a slow cooling scan and a third heating scan after the slow cooling were also recorded. A dry ice/isopropanol bath was used to achieve temperatures as low as ~ $-73^{o}C$ (~210 K). With the bath in place, quenching from $350^{o}C$ at $320^{o}C$/min was efficient down to ~$17^{o}C$ (~290 K). Comparison of slowly cooled and quenched polymer gave some indication of the melt recrystallization and vitrification processes occurring in the various PLCs.

Thermal Gravimetric Analysis

PPT-8-M-b was studied by thermal gravimetric analysis (TGA) to verify that a DSC endotherm was due to vaporization of monomer. The TGA used was a duPont 9900 model. A heating rate of 10^{o}C/min was used.

Viscosity Measurements

The sources of the viscosity measurements quoted herein are published and unpublished results by the synthetic chemists. The measurements were made in various solvents and at various temperatures at a concentration of 0.5 g/dl usually.

Complementary Techniques for Structure Determination

Polarized Light Optical Microscopy

Morphological and mesophase textural changes were observed at up to 320X magnification under crossed polars in a Zeiss microscope (PLOM). Because the Mettler FP-2 hotstage was incorporated in the optical path, short focal length objectives which were able to withstand high temperatures were used. Various types of film were used: Kodak Ektachrome tungsten color slide film, Kodak black and

white print film and Polaroid type 52, 55, and 58 instant film. Magnification was calibrated with a graticule with divisions of 0.01mm (10μm) and a diffraction grating with 600 lines/mm.

X-Ray Scattering

X-ray patterns (WAXS and SAXS) were obtained on flat film in an evacuated Warhus Statton camera (nickel-filtered Cu Kα radiation, operating at 30 mA/40 kV). Powdered samples were placed either directly on the final pinhole or in a flame-sealed, 1.5 mm glass capillary in a heater unit which was set in slot 1 of the camera. Temperature control was ± 2°C. Fibers were taped across the pinhole. By varying the film position, both wide and relatively small, or intermediate, angle patterns were obtained.

A four-circle Siemens D-500 diffractometer equipped with a specially designed, nitrogen-purged heater (Figure 3-1) for capillary enclosed samples was used to obtain the diffractometer scans of powders and melted samples. Capillaries of 1.5 or 2.0 mm diameters were used, therefore, surface orienting effects in these PLCs were not observed and were probably negligible as compared with SMLCs. The heater was controlled within ± 3°C and was calibrated by melting lead and indium standards. The minimum scattering angle, 2θ, obtained on the D-500 was 0.75°.

In the powder patterns there was no preferred orientation. Fibers were taped across the D-500 sample holder: meridional and equatorial scans were taken by changing the fiber axis orientation by 90^{o} from horizontal to vertical.

Small Angle Light Scattering

The basic small angle light scattering (SALS) apparatus, diagrammed in Figure 3-2, consists of a 2 mw polarized He-Ne laser (λ = 632.8 nm), a polarizer film to linearly polarize the incident beam, a sample which scatters light, a second polarizer called the analyzer and various detection devices. A series of incremental neutral density filters attenuate the incident beam. The detection device may be the eye, aided with opalescent glass or paper, photographic film or an electronic detector. The polar angle of interest is chosen by varying the sample to detector distance or by employing a series of lenses (0^{o} to 33^{o} lenses available) to focus the scattering pattern within a given area.

In early SALS studies on PLCs, in which there was no azimuthal dependence of the scattering, the OMA-1 (optical multichannel analyzer) apparatus was used. OMA-1 is a one-dimensional position sensitive detector which consist of 1 track x 500 channels. Two-dimensional scattering patterns

were obtained with OMA-2, a vidicon detector, which has the capability of scanning and storing up to 500 tracks x 500 channels every 5 seconds. Instrument details, calibration procedures and the description of the software for data analysis are given in references [71, 72, 73 and 74]. Four quadrant and quadrant-averaged isointensity contour plots may be obtained from the corrected data.

The Mettler hotstage was used at heating/cooling rates of $2^{o}C$/min and the computer was programmed to take a scan, concurrently, every 1 minute or every 2 degrees. Modifications to the analysis programs were made to facilitate the computation of the many scans taken during thermal programming of the PLC samples.

Lens 1 and lens 2 are stationary in the OMA-1 and OMA-2 set-ups. In order to change the angular range of scattering different lens 3 are necessary. Table 5 lists the lenses used during the course of this work, the polar range and other physical constants.

Both the incident and scattered rays may be linearly polarized in either the horizontal or vertical directions. The two conditions for polarization which were important in this study are H_v or crossed polarization (polarizer is horizontal and analyzer is vertical) and V_v or parallel polarization (both polarizer and analyzer are vertical). If there were no sample or sample which does not cause the depolarization of light, the incident beam would be

Table 5

Lenses used for SALS and their physical constants

Lens Designation	Type	Focal Length (mm)	Angular Range (θ's)
LPX127	plano-convex	63.5	21^{o}
LDX115	bi-convex	50.8	26^{o}
LAG125	aspheric	38.5	33^{o}

extinguished under H_v conditions; such is generally true of an isotropic polymer melt.

The importance of reaching large scattering angles is discussed in Chapter VII. To this end, an aspheric lens was used. Generally, the analyzer may be placed at any location after the scattering sample and before the detector. However, caution must be exercised in the placement of the analyzer when an aspheric lens is used; the analyzer must be located before the lens. If the analyzer is placed after the lens, a four-lobed pattern is observed under both H_v and V_v conditions even for diffusive glass which should not display anisotropy in scattering. Apparently there is significant light reflection, which is partially polarized, from the highly curved surface of the aspheric lens. Furthermore, since the focal distance of the aspheric lens used is only 2 cm, there is a problem of heat dissipation before the plastic analyzer film which is placed between the heated sample and lens 3.

Figure 3-1. Nitrogen purged heater built to accomodate enclosed samples in D-500 diffractometer.

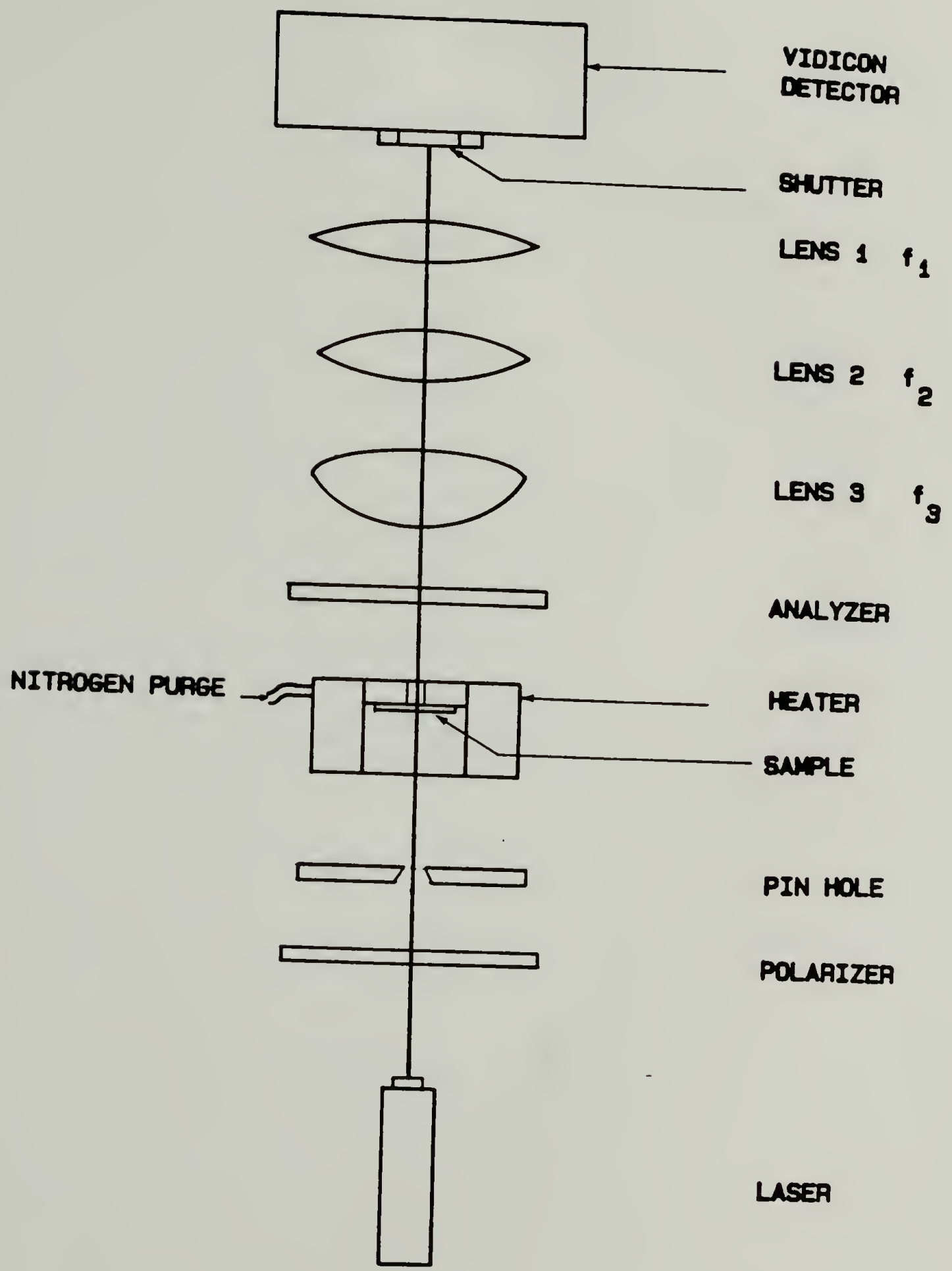

Figure 3-2. Schematic diagram of basic small angle light scattering apparatus.

C H A P T E R IV

ALKYL-SUBSTITUTED POLY(PHENYLENE TEREPHTHALATES)

Introduction

Main-chain PLCs which have no flexible spacers in the polymeric backbone have more potential to find utility as high strength fibers than those with spacers. In these rigid or worm-like chemical structures there is no possibility of chain folding which is the limiting factor to optimization of the strength of PLCs with spacers or, for that matter, a semi-crystalline polymer such as polyethylene. The mesophase of all-aromatic LCn homopolymers is inaccessible because of the symmetry and linearity of the structure resulting in a crystalline ⇒ mesophase transition which is above the degradation point. In this study the transition temperature has been reduced considerably by frustrating the crystalline packing by appending substituents to the backbone. A series of mono-substituted poly(2-alkyl-1,4-phenylene terephthalates), synthesized at the University of Massachusetts, were among the first systematic attempts at structural modification [58, 59]. A similar series of di-substituted poly(1,4-phenylene 2,5-dialkoxyterephthalates) were synthesized and characterized by Ballauff [75]. In the Ballauff series the

number density of the substituents per polymer repeat unit is twice as high and substituents as long as hexamethylene were studied. Thus, the alkyl/aromatic ratio is greater in the Ballauff series than the Majnusz series. A unique mesophase structure, in which the aromatic and aliphatic portions segregate to form a regular, long-range, layered structure where the layers are parallel to the mesogenic axis was discovered.

Results of Characterization Studies

First heating DSC scans of thermotropic PLCs are frequently non-reproducible and, for that reason, great caution and skepticism should be exercised in their interpretation. This will be demonstrated in Chapter V, in which a non-reversible crystal ⇒ crystal transition of solution-cast PLCs with flexible spacers takes place. Other researchers [76] have noted similar phenomena. Problems in dealing with these materials at high temperatures are the possibility of $^{1)}$molecular weight increase by post-polymerization and/or crosslinking and $^{2)}$degradation. Additionally it should be recognized that DSC heating scans of PLCs show a strong dependence on prior thermal history, i.e., quenching versus slow cooling from the mesophase or isotropic state; such effects may be related to behavior under conditions of annealing.

Figure 4-1 shows the first heating and reproducible second heating and cooling DSC scans for the various PPT-8 samples used in this study. The second heating scans, showing two endotherms separated by 5° to 15°C, is typical of the series PPT-R. (See Figure 4-2.) Table 3 listed the transition temperatures obtained for the second heating scan after cooling at 10°C/min. In the paper describing the synthesis of the PPT-R-S samples, the bimodal melting endotherms were incorrectly identified as melting to the simple nematic mesophase, T_m, followed rapidly by isotropization or clearing, T_i or T_c (Table 2 of [59]). The higher of the two transitions, at ~328°C for PPT-8, is currently thought to be the transition to a uniaxial nematic mesophase; the nature of the lower transition was sought. In many of the PPT-R-S samples, degradation occurs before the PLC enters the isotropic phase, thus T_i cannot be observed. However, by placing the sample on a hotplate heated to successively higher temperatures, T_i of PPT-8 has been estimated to be 385°C. The isotropic state of PPT-12-S, which appears as a dark field by PLOM, is accessible at 330° to 350°C. The mesophase PPT-8-M and PPT-8-S show threaded schlieren textures at 340°C (Figure 4-3) as do other members of the series in their mesophase ranges.

The three PPT-8 samples available exhibit complicated thermal behavior. The first heating scans of the samples differ greatly from each other due to different methods of

preparation and workup and possibilities for post-polymerization. Subsequent heating scans show a revealing common thread in their thermal behavior. For example, the first heating of PPT-8-M-b and -M-a show three endothermic peaks. The largest endotherm is likely due to volatilization of residual monomer since the total area under the peaks for subsequent heatings is much less and is quite constant. Also by TGA there is a weight loss of 1.34% at 290^{o}C (Figure 4-4).

The broad thermal event, which has the appearance of a glass transition, observed between ~ 260^{o} and 280^{o}C in the first heating of PPT-8-S is coincident with a perfection of order of the metastable, precipitated and swelled structure as confirmed by x-ray diffraction (see below). In both the PPT-8-M samples which have a higher degree of polymerization, this second order transition is at a slightly higher temperature, 270^{o} to 290^{o}C. It is also evident in other members of the series (see Figures 4-2a and -2c.) Since this temperature is well above the "melting temperature" of the alkyl side-groups, the T_g must be related to motions of the semi-rigid aromatic backbones.

Second heating scans after a slow cooling and after a quench are distinctly different. In all PPT-8 samples there is a T_g at 260^{o} to 290^{o}C and the two apparently first order transitions which shall be designated T_1 (at 300^{o} to 320^{o}C) and T_2 (at 315^{o} to 328^{o}C). As expected, the transitions

occur at lower temperatures in the lower molecular weight, solution polymerized polymer.

After cooling at 10^{o}/min, the area under $T_1 > T_2$ while after quenching below T_g at 320^{o}/min, the T_g is more pronounced than when slowly cooled and the area under $T_1 < T_2$. It has been suggested that this bimodal transition behavior observed in similar PLC systems [75] represents melting of a less ordered crystal at T_1 followed by recrystallization of the melt to a higher melting, more stable crystal which subsequently melts at T_2. The recrystallization exotherm in between is assumed to be masked by the two nearby endotherms. The comparison of slowly cooled and quenched samples refutes this suggestion as one would expect a relatively larger T_2/T_1 area ratio in the slowly cooled versus the quenched sample [77].

Results of Structural Studies

X-Ray: Unoriented

Table 6 lists the values of the scattering angle, 2θ, read from diffraction patterns of selected examples of the as-obtained PPT-R-S polymers at room temperature. In each case there is, at least, an intense diffuse peak at $14^{o} < 2\theta < 24^{o}$ and a small angle peak (Figure 4-5). The position of the broad diffraction peak is fairly constant

Table 6

Small angle x-ray diffraction angles and corresponding d-spacings for PPT-R-S series

number of C atoms in -R	2θ (°'s)	d-spacing (A's)
	PPT-R-S powders	
2	6.80	13.0
4	6.20	14.2
DMB	5.40	16.3
6	5.00	17.6
8	4.70	18.8
12	3.80	23.2
	PPT-R-S fibers	
2	7.65	11.5
4	5.95	14.8
DMB	5.70	15.5
6	5.10	17.7
8	4.10	21.5
12	3.95	22.3

for all the normal alkyl substituents. The dimension in real space represented by the small angle peak is strongly dependent upon the alkyl-substituent length (i.e., the dimension increases as the length increases from ethyl to dodecyl) demonstrating that its origin is likely intermolecular. Proof for this speculation is found in x-ray analysis of oriented specimens.

Additionally, the spacing for PPT-DMB, where the substituent is 4 methylene units "long" but 6 carbon atoms "big", is in between the spacings for PPT-4 and PPT-6 (Figure 4-6). This intermediate packing distance for the branched substituent indicates a size or bulkiness effect present in addition to a length effect.

The diffraction pattern of PPT-2-S, contains a greater number of peaks which indicates more crystalline order. The very high melting point of this PLC supports this view.

Although patterns of unoriented samples such as these, containing a small angle peak and a diffuse scattering peak, are typical of simple smectic mesophases [78], the small angle peak in this case does not arise from a layered ordering of the mesogens perpendicular, or at some small tilt angle, to the mesogenic long axis. Evidenced by its dependence upon alkyl-substituent length, it is due to intermolecular interferences. Added evidence in the assignment of the structural origin of the diffraction peaks

was sought from diffraction patterns of specimens which were oriented in the mesophase and subsequently quenched below their glass transition temperature and by correlation of diffraction patterns to morphological transitions inferred from DSC and PLOM.

X-Ray: As a Function of Temperature

Figure 4-7 contains diffractometer scans at a series of temperatures (up to the limit of the heater) of PPT-8-S. At 25°C the pattern (of the as-synthesized, swelled polymer) consists of this "amorphous halo" centered at $2\theta = \sim 20^{\circ}$ and a small angle peak corresponding to 18.8A (calculated by Bragg's law from $2\theta = 4.7^{\circ}$). Over the temperature range from 25° to 250°C the small angle peak continuously intensifies, becomes narrower and moves to smaller angles, finally representing a dimension of 23.2A ($2\theta = 3.8^{\circ}$). At 285°C an additional small angle peak develops which corresponds to 31.5A ($2\theta = 2.9^{\circ}$).

Sample PPT-8-M-b shows two small angle peaks from room temperature (Figure 4-8). Thus, there is no change in the diffraction pattern at 285°C except for a slight shifting and intensification of the two peaks. This material was obtained directly from the melt polycondensation and was not subjected to the solvent swelling that PPT-8-S was. Since this sample was also of higher purity, it was more stable

under nitrogen at high temperatures for the extended time required for collection of the x-ray scans. Between 320° and 340°C the intensity of the two peaks decreases but the 2.9° peak decreases relatively faster with respect to the 3.8° peak. Above 340°, the temperature at which the material visually becomes fluid and exhibits the threaded texture of a nematic, the small angle peak has disappeared leaving diffuse scattering at both small and wide angles. This is the scattering one would expect of a uniaxial nematic mesophase.

A sample heated to the mesophase at 350°C and quenched shows a single small angle peak, while one slowly cooled to room temperature shows two small angle peaks in addition to other wide angle reflections (see Figure 4-9). The slowly cooled specimen is likely semi-crystalline.

X-Ray: Oriented

Figure 4-10 shows the x-ray diffraction pattern of a monofilament (60 hours exposure time) of PPT-8-M-a which was extruded and drawn. The prominent features of the pattern are two peaks on the equator, one at a wide angle the other at a small angle, and four lines located on the meridian. Another feature is the apparent separation of the wide angle amorphous halo into two components, one equatorial and one meridional, even though there is some intensity at $2\theta \sim 20^{\circ}$

at all azimuthal angles. Diffractometer scans along the equator and meridian are plotted in Figure 4-11 and corroborate the indistinct features of the diffraction pattern.

The two major equatorial peaks correspond to those observed in the unoriented sample, PPT-8-S. The peaks have sharpened considerably and are at somewhat different values of 2θ, however. The peak at 2θ = 20.5^{o} corresponds to an intermolecular distance of 4.3A. This distance is slightly larger than the aromatic ring, face to face packing of 3.7A in the crystalline state of polyphenyls and fused aromatic structures [79]. The peak at 2θ = 3.8 corresponds to a spacing of 23.2A, close in value to the spacing of a PPT-8-S sample heated to 285^{o}C. The equatorial placement is the result of inter-chain interferences perpendicular to the fiber axis and, therefore, to the PLC main-chain separation. This evidence confirms the speculation that the alkyl chain-length-dependent, small angle peak arises from the distance between the aromatic cores separated by the aliphatic side-groups.

Equatorial scans (Figure 4-12) of fibers of other members of the series show the same relationship between d-spacing of the small angle peak and alkyl chain length as in the unoriented state. The distance observed by x-ray diffraction is intermediate between that calculated for the distance between two aromatic cores of polymer

backbones if separated by two alkyl chains which are fully extended (that is, all-trans conformation) and abutting and by two fully extended alkyl chains which are interdigitated.

The first prominent layer line is in excellent agreement with the intra-chain correlation of regularly spaced polymer repeat units calculated from literature values of bond lengths to be ~ 12.5A in length.

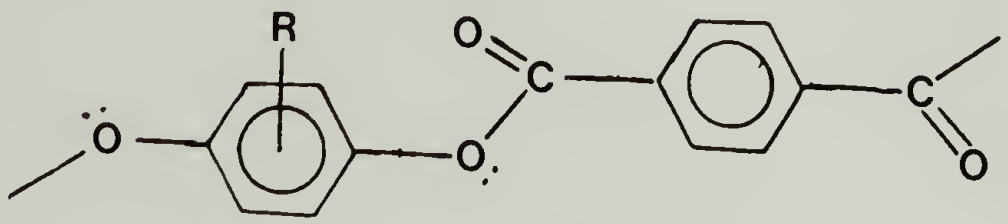

The lines at periodic intervals along the meridian correspond to 1/2, 1/3 and 1/4 the value of the molecular transform.

Fibers annealed at 295^{o}C in the DSC for 20 minutes show the development of a second peak at small angle in addition to the peak for the quenched fiber (Figure 4-13). This situation is analogous to the unoriented case of rapidly and slowly cooling the sample.

The DSC of the as-obtained fiber, prior to annealing, is shown to be identical to the DSC of unoriented polymer which has been quenched in Figure 4-14.

Discussion: Crystalline, Biaxial Nematic and Uniaxial Nematic Structures

Above T_2 (315° to 328°C), PPT-8 displays properties of a typical nematic liquid crystalline polymer: rheologically the sample has low viscosity and potential for formation of highly oriented fibers, microscopically it displays a threaded appearance, and the x-ray scattering consists of only diffuse scattering at wide angles. In the unoriented solid and quenched fiber states, the small angle x-ray peak is of intermolecular origin based upon its dependence on alkyl-substituent length and equatorial location in the fiber pattern. Thus, between T_1 (300° to 320°C) and T_2 (315° to 328°C), depending upon the particular sample studied, a nematic structure is formed which may best be described a biaxial nematic. The term biaxial nematic connotes a structure in which both the long mesogenic axes and flat surfaces tend to be parallel which still allows translational freedom along the mesogenic long axis. A cylindrical or rod-like structure will form a uniaxial nematic mesophase whereas a lath-like structure has the potential of forming a lower energy biaxial nematic mesophase (Figure 4-15). Thus, it appears that upon cooling PPT-8 undergoes a restriction in rotation enhanced by coplanarity of the aromatic rings or ester groups which results in a lath-like structure and favors a face to face

orientation. If a sample, quenched from the uniaxial nematic mesophase or swelled by solvent, is annealed, a second equatorial small angle peak develops at ~285^{o} to ~290^{o}C. This peak has not been indexed but may be related to crystalline order.

Indirect evidence of a biaxial nematic mesophase has been obtained by Wood [80] for PLCs with alternating mesogens and flexible spacers by electron diffraction and by Viney et al. [81] for random poly(hydroxybenzoic acid-co-hydroxynaphthoic acid) and hydroxybenzoic acid-co-poly(ethylene terephthalate) by microscopic techniques. Very different electron diffraction patterns were obtained by annealing slowly cooled and quenched specimens of the PLC which previously had been seemingly structurally equivalent by electron diffraction. The mesogenic units of this study had no or small substituents and thus the dimensions along the two orthogonal axes were approximately equivalent. Packing along the two axes were not differentiable by diffraction, but upon annealing, the slowly cooled biaxial morpholgy was able to crystallize with ease whereas the quenched uniaxial morpology could merely perfect the fiber texture. In samples for this research, the inherently plate-like profile of the the benzene ring has been enhanced by the addition of alkyl substituents extending outward to the side, thus, the dimensions along the minor axes of the homologous series are differented to a greater extent.

Ballauff gives convincing evidence of a unique nematic structure with translational freedom where there is, in addition, microphase segregation of the aromatic cores and flexible aliphatic side-groups to form a regular, periodic layered structure. The x-ray diffraction pattern consists of sharp Bragg peaks corresponding to a layer thichness between aromatic cores filled with interdigitated alkyl chains which crystallize upon cooling. The layer perfection and degree of microphase segregation increase with increasing length of the alkoxy substituent; two orders observed in the didodecyloxy PLC and three orders in the dihexadecyloxy PLC (Figure 4-16).

In the monosubstituted series of this study, microphase segregation probably contributes to the biaxial ordering but an extended layered structure is absent. There is only a single order of diffraction which is much broader than the Ballauff study. Moderate Hosemann distortion [82] of the second kind would be sufficient to damp out higher order reflections. Two variables in the Ballauff experiment may also have encouraged more rapid formation of the more stable equilibrium structure: 1) the lower degree of polymerization of the samples and 2) surface orienting effects of the x-ray reflection-mode heater.

One must also compare the packing requirements peculiar to each system. If one could speak of a "unit cell" for PPT-8 in the biaxial nematic LCn state, the dimensions of

the "cell" as obtained by x-ray scattering would be 4.4A x 23.2A x 12.5A. A simple calculation yields as a requirement, two momomer repeat units/"unit cell" (352.4g/mole), in order to arrive at a reasonable specific density for an organic polymeric material in the condensed phase based on calculations of molecular packing density. A lath-like structure arranged on a distorted two-dimensional lattice is pictured as the morphology of the quenched PLC or unannealed fiber. The transition in PPT-8 at T_2 from this biaxial nematic mesophase to a uniaxial nematic mesophase is depicted in Figure 4-17. The transition from the uniaxial to biaxial nematic states is predicted to be second order, however, the propensity of forming a layered morphology may result in some first order contribution.

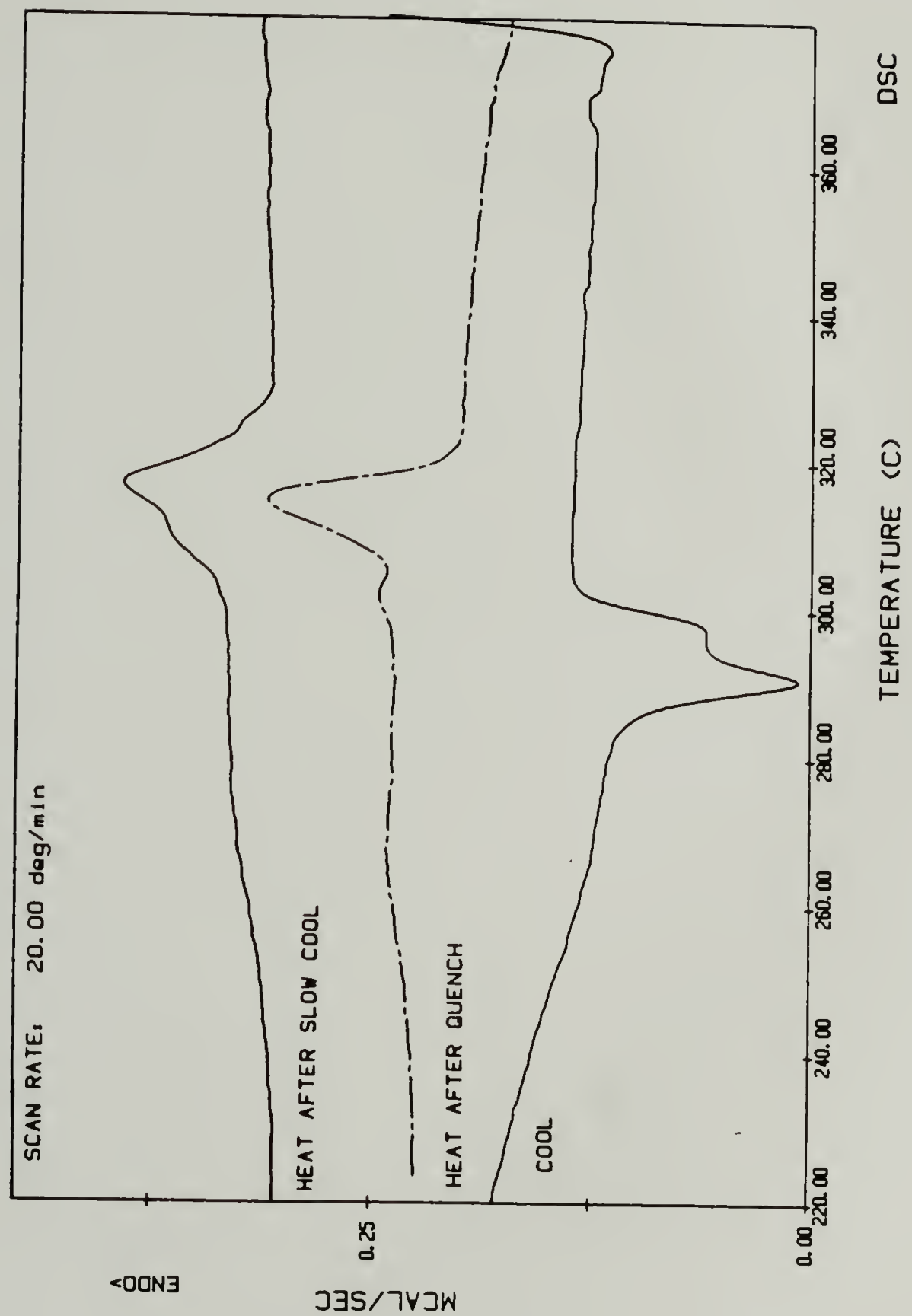

Figure 4-1. DSC scans of a) PPT-8-S,

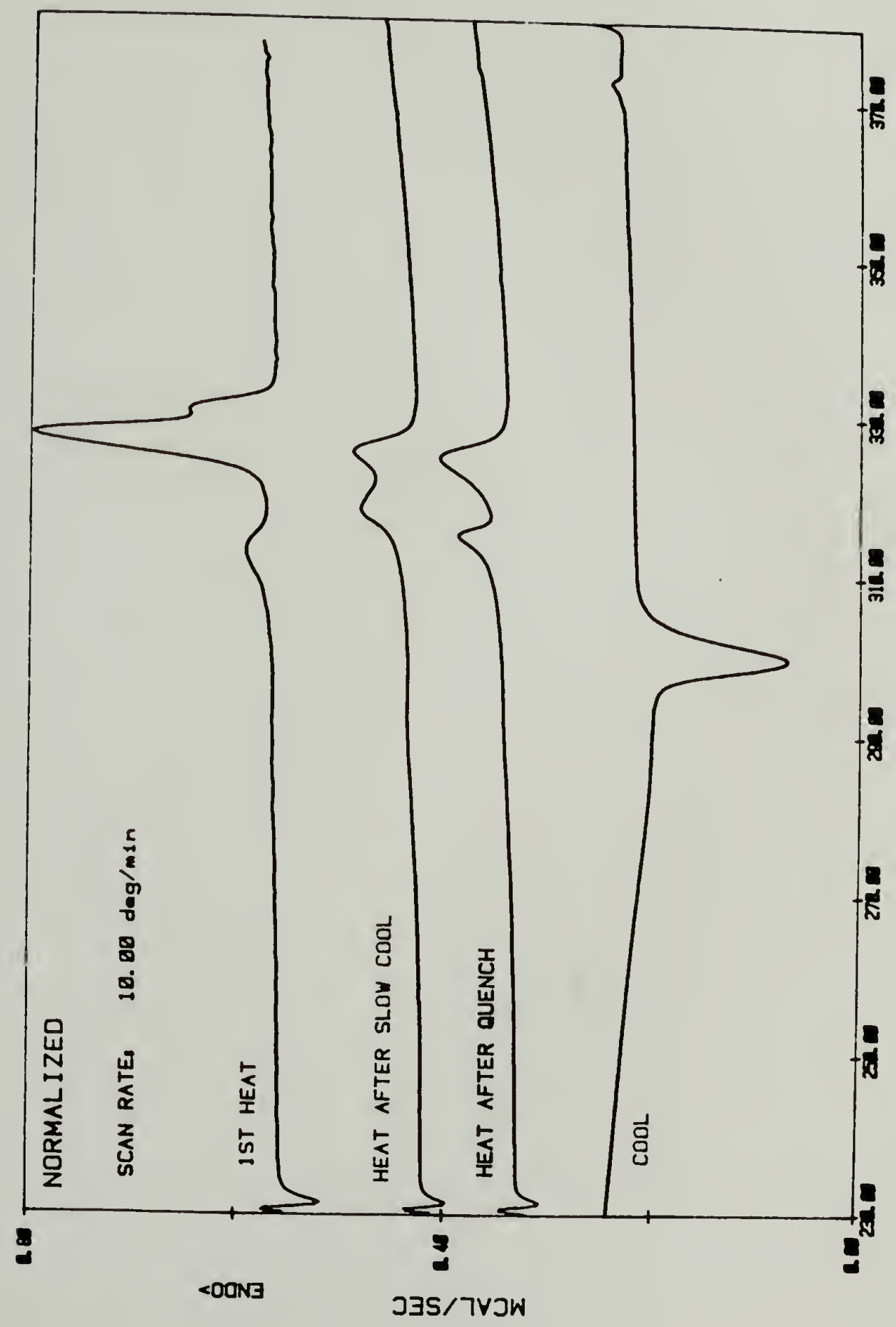

Figure 4-1. b) PPT-8-M-b and

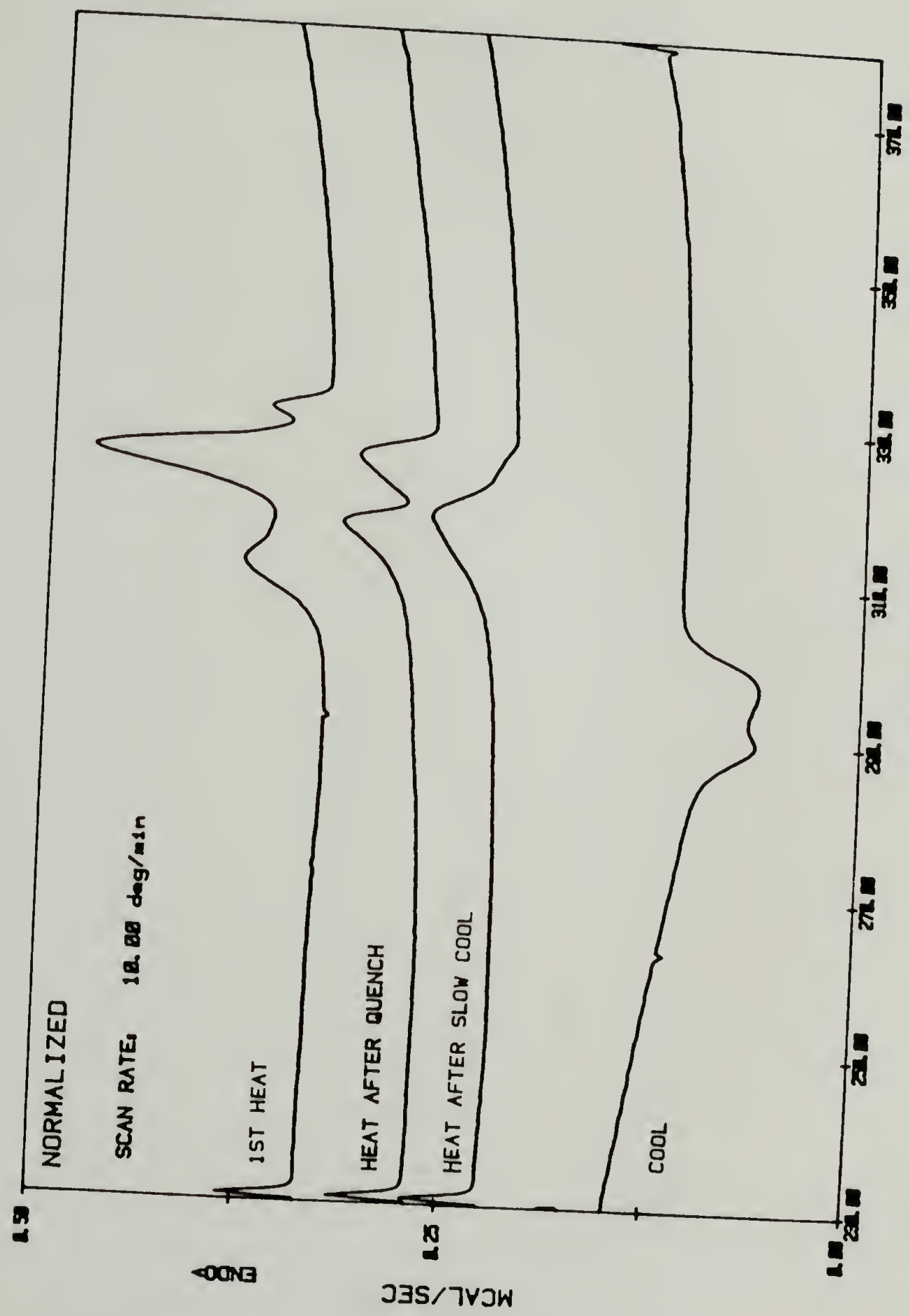

c) PPT-8-M-a.

Figure 4-1.

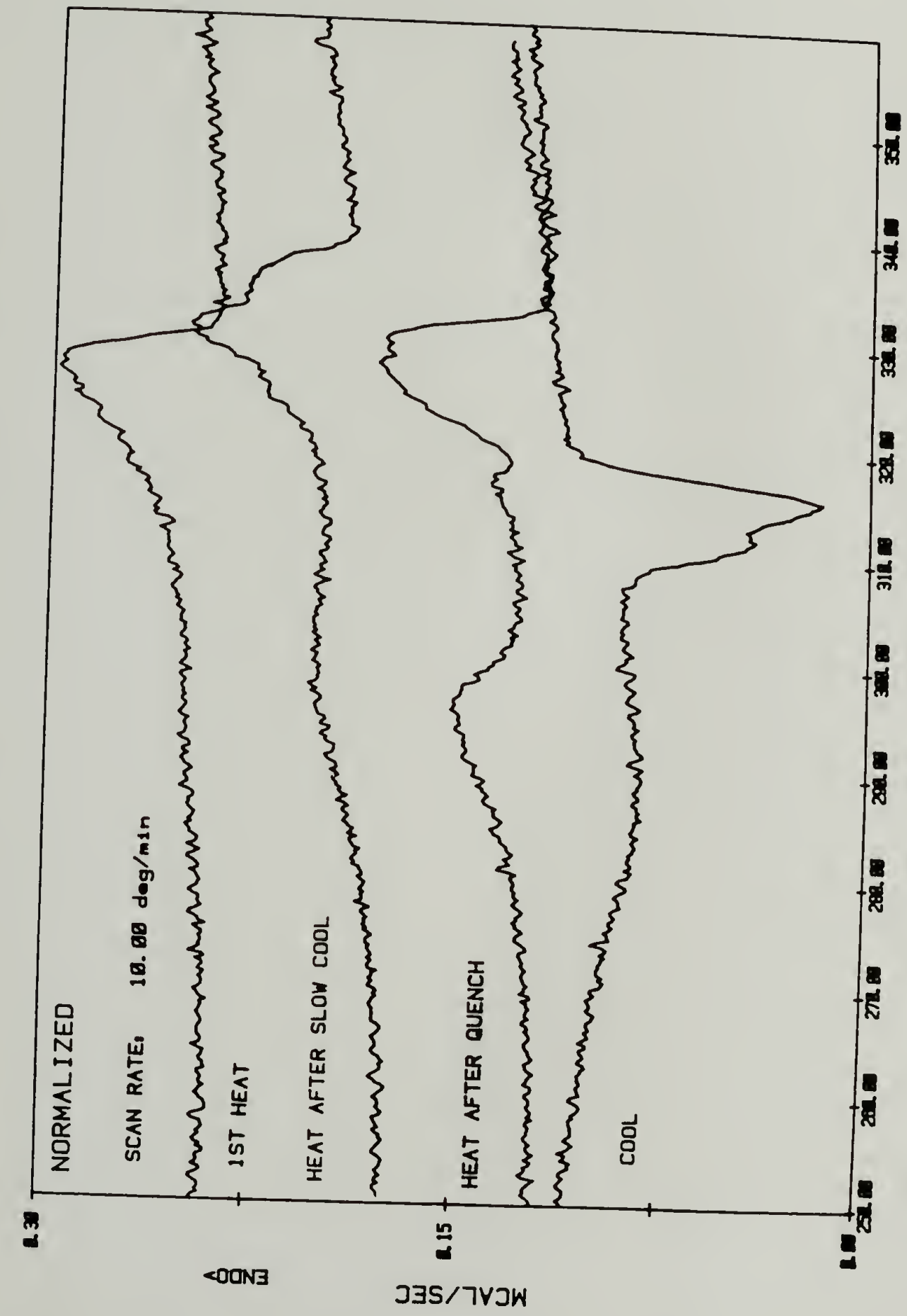

Figure 4-2. DSC scans of a) PPT-6-S,

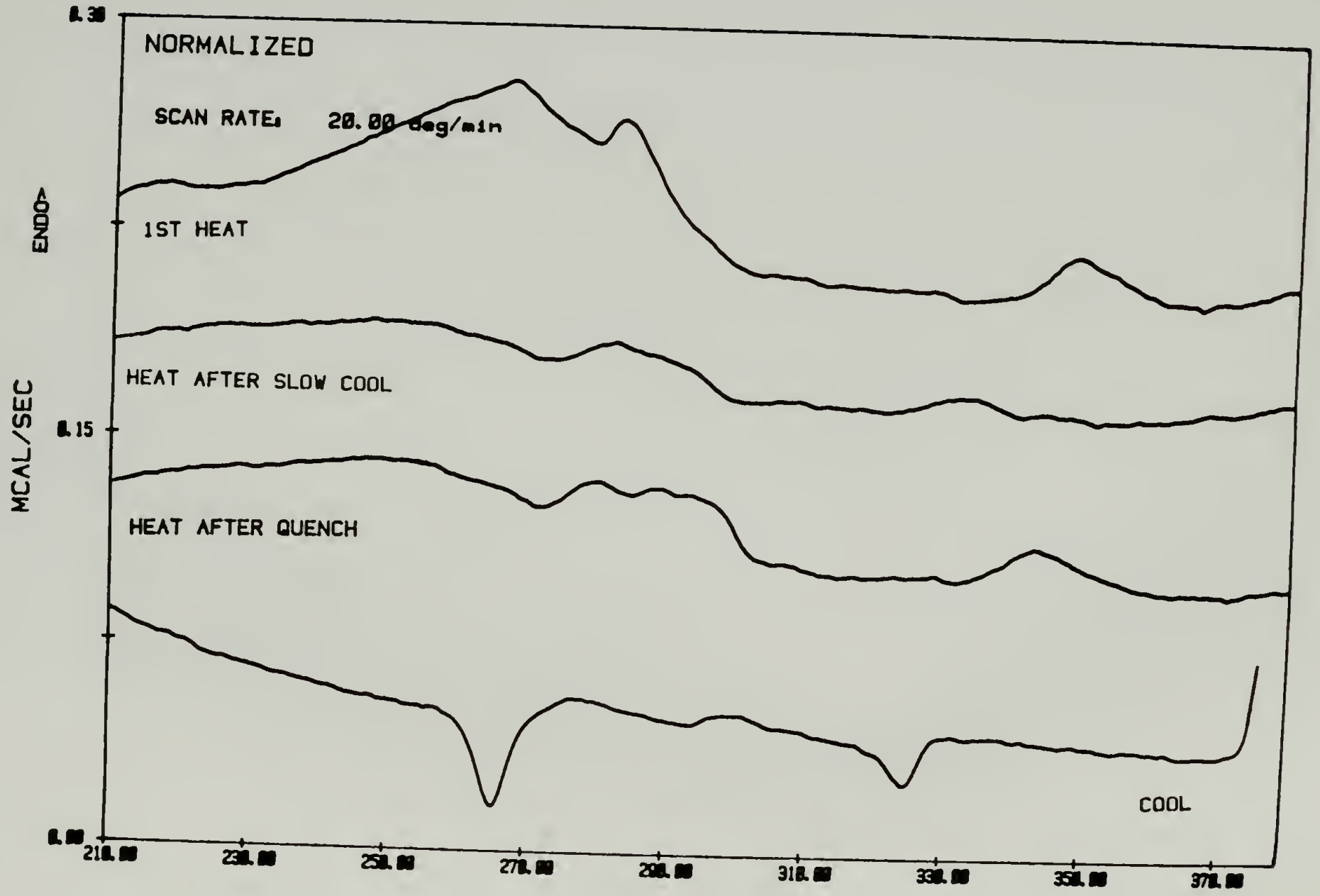

Figure 4-2. b) PPT-12-S and

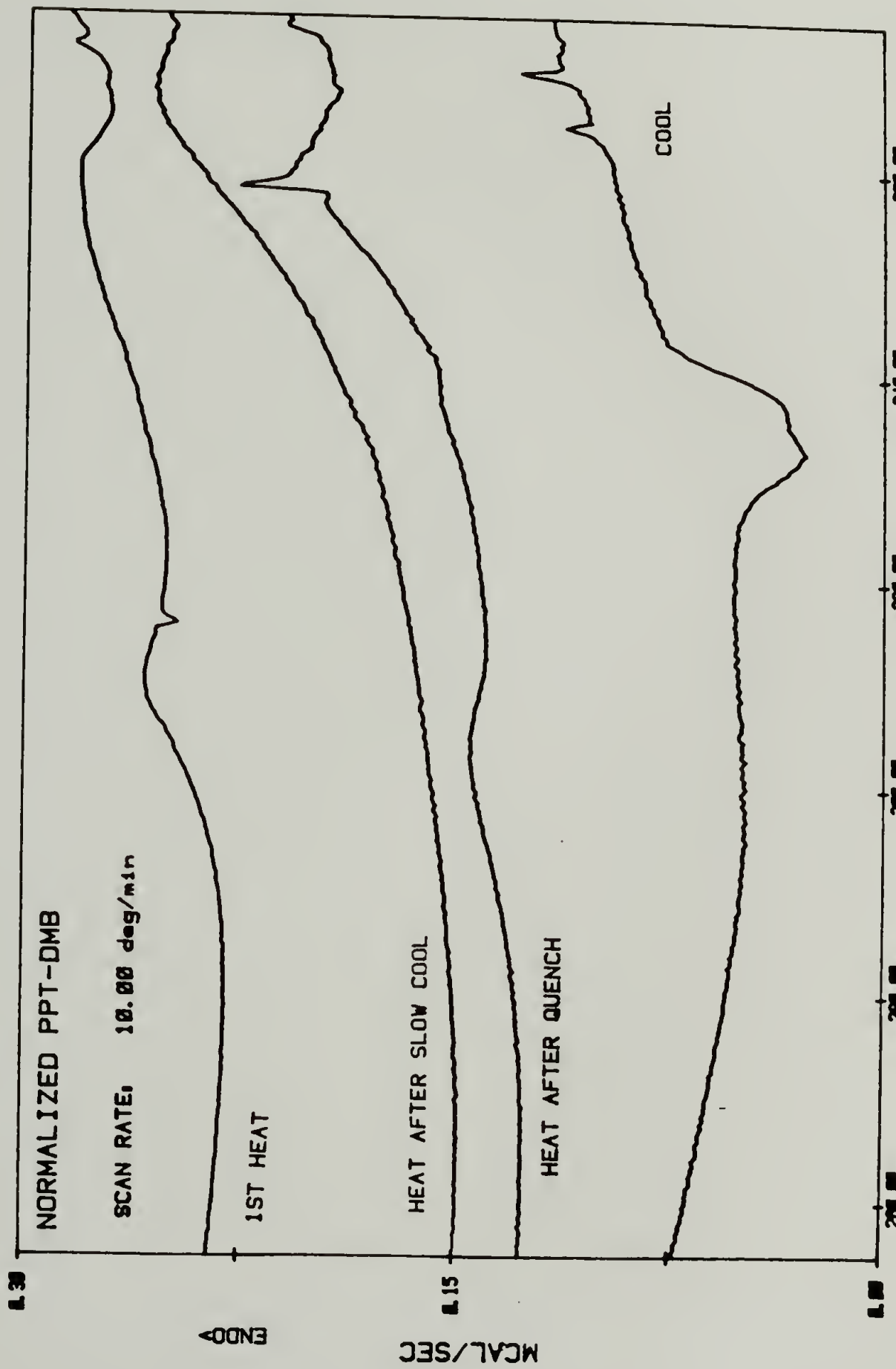

Figure 4-2. c) PPT-DMB-S.

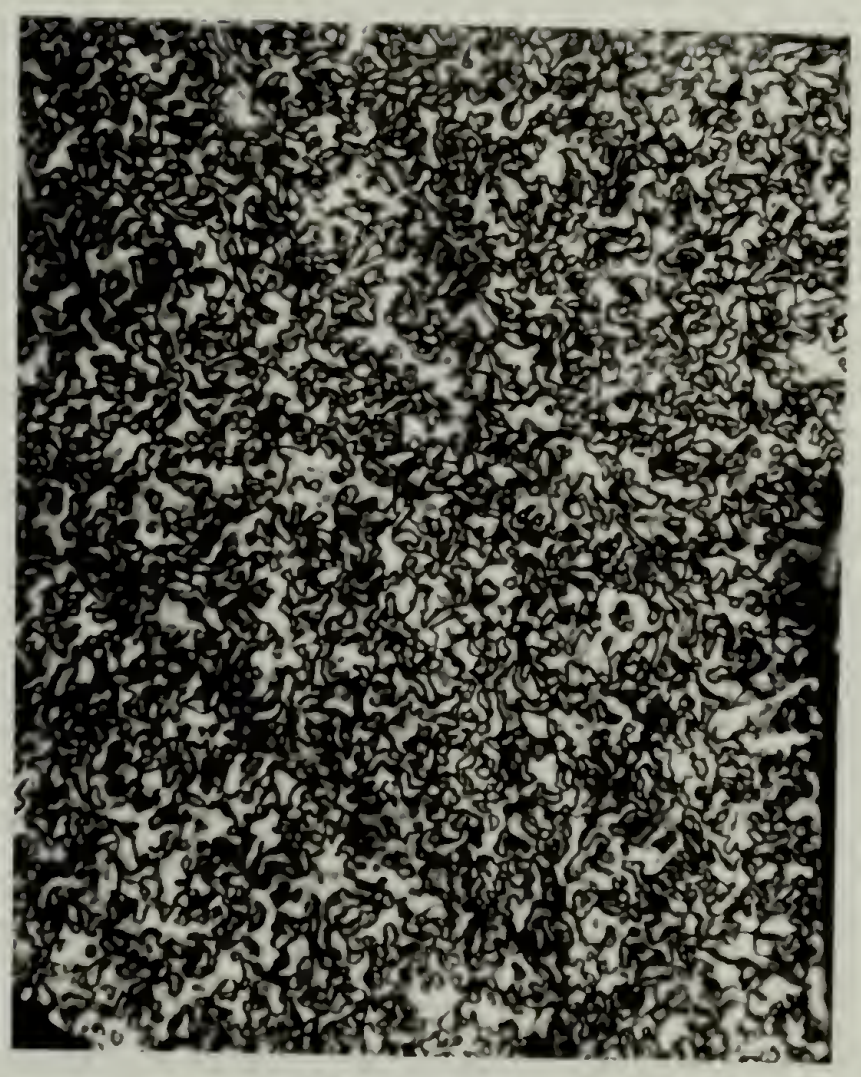

Figure 4-3. Optical micrograph of PPT-8-S at 340^{o}C showing threaded texture.

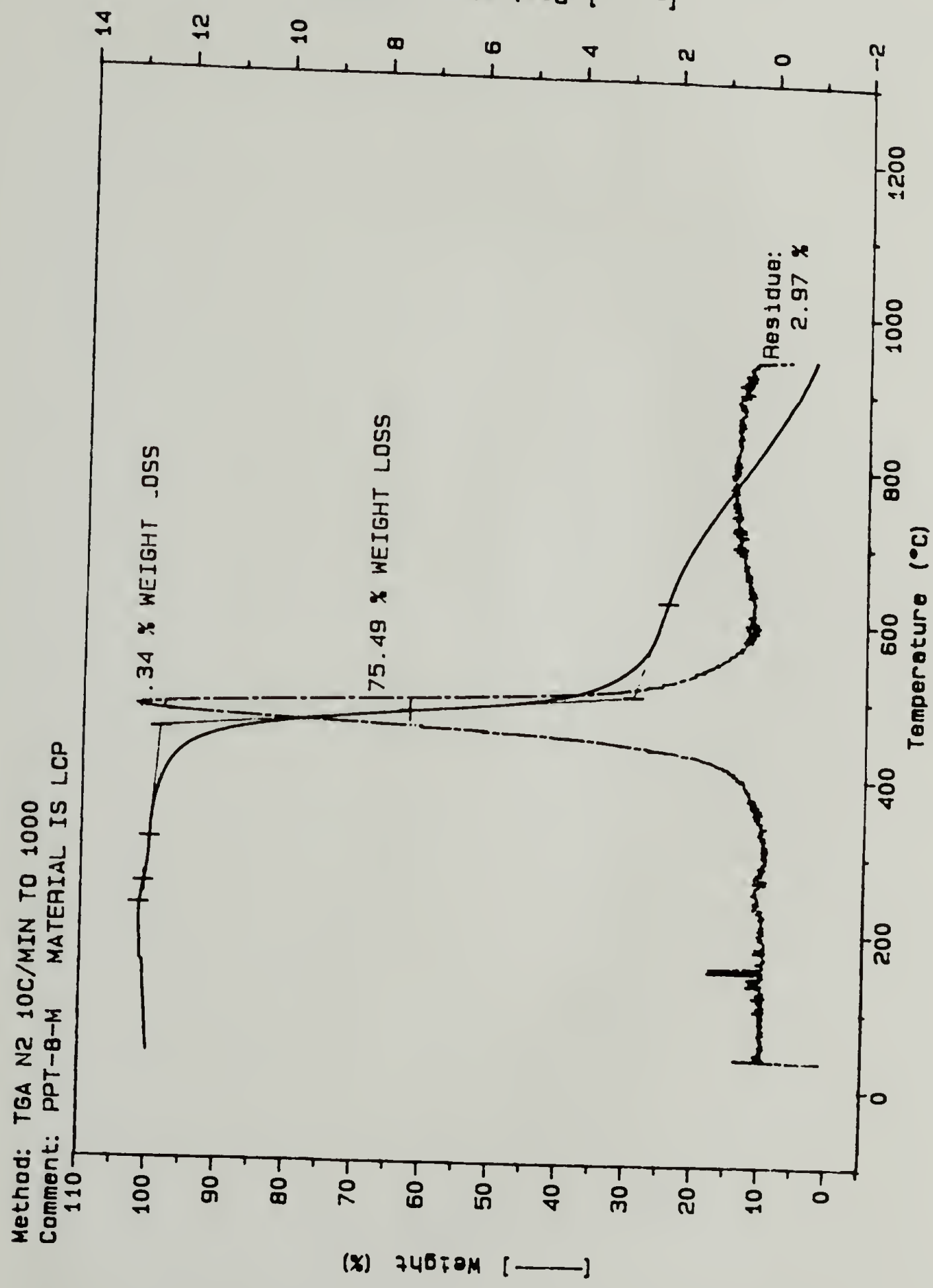

Figure 4-4. TGA of PPT-8-M-b.

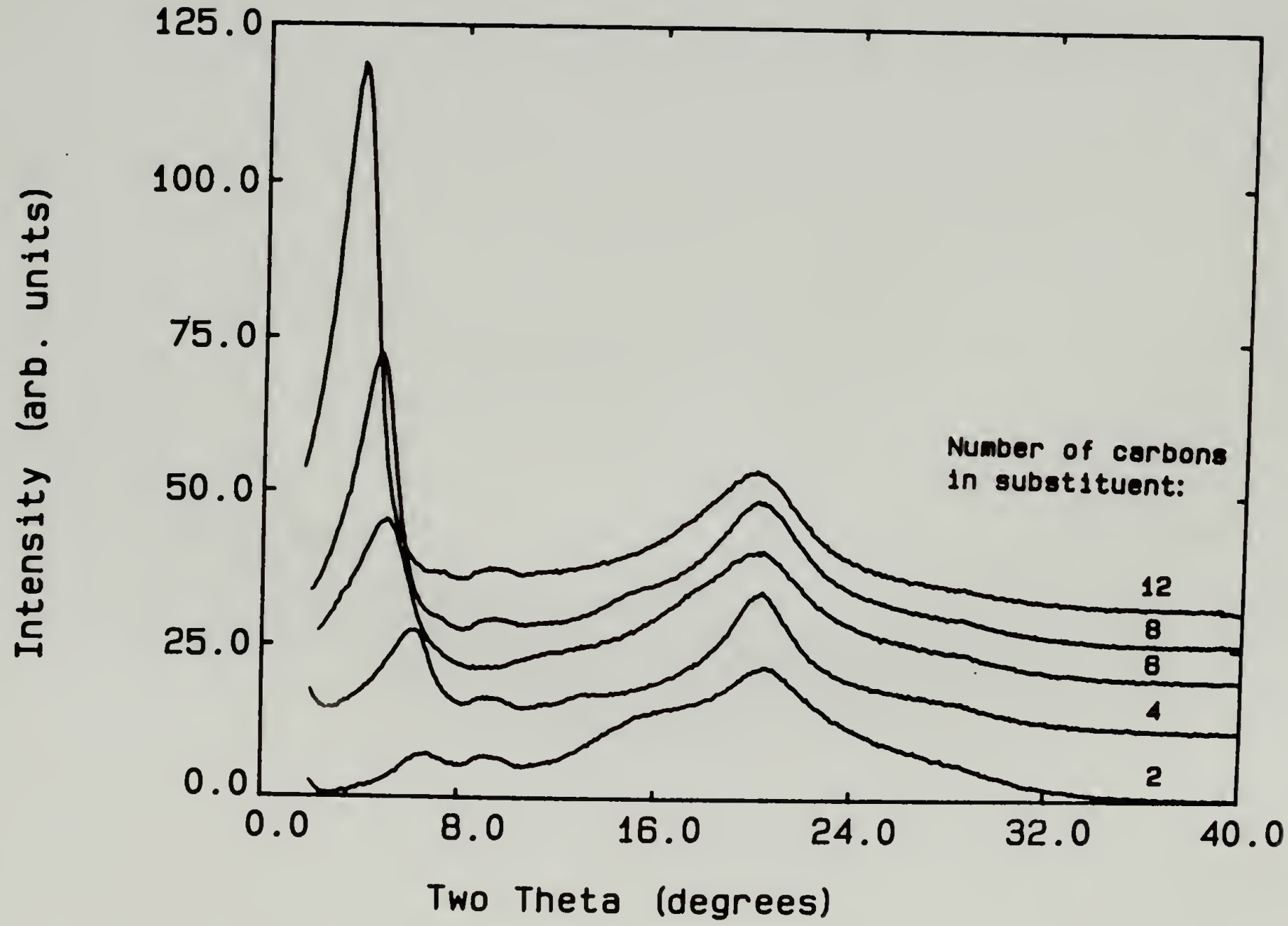

Figure 4-5. Diffractometer scans of powdered PPT-R-S samples before heating.

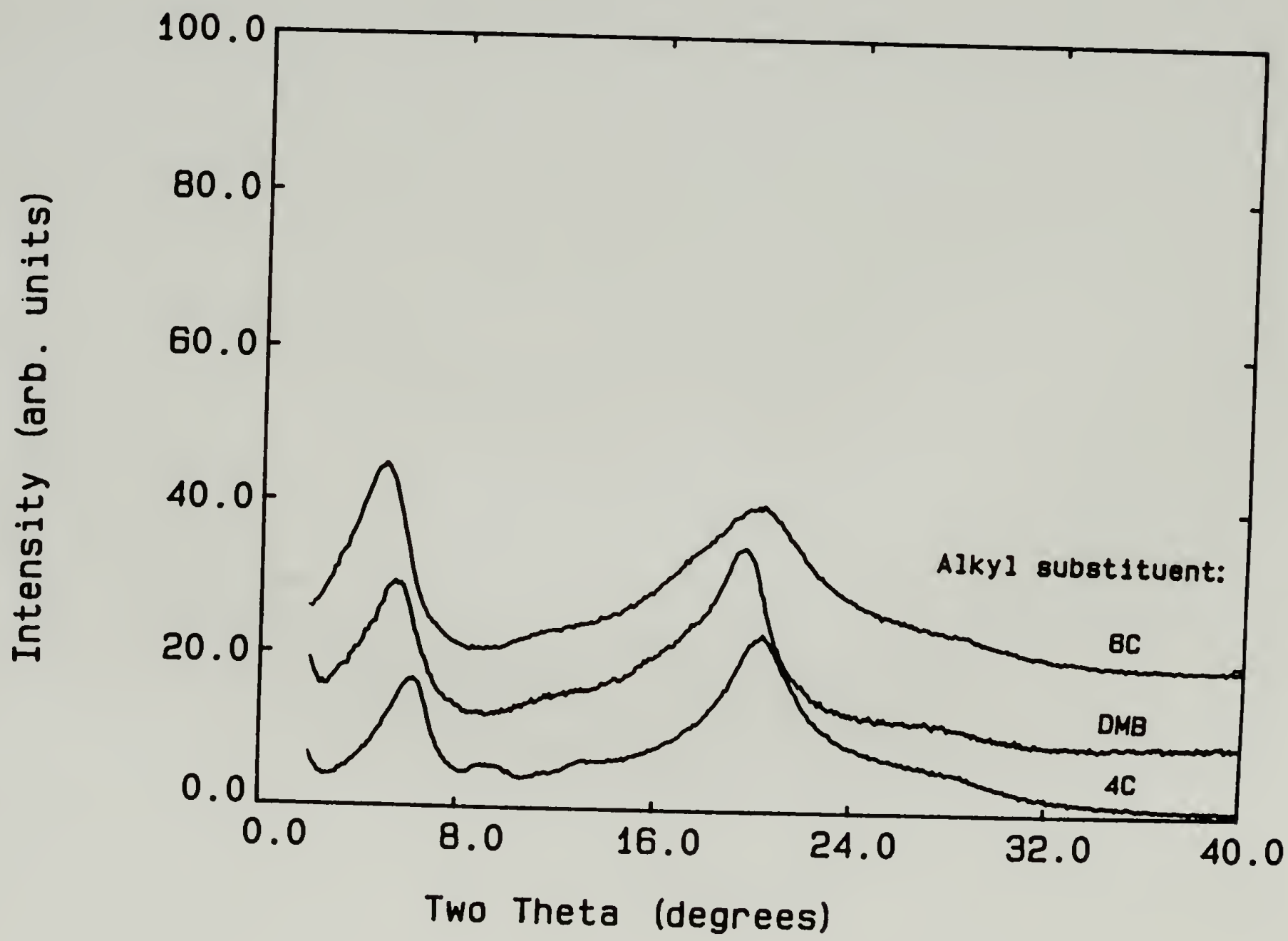

Figure 4-6. Diffractometer scans of PPT-4, PPT-6 and PPT-DMB.

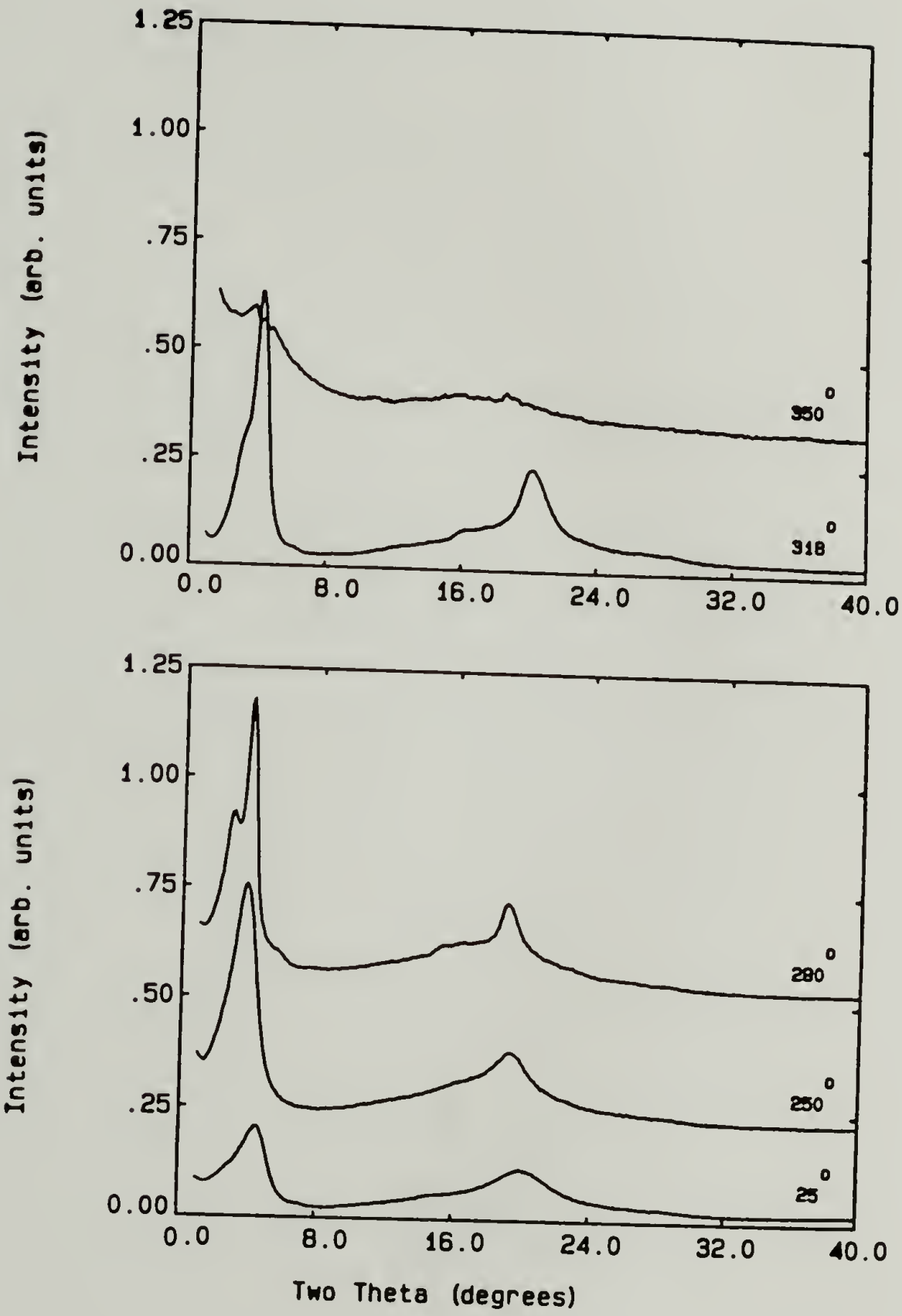

Figure 4-7. X-ray diffractometer scans of PPT-8-S at various temperatures during heating to the nematic mesophase.

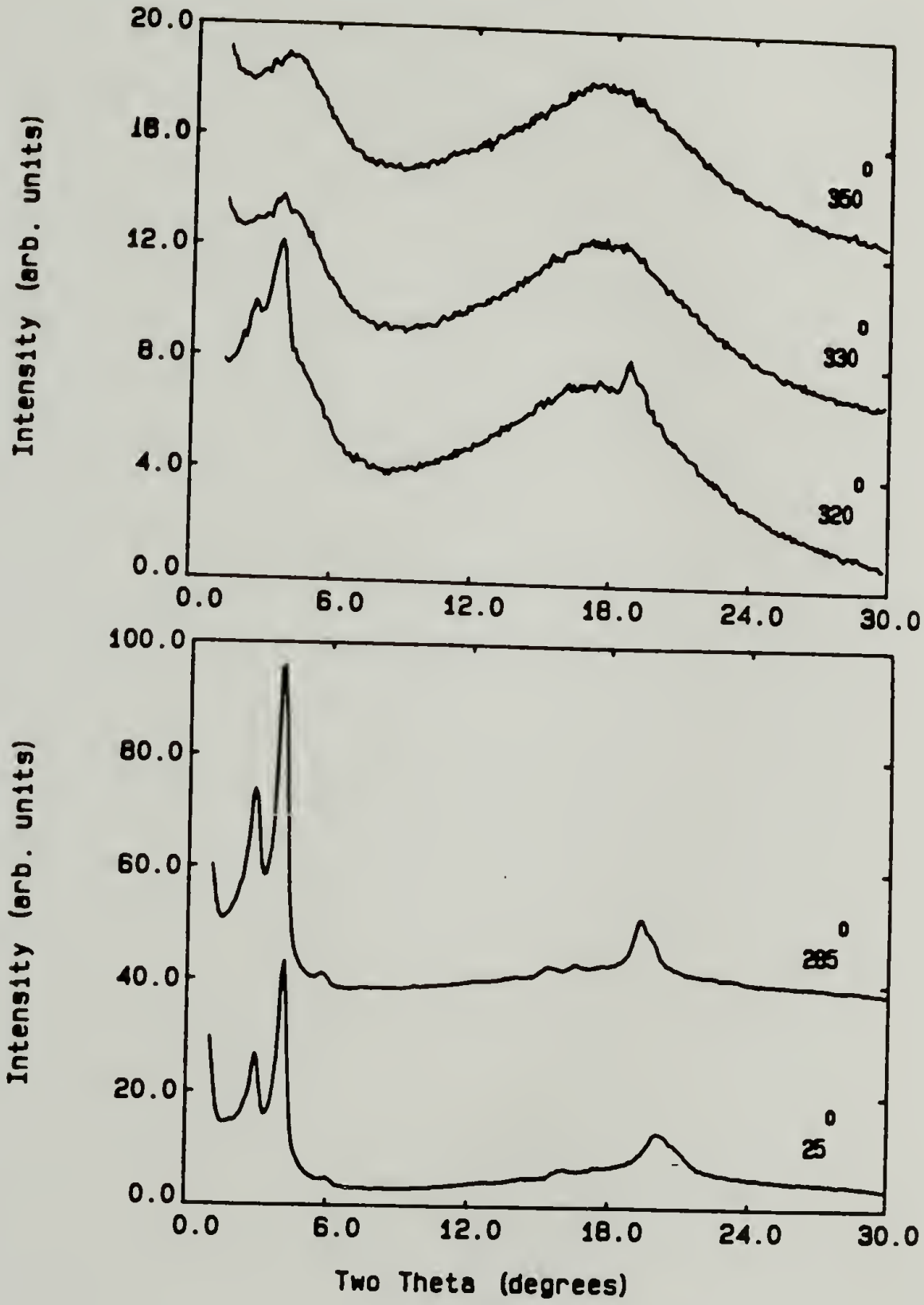

Figure 4-8. X-ray diffractometer scans of PPT-8-M-b at various temperatures during heating to the nematic mesophase.

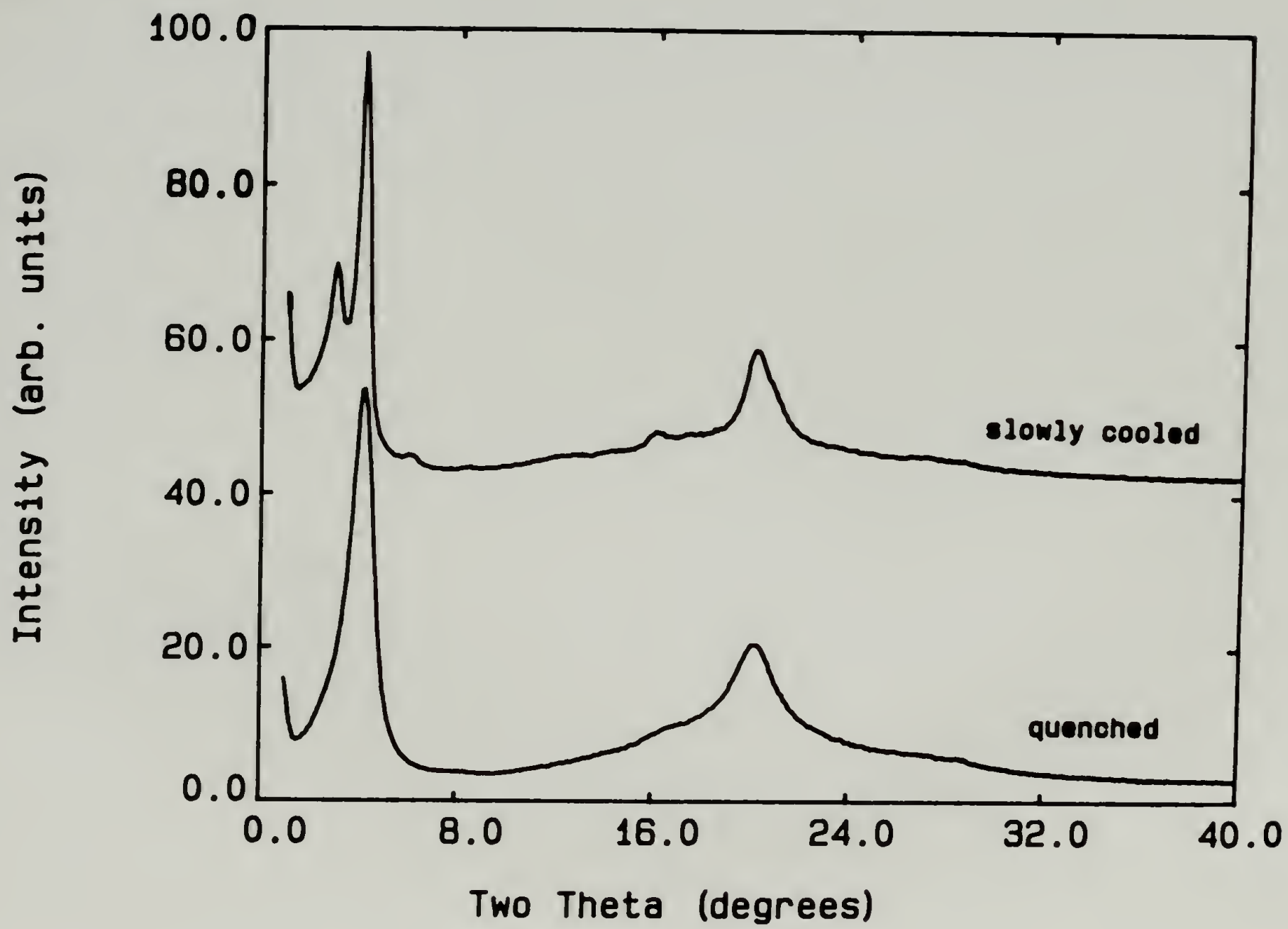

Figure 4-9. X-ray diffractometer scans comparing the small angle scattering of quenched and slowly cooled PPT-8-M.

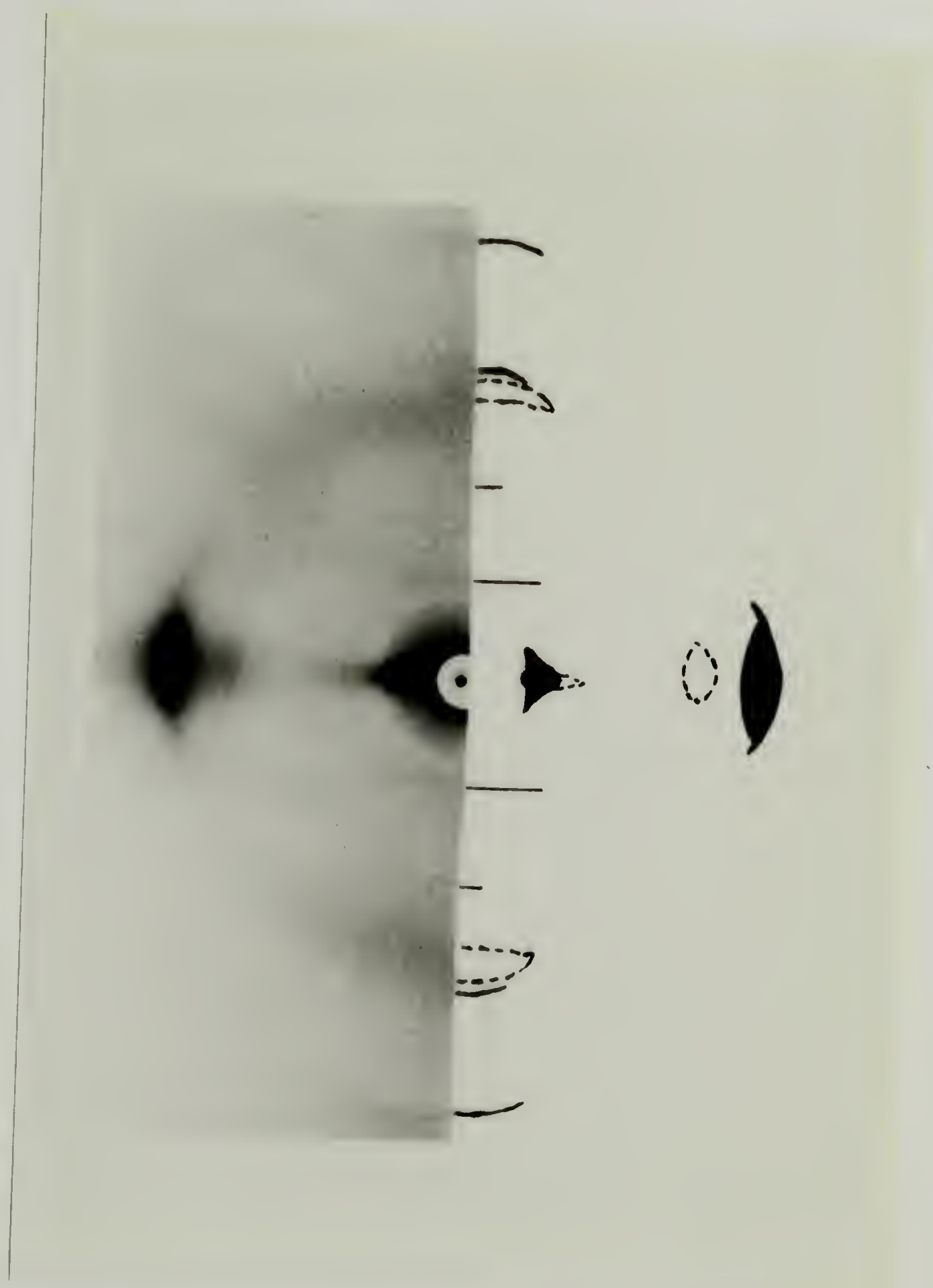

Figure 4-10. Fiber diffraction pattern of monofilament of PPT-8-M-a.

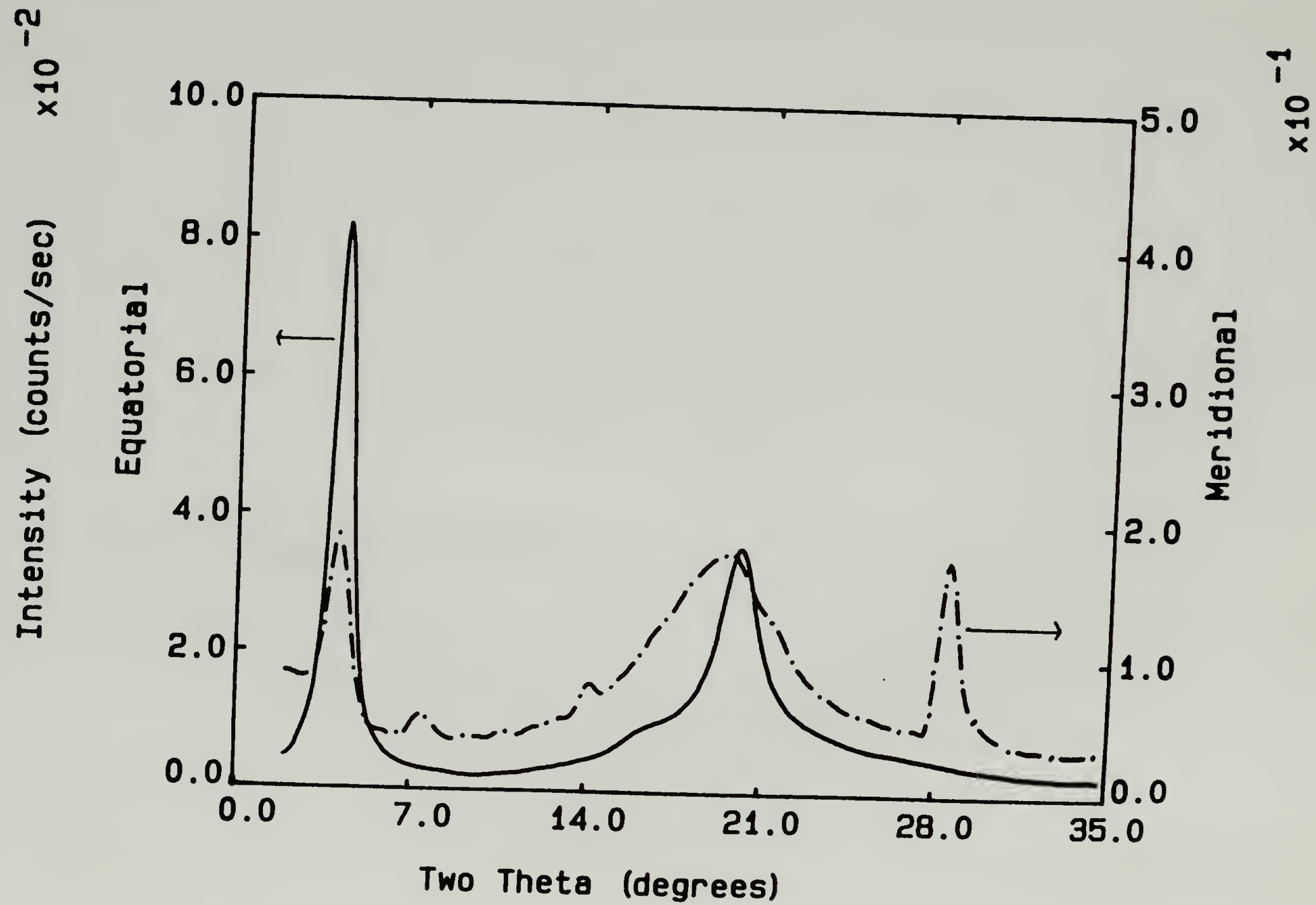

Figure 4-11. Equatorial and meridional scans of a bundle of of PPT-8-M-a fiber.

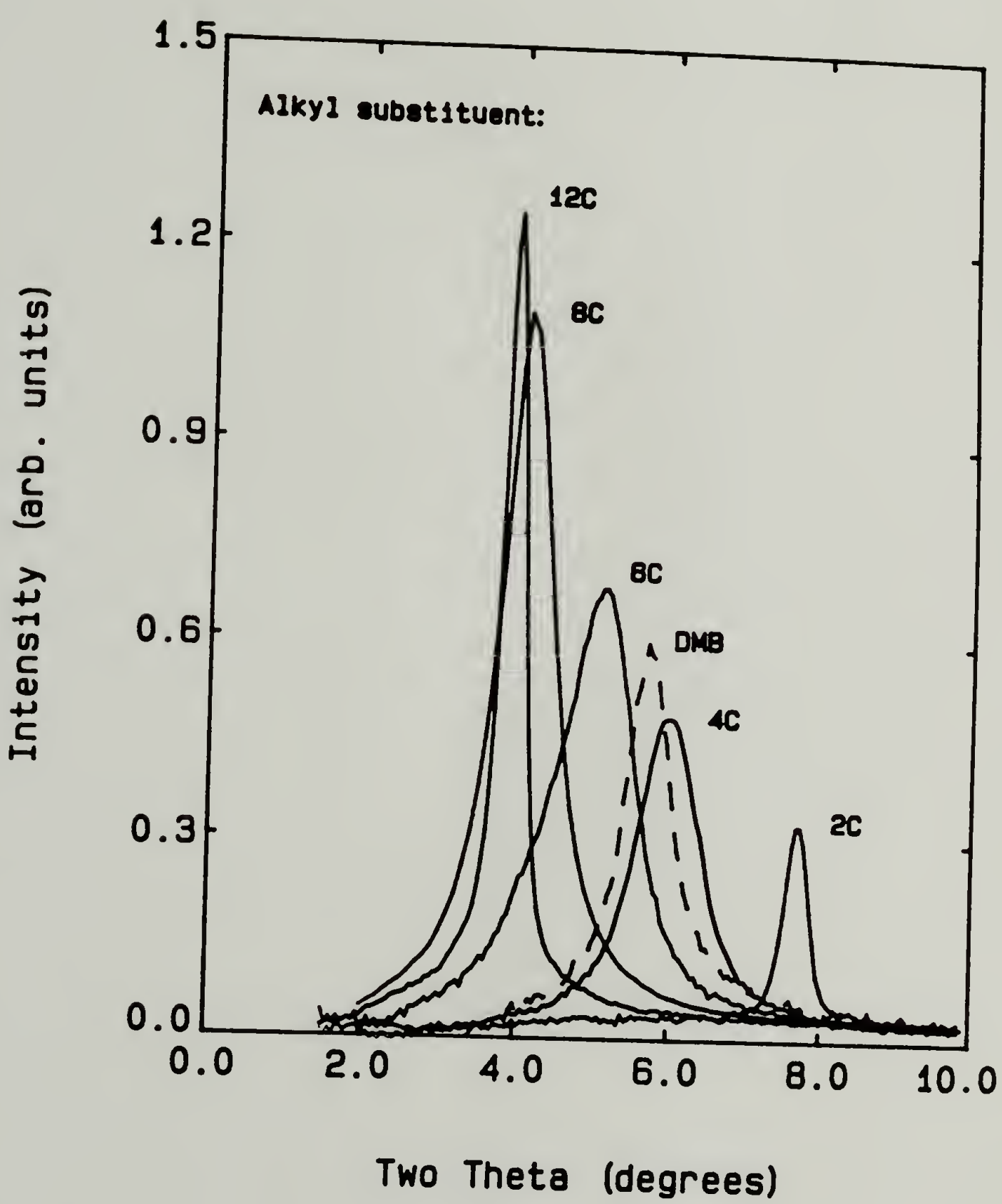

Figure 4-12. Equatorial scans of PPT-R fibers.

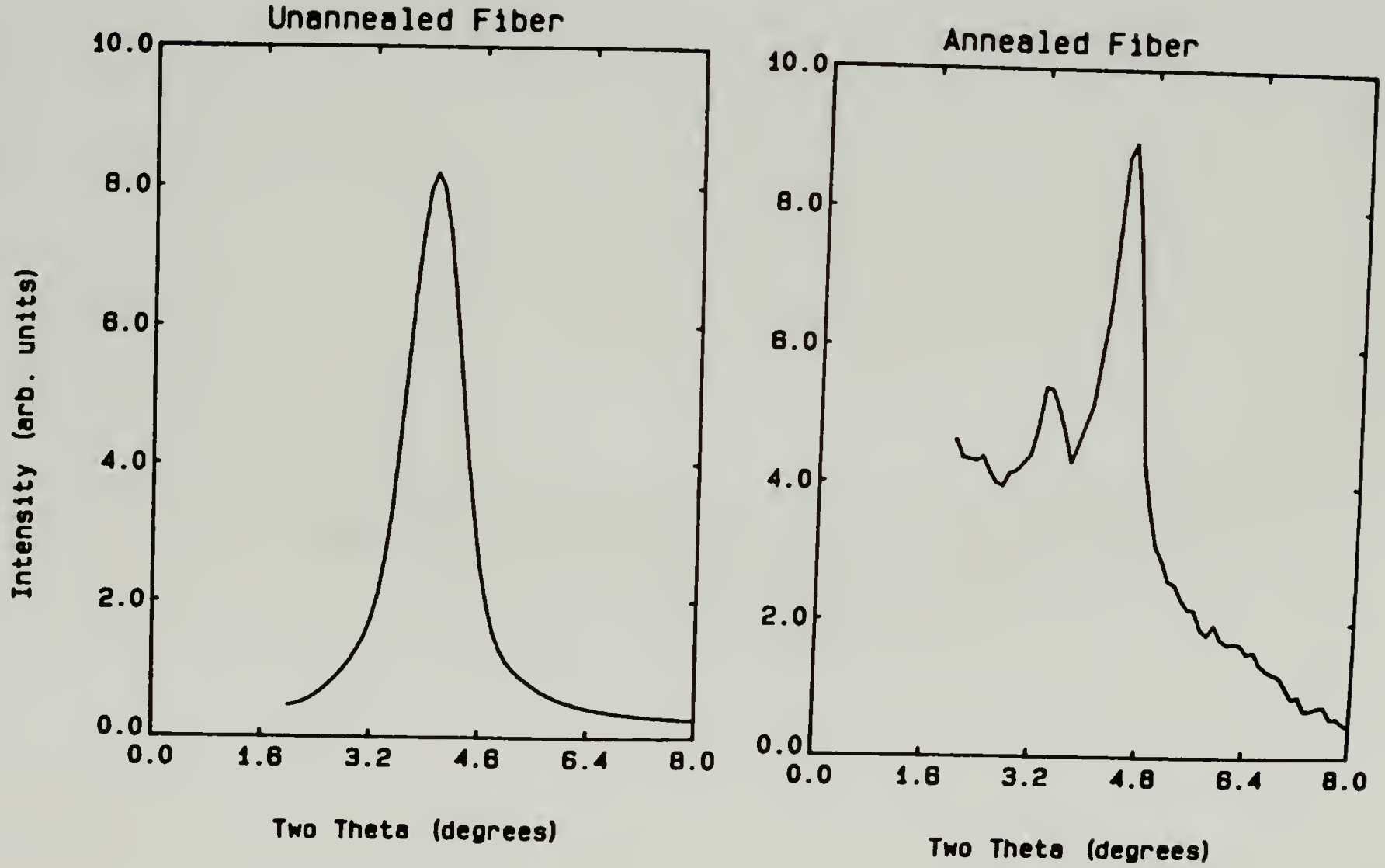

Figure 4-13. Equatorial scans of unannealed and annealed fibers of PPT-8-M-b.

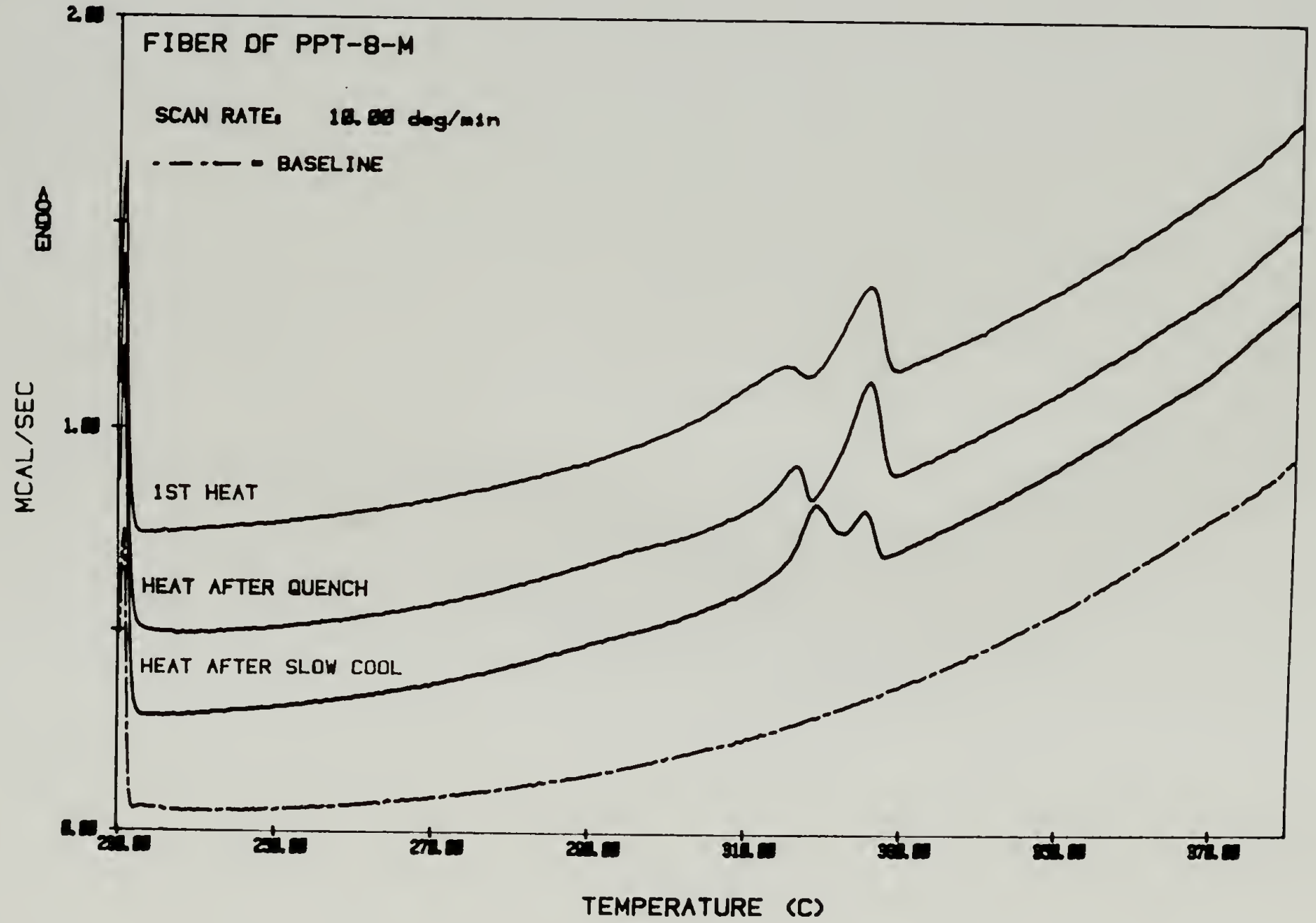

Figure 4-14. DSC scans of PPT-8 fibers.

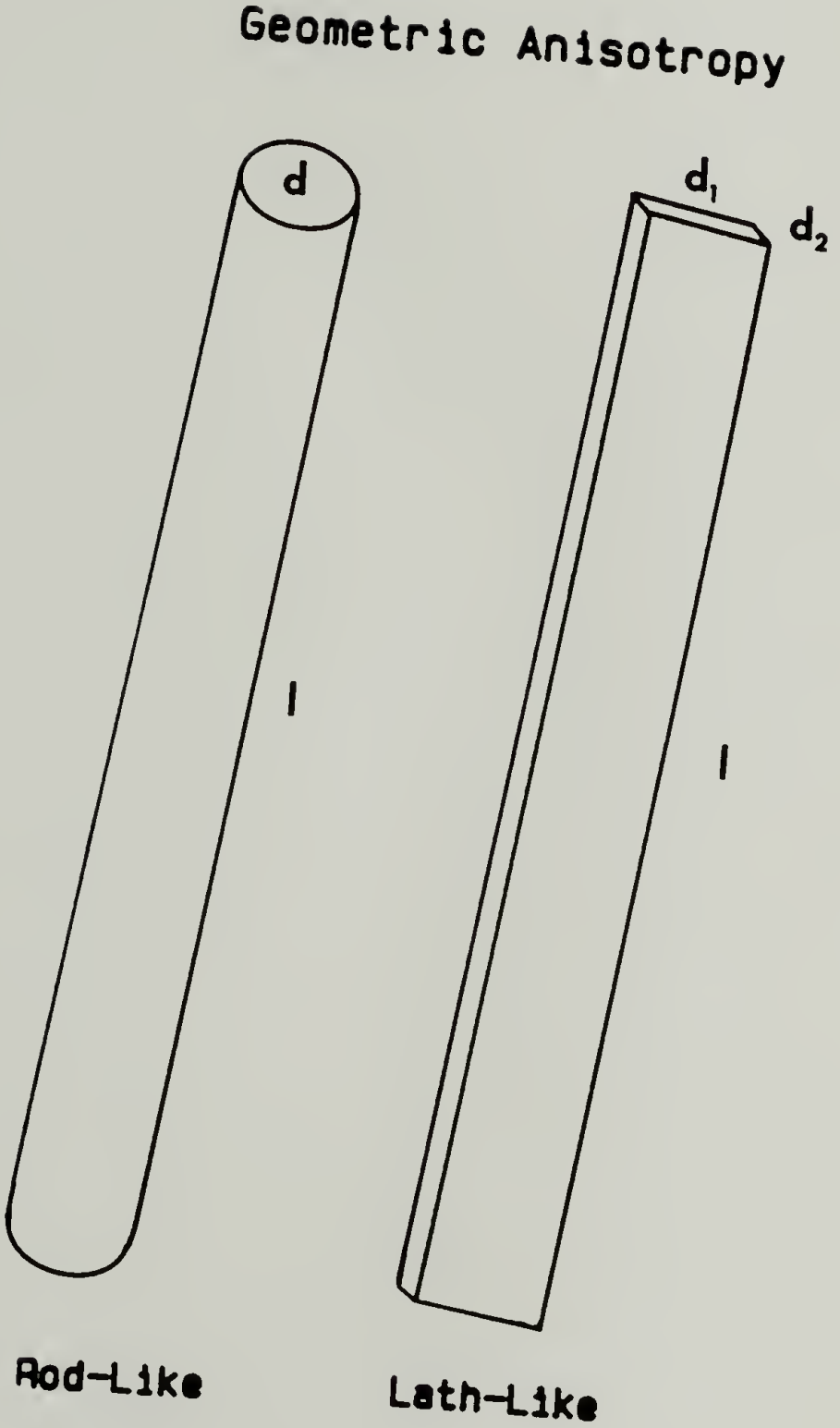

Figure 4-15. Rod- and lath-like structures.

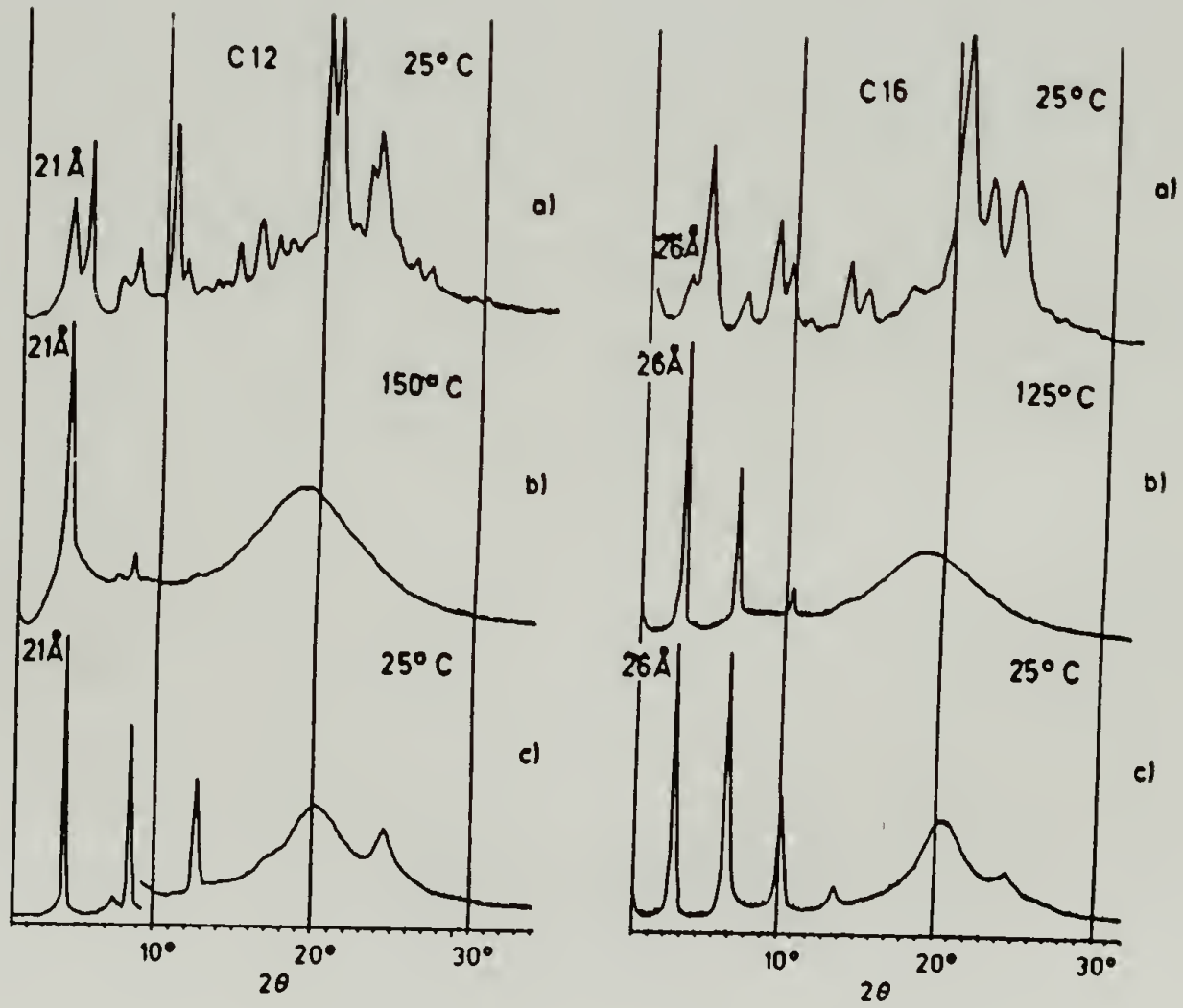

Figure 4-16. X-ray diffraction of disubstituted lath-like structures [75].

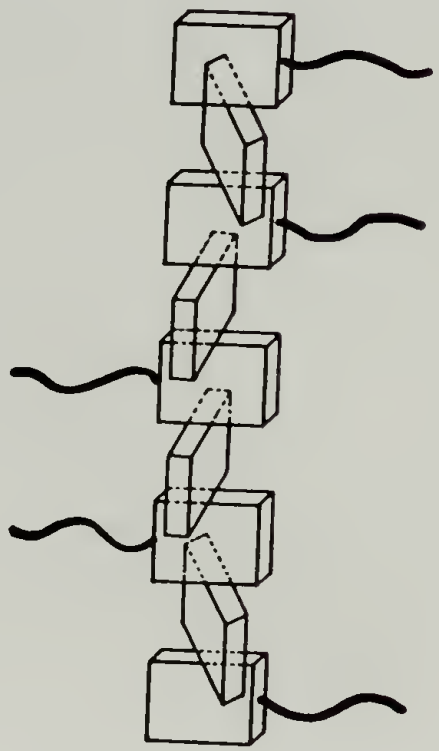

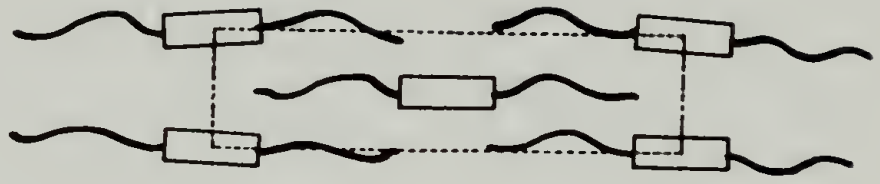

Biaxial Nematic

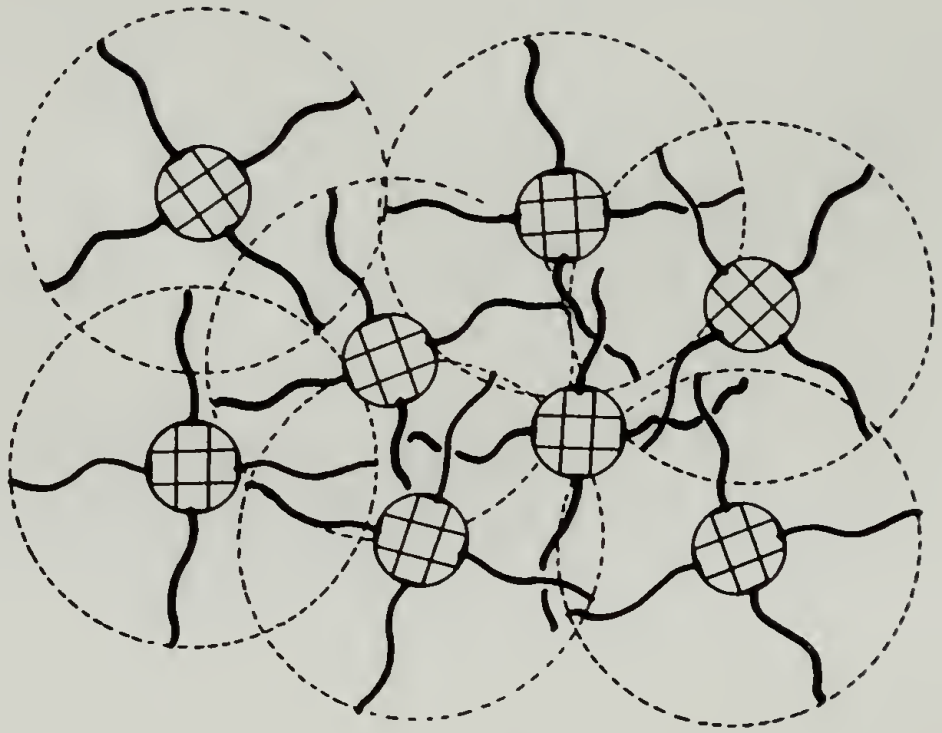

Uniaxial Nematic

Figure 4-17. Schematic diagram of biaxial to uniaxial nematic mesophase transition.

C H A P T E R V

POLYMERIC LIQUID CRYSTALS WITH ALTERNATING MESOGENIC AND FLEXIBLE UNITS

Introduction

Introduction of flexible spacers and alkyl substituents greatly enhance the solubility of PLCs in addition to decreasing the melting and isotropization temperatures. The use of different solvents for casting the PLCs in various morphological states may be used to tailor the initial morphology of a specimen for further study. The PLCs of this type listed in Table 3 show interesting trends when cast from slowly evaporating solvents such as p-chlorophenol (boiling point = 220^{o}C). Figure 5-1 shows the inhibition of folded-chain lamellar spherulitic super-structural morphology when the length of the flexible spacer in the HTH series is decreased from 12 carbons (banded spherulites) to 9 carbons (no banding and spherulites with poorly defined internal structure) to 5 carbons (ability to form spherulites all but eliminated). The minimum conformation of polymethylene to form a tight fold, assuming adjacent reentry, is $tg^{+}tg^{-}$ which requires five carbon atoms. By adding bulkier substituents to the TQT-10 series (Figure

5-2) crystal packing is frustrated to some extent and less perfect crystallites and a less organized super-structure is formed. By rapid casting from a good, yet volatile, solvent such as hexafluoroisopropanol (boiling point = 59^{o}C), the PLCs can be trapped into a morphology with a texture under the microscope reminiscent of the threaded schlieren texture. No evidence of chain folding was observed in the rod-like PPT-R series even when cast slowly from p-chlorophenol (Figure 5-3).

Morphological Transitions of HTH-12

Thermal Analysis

The DSC scans of HTH-12 for the first heating, heating after slow cooling and after rapid cooling and for cooling are shown in Figure 5-4. In the first heating of the polymer recrystallized form p-chlorophenol three endotherms are evident at 165^{o}C, 175^{o} and 182^{o}C which do not appear in any subsequent heating curves, yet the two at 200^{o} and 210^{o}C do. The recrystallization is a similar treatment to solution casting from p-chlorophenol and, in essence, has erased any memory of the thermotropic potential of the PLC. At the 210^{o} transition, typical mesophase fluidity is observed microscopically. The banded spherulites obtained by solution casting of HTH-12 onto cover glass vary in size

with the rate of evaporation. The internal structure of the spherulites is unchanged until the 210°C transition at which they rapidly melt.

SALS Analysis

A spherulitic, four-lobed photographic SALS pattern with outer lobes corresponding to the twist period of the radial lamellae in the spherulites is observed under crossed polars (Figure 5-5). On heating from 25° to 165°C and, further, to 210°C, no change in the shape of the SALS pattern is observed. Photometrically an increase in H_v intensity is detected between 165° and 210°C, corresponding to an increase in birefringence observed visually under the microscope. At 210°C the H_v SALS pattern becomes circularly symmetric about the incident beam, characteristic of random orientation fluctuations giving rise to the scattering of light by the mesophase (as will be discussed in detail in Chapters VI and VII). As the temperature is increased over the range of the mesophase, the intensity of scattering decreases until, at $T_i \sim 230°C$, the isotropic melt or liquid scatters no light under conditions of H_v polarization. On cooling through the mesophase region at a rate of 2°C/min, the circularly symmetric scattering pattern redevelops and is quenched in below 210°C. At the edge of the quenched sample, a four-lobed pattern without maxima is observed

indicating rod-like super-structures. (Boundary conditions may play an important role in creating this morphology.) The banded spherulite morphology of solution casting does not redevelop by melt casting.

X-Ray Analysis

By x-ray techniques, one can observe sub-structural changes of atomic dimensions. The reason for the major 165^{o}C endotherm, undetected by microscopy and SALS, becomes apparent by x-ray diffraction (Figure 5-6). At this temperature, the relative intensities in the wide angle region change and several small angle peaks, representing dimensions larger than the monomer repeat unit length and which are related to the flexible spacer length, disappear. Apparently, "melting" of the flexible spacer occurs at this temperature. Thus, this may be considered a transition from a more ordered ⇒ less ordered crystal. Transitions at 175^{o}, 185^{o} and 200^{o} were not identified but are also probably due to increased rotational or configurational freedom of a part of the molecule but which does not disrupt the super-structural spherulitic morphology until 210^{o}C.

The small angle peak which remains after the 165^{o}C transition stays constant throughout the smectic mesophase regime. From crystallographic features of the solid state, Bernal and Crowfoot [83] found for the SMLCs, p-azoxyanisole

and p-azoxyphenetole, the first mesophase upon heating may be predicted. That is, a nematic mesophase will follow an imbricated crystal structure while a layered crystal structure will give rise to a layered smectic mesophase. Throughout the smectic regime, 210° to 240°C, the small angle peak due to diffraction from the smectic layers decreases in intensity and broadens to some degree. This is the result of increasing disorder in the layers and less volume of smectic material as T_i is approached.

Summary

HTH-12 provides an example of the complementary nature of the techniques of SALS, SAXS and WAXS in conjunction with tailoring of the initial morphology, thermal analysis and optical microscopy to understand the stepwise disordering of matter which occurs in polymeric liquid crystal in going from the semi-crystalline state to the isotropic state. The various techniques probe different levels of order and structure. Super-structural morphological changes (of the scale of 5000 to 50,000A) may be detected by PLOM and, quantitatively, by SALS while information about sub-structural details of the 1 to 100 A scale are detected by x-ray techniques.

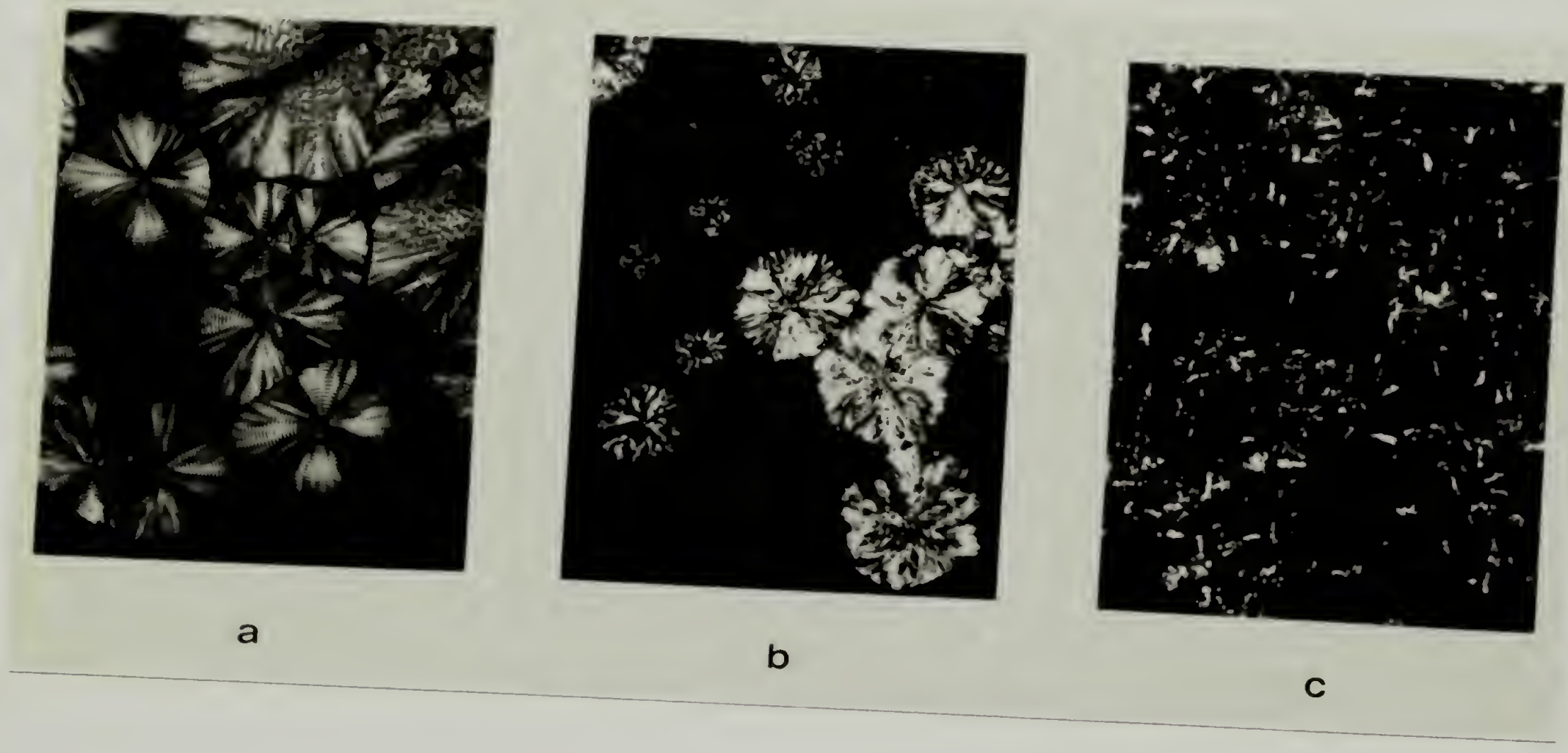

Figure 5-1. Optical micrographs of solution cast: a) HTH-12, b) HTH-9 and c) HTH-5.

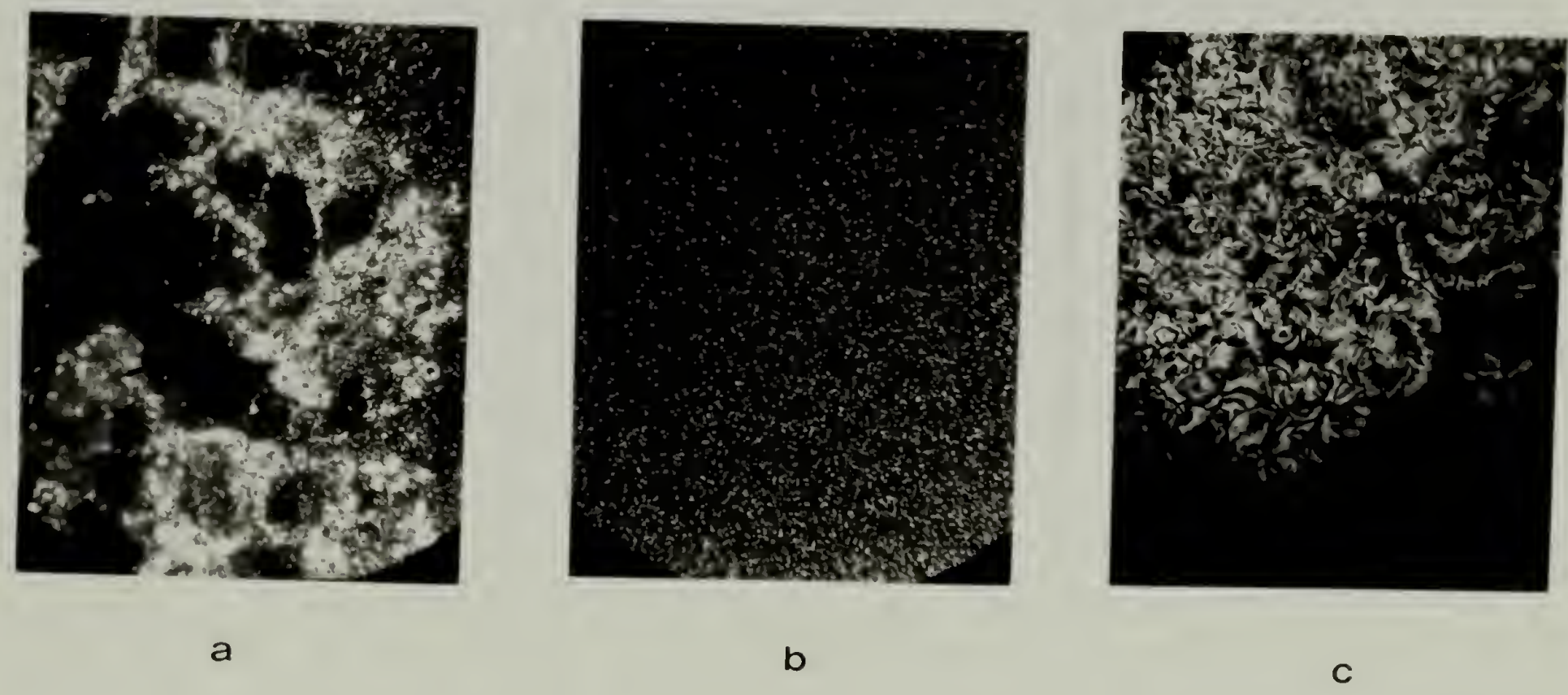

Figure 5-2. Optical micrographs of solution cast: a) TQT(H)-10, b) TQT(Me)-10 and c) TQT(Et)-10.

Figure 5-3. Optical micrograph of solution cast PPT-8-M-b.

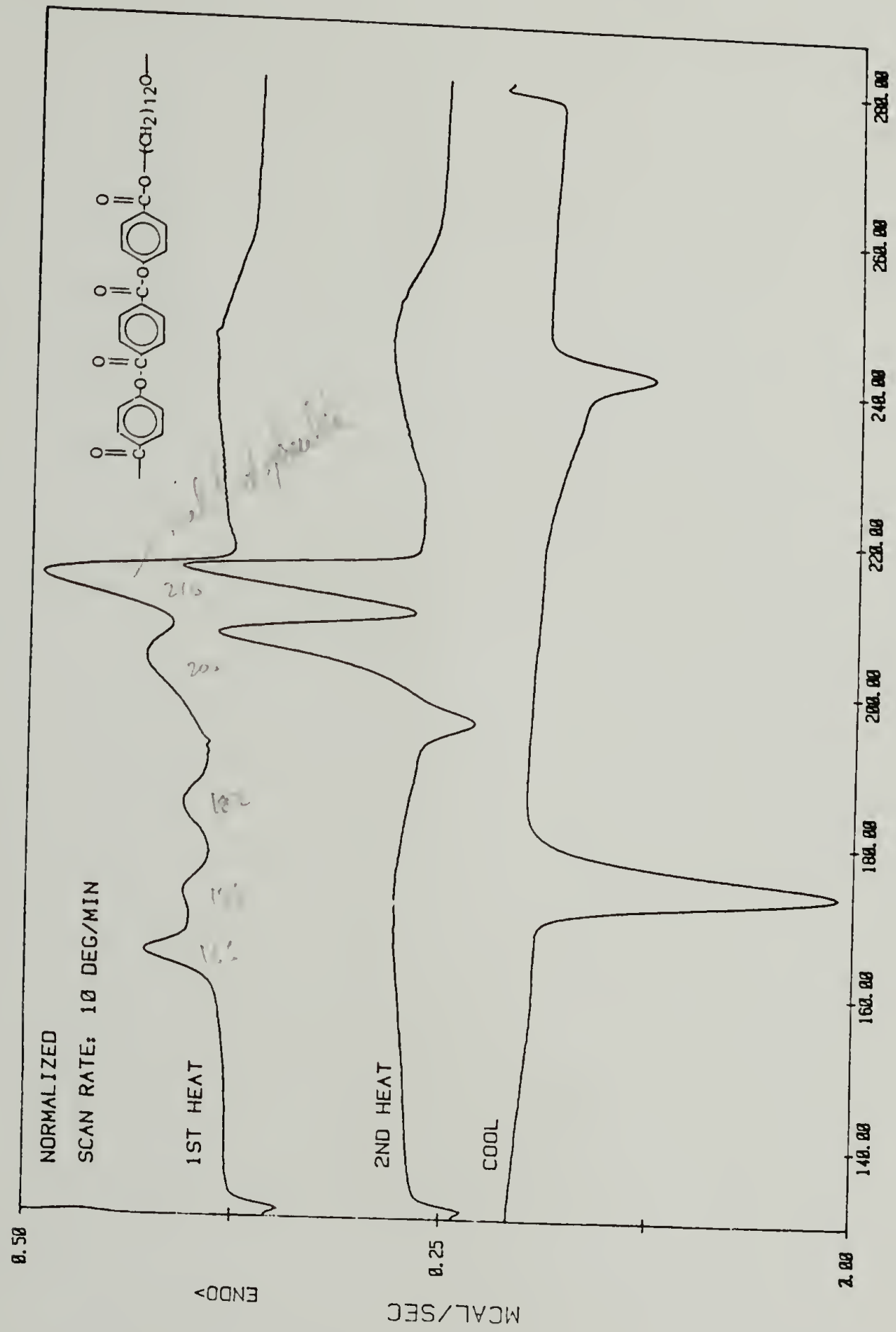

Figure 5-4. DSC scan of HTH-12.

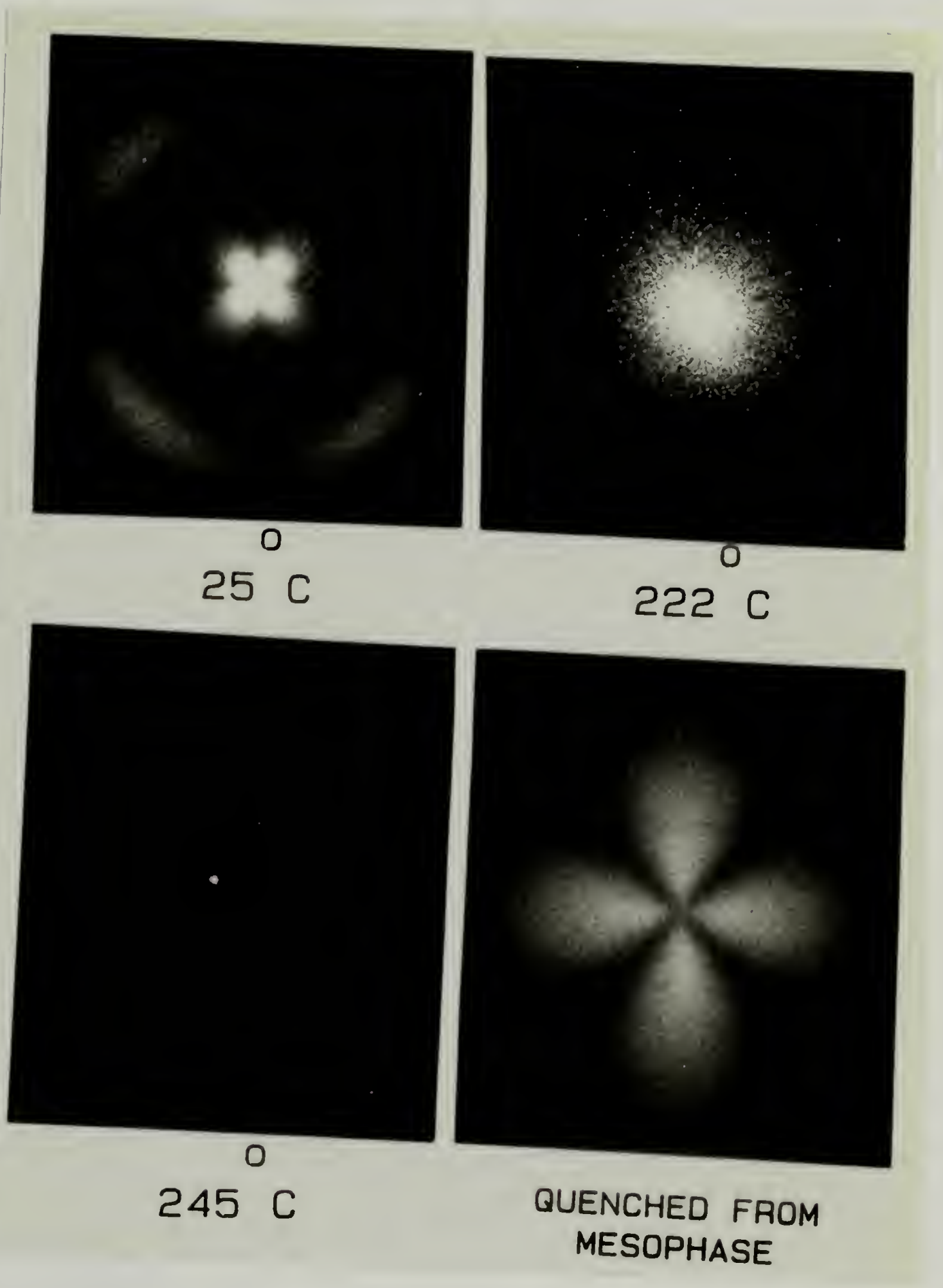

Figure 5-5. Photographic light scattering patterns of HTH-12 at various temperatures during first heating cycle.

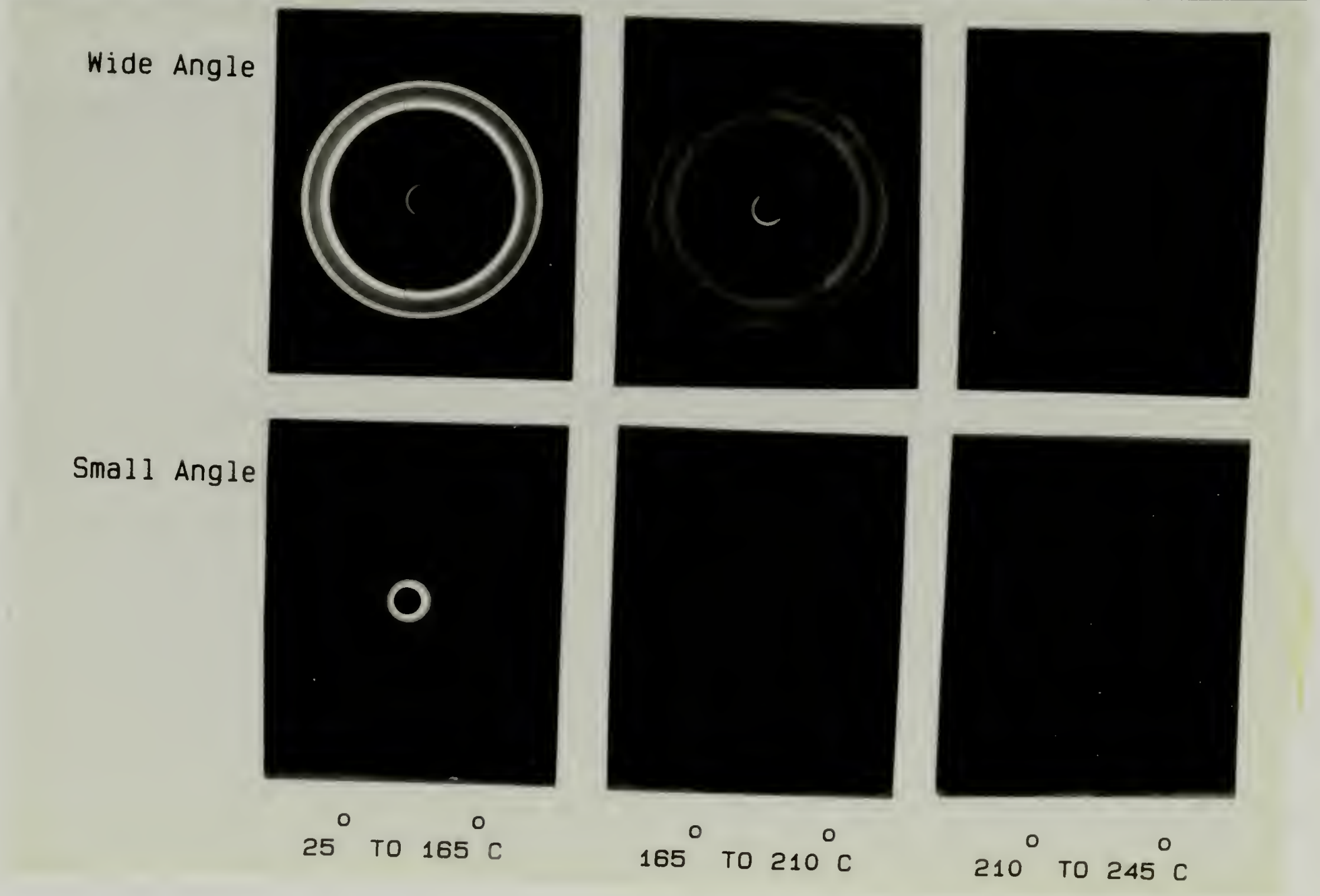

Figure 5-6. X-ray diffraction of HTH-12 as a function of temperature.

C H A P T E R VI

THEORY OF SMALL ANGLE LIGHT SCATTERING

Introduction

Domain Discussion

The hallmark of the thermotropic mesophase is a fluid, yet turbid, melt. In order for the phenomena of turbidity to be visible to the eye, it must be due to the scattering of light by "structures" with a size of the order of magnitude of the wavelength of light. Volume elements throughout which there is a narrow distribution of orientations of the principal molecular axis of mesogenic units centered about the orientation of the director, $\hat{n}$, have been called "domains" and constitute the scattering "structures." This terminology was used originally to describe the super-structural morphology of the mesophase of SMLCs and has been adopted for PLCs. We have purposely left the definition of the "domain" vague as several must be considered in the description of the morphology of the mesophase of thermotropic PLCs.

In the mesophase which has no externally applied orienting forces, the directors are pictured as being randomly oriented in space (Figure 6-1). This polydomain

structure may be kinetic in origin. There is some debate as to whether the mesophase is formed by nucleation and growth or spinodal decomposition processes. It is observed by PLOM on the polymeric liquid crystals utilized in this study that, upon cooling from the isotropic state at either 0.2^{o} or 2.0^{o}C/min, specks of birefringence form first in a dark field, followed very rapidly by formation of a highly birefringent field of view, uniform in intensity. The disappearance of the mesophase upon heating is very dissimilar; there are large "pools" of birefringence surrounded by isotropic liguid, dark under crossed polars, the area of which grows at the expense of the mesophase as the temperature is raised through the broad, biphasic regime of the isotropization transition. This suggests that nucleation and growth controls mesophase formation upon cooling from the isotropic state, hence, several Avrami treatments of the kinetics of mesophase formation have appeared [84, 85]. Recent evidence for fractionation by molecular weight explains the clearing behavior [86].

The detailed description of a domain is a topic of much debate. Models (Figure 6-2) which have been suggested are $^{1)}$sharp-boundaried domains [87], $^{2)}$diffuse-boundaried domains and $^{3)}$continuously changing mesogen orientation but with a preference for parallel orientation with the nearest neighbors. Most recently, $^{4)}$a description in which there is no preferred orientation has been proposed by Marrucci [88]

to explain rheological phenomena.

Sharp-boundaried models are analogous to the concept of grain boundaries observed in metals. There is certainly more justification for this description in SMLCs than in main-chain PLCs where inter-domain "tie molecules" would be likely and would blurr the abruptness of orientational change. On the other hand, polymer chain defects (chain ends and short branches) and low molecular weight fractions could constitute the boundary zone. As was shown in Chapter V, the likelihood of chain folding is great in main-chain PLCs with alternating mesogenic units and flexible spacers. This would reduce the probability of "tie molecules;" chain folding with tight folds is impossible in the stiffer, rod- or worm-like PLCs.

Under the influence of an external magnetic, electrical or mechanical orienting field, the directors align in a parallel fashion as, obviously do, all the mesogenic units which they represent. Thus the structure approaches a monodomain (Figure 6-1). Thermodynamic equilibrium is not usually observed in polymers because of their sluggish, long-chain nature. If equilibrium were achievable, the monodomain super-structure would be expected to prevail in PLCs. Upon cessation of the orienting field, the monodomain appears to break-up by optical microscopy. This is probably caused by elastic recoil due to residual stresses.

Orientational Order

In PLCs, orientational order must be described at both the local and global levels [89] which necessitates several different parameters. The order parameter, s, was first used by Tsvetkov [90] for SMLCs to express the state of orientational order. It is defined for three and two dimensions, respectively, as

$$s = [3\langle\cos^2\theta_i\rangle - 1]/2 \qquad (6\text{-}1a)$$

$$s = [2\langle\cos^2\theta_i\rangle - 1] \qquad (6\text{-}1b)$$

where θ_i is the angle between the characteristic axis of the mesogenic moiety, given as the unit vector, $\hat{m}$, and the director, $\hat{n}$. The symbol $\langle\rangle$ is used to designate a spatial average over the domain. Only local preferred orientation is specified by the director. For the sake of simplicity, let us assume the molecular and mesogenic axes to be coincident. Further,

$$\hat{m}_i \cdot \hat{n} = \cos\theta_i \qquad (6\text{-}2)$$

and the sum over the domain is necessarily

$$\sum_i (\hat{m}_i \cdot \hat{n}) = 0. \qquad (6\text{-}3)$$

In a macroscopically disordered LCn sample, the directors are taken to be randomly oriented in space. Small molecule LCs are easily oriented by electric and magnetic fields or by surface treatments. A macroscopic monodomain, in essence, is achieved by such processes; the order

parameter of the macroscopic sample becomes that of the individual domain.

Magnetic and electric fields and surface treatments are not, in general, as effective in orienting ordinary polymeric chain backbones. (To orient main-chain PLCs, magnetic field strengths of 15 Tessla were used in comparison to 1.5 Tessla which is sufficient for SMLCs and side-chain PLCs.) Extensional flow results in a high degree of orientational order in polymers which can be quantified by specifying the order parameter. Let the angle between the polymer chain axis and the macroscopic orientation direction be θ_o. When the polymer (amorphous or semi-crystalline) is orientationally disordered, $\langle \cos^2\theta \rangle = 1/3$ thus $s = 0$. But for perfectly aligned or oriented chains, $\theta_o = 0^o$ and $s = 1$. The distinction between local and macroscopic levels of orientational order does not exist for ordinary amorphous polymers as it does for semi-crystalline and liquid crystalline polymers and SMLCs. In semi-crystalline polymers, the local order parameter is taken to be 1 within a crystallite, i.e., perfect alignment of polymer chains.

$P^{(2)}$, Hermans orientation function, is the second coefficient in the expansion in spherical harmonics of the orientation distribution function and describes the macroscopic orientational order in polymers. For a macroscopically unoriented system,

$$P^{(2)} = [3\langle\cos^2\theta_o\rangle - 1]/2 = 0. \qquad (6\text{-}4)$$

Another parameter to describe the degree of parallel orientation of two molecules, 1 and 2, separated by a vector distance, r_{12}, and where θ_{12} is the angle between the principal mesogenic axes of the individual molecules is the orientation correlation function given as

$$P_{12}(r) = [3\langle\cos\theta_{12}^2\rangle_r - 1]/2 . \qquad (6\text{-}5)$$

This function decays from a value of unity when the molecules are coincident, i.e., $|r_{12}| = 0$, to zero when the separation approaches infinity, i.e., no correlation in orientation in a system not possessing long-range order.

Let us assume the sharp-boundaried domain description where the orientation of individual mesogens, $\hat{m}$, about the director, $\hat{n}$, is given by some function symmetric about zero. In general, a mesogen in the neighboring domain has a different direction, $\hat{m}$. The orientation correlation function between two mesogens within the same domain is s^2, but when mesogens in different domains are considered, $\langle P_{12}(r)\rangle = 0$. The order parameter and the orientation correlation function may be related by

$$s = \left[\int_{V_D} P_{12}(r)dr^3 / \int_{V_D} dr^3\right]^{1/2} \qquad (6\text{-}6)$$

It may be instructive to consider the relationship between the measures of orientational order on the local and global scales, that is, s defined in terms of θ_m and $P^{(2)}$

defined in terms of θ_o, respectively. The order parameter and the orientation function can be related by invoking, $P_D^{(2)}$, the orientation function of a domain director, $\hat{n}$, defined by

$$P_D^{(2)} = [3\langle\cos^2\theta_D\rangle - 1]/2 \qquad (6\text{-}7)$$

where θ_D is the angle between $\hat{n}$ and the macroscopic orientation direction of the sample. The relationship becomes

$$P^{(2)} = s\cdot(P_D^{(2)}). \qquad (6\text{-}8)$$

The various schenarios for s, $P^{(2)}$ and $P_D^{(2)}$ are illustrated in Figure 6-3. The foregoing development assumes, of course, that the applied field which is required to orient the domains does not affect s. The utility of the light scattering technique is to be able to determine the state of orientation in a macroscopically unoriented sample.

Theory

Small angle light scattering (SALS) of ordinary polymeric films has been approached by two methods: the model description and the statistical description [91]. The model description is useful when scattering arises from a collection of structurally definable (in terms of size and shape) objects such as spherulites in polymeric films or an assembly of rods as in mesomorphic materials. Obtainable

quantities are the third moment average spherulite radius [92],

$$R = \frac{3.9\ \lambda}{2\ \pi\ \sin\ \theta_{max}}, \qquad (6\text{-}9)$$

and the pitch in ringed spherulites [93],

$$P = \lambda \backslash \sin(\theta_{max}/2), \qquad (6\text{-}10)$$

where θ_{max} is the scattering angle at which the maximum in intensity occurs and λ is the wavelength of light in the medium.

Density and Orientation Correlations

The statistical description is more general and is frequently used for more random, non-particulate systems in which heterogeneities are described as fluctuations from an average value and in which correlation lengths quantify the extension of heterogeneities present in the sample. Both descriptions must be employed in the PLC systems under study in order to fully describe the structural variety of the phases observed upon thermal programming. PLC domains may best be described statistically while a single domain may be considered to be an assembly of rod-like scatterers [94, 95].

The general scattering equation is given by:

$$I = K\ \Sigma\Sigma\ (M_i \cdot \hat{O})\ (M_j \cdot \hat{O})\ \cos\ [k(r_{ij} \cdot s)] \qquad (6\text{-}11)$$

where M_i and M_j are the induced dipole moments of the i^{th}

and j^{th} volume elements, $\hat{0}$ is a unit vector, given for parallel (//) and crossed (+) experimental conditions, in the analyzer plane of polarization and along M given for various possible experimental conditions:

$$\hat{0}_{//} = (\sin\psi \sin\theta)\hat{i} + (\sin\psi \cos\theta)\hat{j} + (\cos\psi)\hat{k} \quad (6\text{-}12)$$

$$\hat{0}_{+} = (\cos\psi \sin\theta)\hat{i} + (\cos\psi \cos\theta)\hat{j} + (\sin\psi)\hat{k}$$

where ψ is the angle by which the polarizer is rotated from the vertical direction and θ is the polar scattering angle. r_{ij} is the vector connecting the two volume elements and s is the vector, $s = \hat{s}_o - \hat{s}'$, where $\hat{s}_o$ and $\hat{s}'$ are unit vectors along the incident and scattered rays, respectively. The wave number, k, is $2\pi/\lambda$.

Let E be the effective incident field strength at an arbitrary volume element i. Then,

$$M_i = (\alpha_1)_i (E \cdot \hat{a}_{1,i}) \hat{a}_{1,i} + (\alpha_2)_i (E \cdot \hat{a}_{2,i}) \hat{a}_{2,i} \quad (6\text{-}13a)$$

where α_1 and α_2 are the longitudinal and transverse polarizabilities of a cylindrically symmetric anisotropic volume element and $\hat{a}_1$ and $\hat{a}_2$ are the respective unit vectors in these directions (Figure 6-4). Defining δ, the anisotropy of polarizability of the volume element, to be $(\alpha_1 - \alpha_2)$, then

$$M_i = \delta_i (E \cdot \hat{a}_{1,i}) \hat{a}_{1,i} + \alpha_2 E \quad (6\text{-}13b)$$

$$= \delta_i (E \cdot \hat{a}_{1,i}) \hat{a}_{1,i} + (\alpha_i - 1/3\ \delta_i) E \quad (6\text{-}13c)$$

As seen in eq. 6-11, scattering arises from relative fluctuations in the induced dipole moment (with respect to $\hat{0}$) in the i^{th} and j^{th} volume elements. Eqs. 6-13 could be

modified to take account of fluctuations about the average in:

1-1) polarizability (α) of the volume element, $\eta_i = \alpha_i - \overline{\alpha}$ (also called density fluctuations).

2-1) anisotropy (δ), $\Delta_i = \delta_i - \overline{\delta}$

3-1) orientation of the principal optic axis, $\hat{a}_{l,i}$, and

4-1) optical rotation.

The corresponding correlation functions which are of interest are:

1-2) $\gamma(r) = \langle \eta_i \eta_j \rangle_r / \langle \eta^2 \rangle$

2-2) $\Psi(r) = \langle \Delta_i \Delta_j \rangle_r / \langle \Delta^2 \rangle$

3-2) $P_{l2}(r) = [2\langle \cos^2 \theta_{ij} \rangle_r - 1]$ (for 2D) and

$= [3\langle \cos^2 \theta_{ij} \rangle_r - 1]/2$ (for 3D)

where θ_{ij} is the angle between the principal optic axes of two volume elements. (For the sake of simplicity, we will assume the optic axis and the mesogenic axis in the case of main-chain PLCs to be coincident.) $\langle\ \rangle_r$ denotes an average over all space for a constant separation r_{ij} [91].

Random Orientation Approximation

Debye and Bueche [96] looked at isotropic (i.e., random - $\delta^2 = \langle \Delta^2 \rangle = s$) density fluctuations only and obtained the equation:

$$I = K \langle \eta^2 \rangle \int \gamma(r) \frac{\sin qr}{qr} r^2 dr. \qquad (6\text{-}14)$$

q is given as $q=(4\pi/\lambda)\sin(\theta/2)$ where θ, the scattering angle, is the angle between the incident ray and scattered ray and λ is the radiation wavelength in the medium.

Goldstein and Michalek [97] generalized the approach to include fluctuations 1, 2, and 3 which may all be interdependent, thus resulting in a very complex situation. Stein and Wilson [98] made the mathematical simplification of the random orientation approximation. It is assumed that θ_{ij} is independent of the angular coordinates of r_{ij} and, only dependent on the magnitude, $r_{ij} = |r_{ij}|$: that is, the angle between the principal polarizability axes of i and j depends on the scalar separation between them but not direction and θ_{ij} is not correlated with θ_i. The scattering system has spherical symmetry and the scattering pattern is cylindrically symmetric about the incident beam.

Further simplifications include: 1) all r_{ij}'s are equally probable for an unoriented system and not correlated with the orientation of the principal polarizability axis, 2) $\Psi(r)$ is not correlated with $\gamma(r)$ and 3) fluctuations in δ_i are due to fluctuations in α_i when the polarizability elipsoid may be considered constant due to an invariant chemical structure. This last approximation is given as:

$$\frac{\langle \Delta^2 \rangle}{\delta^2} = \frac{\langle \eta^2 \rangle}{\alpha^2} \qquad (6\text{-}15)$$

The above treatment allows one to separate the contribution to scattering due to density fluctuations from that due to orientation fluctuations by performing SALS experiments under conditions of both parallel (V_v) and crossed (H_v) polarization and performing the requisite subtraction. The equations for scattered intensity are as follows:

$$I_{Vv} = K[\langle\eta^2\rangle \int \gamma(r) \frac{\sin qr}{qr} r^2 dr + \frac{4\delta^2}{45} \int p_{12}(r)u(r) \frac{\sin qr}{qr} r^2 dr] \quad (6\text{-}16a)$$

$$I_{Hv} = K[\frac{\delta^2}{15} \int p_{12}(r)u(r) \frac{\sin qr}{qr} r^2 dr] \quad (6\text{-}16a)$$

$$I' = I_{Vv} - 4/3\ I_{Hv} \quad (6\text{-}16b)$$

$$= K[\langle\eta^2\rangle \int \gamma(r) \frac{\sin qr}{qr} r^2 dr \quad]$$

The definition of $u(r) = 1 + \frac{\langle\Delta_2^2\rangle}{\delta^2} \Psi(r) \simeq 1 + \frac{\langle\eta_2^2\rangle}{\alpha^2} \gamma(r)$. (6-16c)

The variation of the density correlation function, $\gamma(r)$, and the orientation correlation function, $p_{12}(r)u(r)$, obtained from I_{Hv} and I' respectively, with temperature gives us a working model to quantitatively characterize the structural changes in LCn domains relating to the extent of polarizability and orientation fluctuations. An exponential form of the correlation functions has been shown to be valid for density [99] and orientation [100] fluctuations in other systems. This approach was taken previously for TQT(BR)-10 [101] and will be discussed in Chapter VII. It can be shown that by substituting

$$p_{12}(r)u(r) = e^{-r/a} \quad \text{and} \qquad (6\text{-}17a)$$

$$\gamma(r) = e^{-r/a} \qquad (6\text{-}17b)$$

in eqs. 6-16b and c respectively, integrating and taking the inverse that

$$[I_{Hv}]^{-1/2} = [K'\delta^2 a_o{}^3]^{-1/2} (1 + q^2 a_o{}^2) \qquad (6\text{-}18a)$$

$$[I']^{-1/2} = [K'\langle\eta^2\rangle a_p{}^3]^{-1/2} (1 + q^2 a_p{}^2). \qquad (6\text{-}18b)$$

By plotting the respective $I^{-1/2}$ vs q^2, one may obtain the correlation lengths, a_o and a_p, from the square root of slope/y-intercept ratio. It is also evident that from the ratio I_{Hv}/I', the relative strengths of contributions of anisotropy and polarizability to scattering, $\delta^2/\langle\eta^2\rangle$, may be evaluated.

An alternate method of data interpretation which will be adopted in Chapter VII is to perform a Fourier inverse of the I vs q data to obtain the correlation function vs r:

$$p_{12}(r)u(r) = A/r \int I_{Hv}\, q \sin qr\, dq \qquad (6\text{-}19a)$$

$$\gamma(r) = B/r \int I'\, q \sin qr\, dq \qquad (6\text{-}19b)$$

A comparison of the extent of heterogeneities for different samples, different temperatures, or different types of heterogeneities may be obtained by examining the r values at a constant correlation function value (say $\gamma(r)=0.5$).

Anisotropic Orientation Fluctuations

It is a reasonable prediction that the random placement of the centers of gravity of the mesogens in a nematic

mesophase would give rise to random fluctuations in orientation and circular symmetry in the light scattering pattern. Consider the more complex situation in which correlation in orientation is a function of the angular dependence of r_{ij} as well as its magnitude, as may be predicted for the smectic mesophase. This is referred to as anisotropic orientation fluctuations and requires a more complex analysis [91]. Separation into shape (G) and size (p_{12}) factors

$$F(r_{ij}) = G(\alpha_{ij},\beta_i)\ p_{12}(r_{ij}) \qquad (6\text{-}20)$$

may be instructive (angles defined in Figures 6-4 and 6-5). By defining a shape anisotropy parameter, ε, with the values of +1, -1 and 0 for rod-like, disk-like and random orientation, the azimuthal angular (μ) dependence of various scattering patterns may be duplicated (see Figure 6-5). To improve upon the scattering angle (θ) dependence of I versus μ variation, ε is considered to be a function of r_{ij}:

$$\varepsilon(r_{ij}) = \varepsilon_o \exp -[r_{ij}/a_s]^2 \qquad (6\text{-}21a)$$

Here, ε_o refers to the shape factor for closely spaced scattering elements and a_s is the correlation distance for persistence of this shape.

Smectics, in which the mesogens are normal to the layer planes, have disk-like orientation superimposed on the rod-like orientation of nematics and, thus, an $\varepsilon(r_{ij})$ which may assume positive values for certain r_{ij}'s and negative values at other r_{ij}'s may be more correct:

$$\varepsilon(r_{ij}) = \varepsilon_o \{x \exp -[r_{ij}/a_r]^2 - (1 - x) \exp -[r_{ij}/a_d]^2\} \quad (6\text{-}21b)$$

where x is the fraction of rod-like orientation at $r_{ij} = 0$. Smectics and nematics could be theoretically differentiated by the a_r/a_d ratio which would be larger for nematics.

A more general approach is required for the tilted smectic mesophases since the shape anisotropy parameter can only describe cases where β_i is 0^o or 90^o. For a two-dimensional system, the probability of a given angle, θ_{ij}, between the i^{th} and j^{th} scattering elements may be expanded in a Fourier series as

$$P(\theta_{ij}) = L_0 + L_1 \sin \theta_{ij} + L_2 \sin 2\theta_{ij} + \ldots\ldots + M_1 \sin \theta_{ij} + M_2 \sin 2\theta_{ij} + \ldots\ldots . \quad (6\text{-}22)$$

The coefficients of the series may be expressed as averages of the distributions of θ_i, θ_j and θ_{ij} and further expanded as Fourier series in β_i with proper symmetry conditions. Many-parameter equations duplicate the shape of H_v and V_v scattering patterns.

Hashimoto et al. [95] have also considered the problem of rod-like scattering in semi-crystalline and liquid crystalline polymers (poly(γ-benzyl-L-glutamate), poly(tetrafluoroethylene) and collagen) which exhibit anisotropic rod-like textures. They considered a rod to be composed of a parallel alignment of isolated rods where ω_o is the angle between the optic axis, $\hat{m}$, and the rod axis, $\hat{r}_i$, (see Figure 6-6). Thus, rod-like ($\omega_o = 0^o$), disk-like ($\omega_o = 90^o$) and tilted ($0^o < \omega_o < 90^o$) are all described as

rods. It was found that a larger assembly of rods, randomly oriented in space and incorporating one-dimensional paracrystalline disorder, where ξ is the angle between the assembly long axis, $\hat{r}_a$, and $\hat{r}_i$, dominates scattering at small angles. Thus, complex patterns which are composites of +-type and x-type scattering can be accounted for based upon inter-rod interference considerations (inter-assembly interferences neglected).

Summary

Recalling Chapter II, the failure of the mean-field approximation for LCs stems from its neglect of short-range, anisotropic, repulsive forces. Such forces are responsible for the structure of simple liquids while long-range, attractive forces merely serve to maintain the high density of liquids. A correction factor to fit experiment to theory involves small clusters of molecules with high orientational order. The anisotropy of the cluster is assumed lower than that of a single mesogen and is presumed to persist into the isotropic state. Leadbetter [26] has shown by x-ray and neutron scattering techniques, that the short-range structure, as obtained from the radial pair distribution function of p-azoxyanisole and some 4,4′-disubstituted cyanobiphenyls, are essentially identical in the nematic and isotropic states.

The terminology of these clusters has been incorrectly confused with that of "swarms" [23, 24, 25]. According to Luckhurst [26]:

> "Such an inadequate description may be avoided by using the language of the distribution function. Then the word cluster would be a shorthand for the statement that the pair distribution function for parallel alignment is large and essentially constant over distances comparable to several molecular dimensions. In addition [the distribution function] model would require that the short-range part of [the pair distribution function] does not change at the isotropic to nematic transition. Consequently, the variation in the orientational properties of the nematogen at the phase transition must be caused by that part of the pair potential for which the intermolecular separation is greater than the distance over which the pair potential is constant."

Such is the information which we seek for PLCs by studying the small angle light scattering from these materials under conditions of H_v polarization and the long-range orientation correlation function derived from the experimental data.

A final word concerning the use of the term "domain" structure, loosely used to describe the morphology of these PLC films in the mesophase: the boundary limits of a domain may be defined as the distance over which the molecular axes (coincident with the optic axes for these PLCs) are orientationally correlated with the director, $\hat{n}$, given an arbitrary, but reasonable, misorientation angle. The correlation lengths serve as a measure of the size of the correlated region. When a larger misorientation angle is allowed, a larger correlation length will be sampled

resulting in a larger effective domain size. Thus, this approach is able to describe both the continuum description, in which one would expect small correlation lengths and might allow large misorientation angles, and the sharp-boundaried domain description of the mesophase.

no force field: polydomain

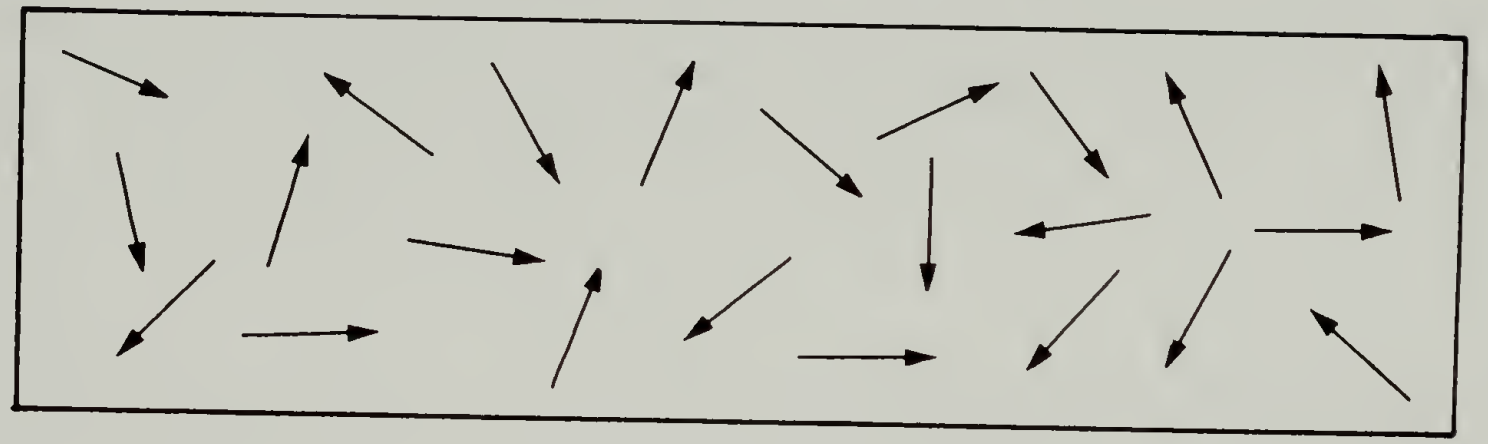

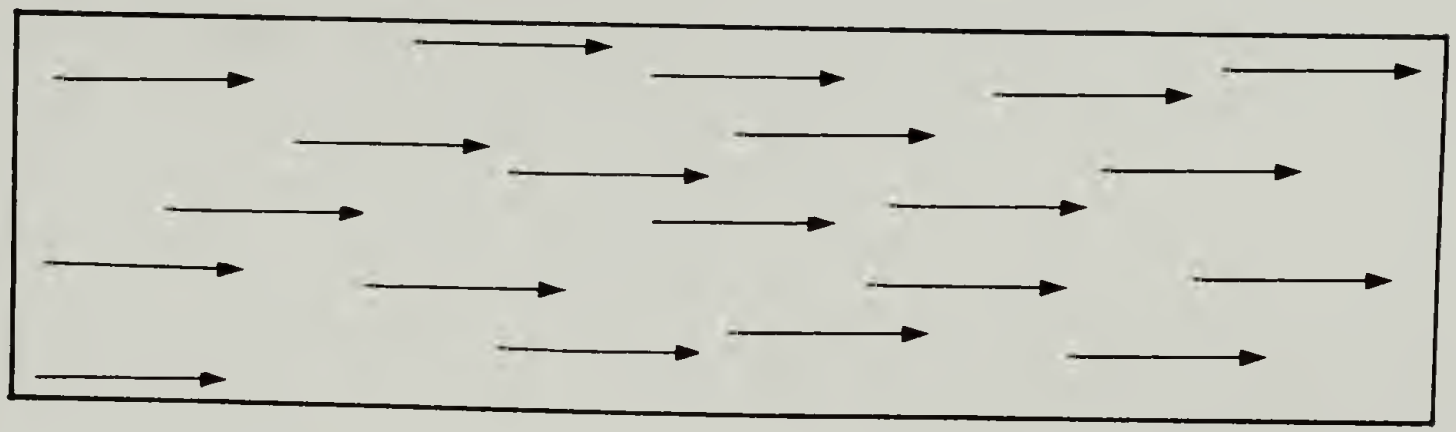

with force field: monodomain

Figure 6-1. Schematic diagram of the transition from a polydomain morphology to a monodomain morphology for LCs experiencing an orienting field.

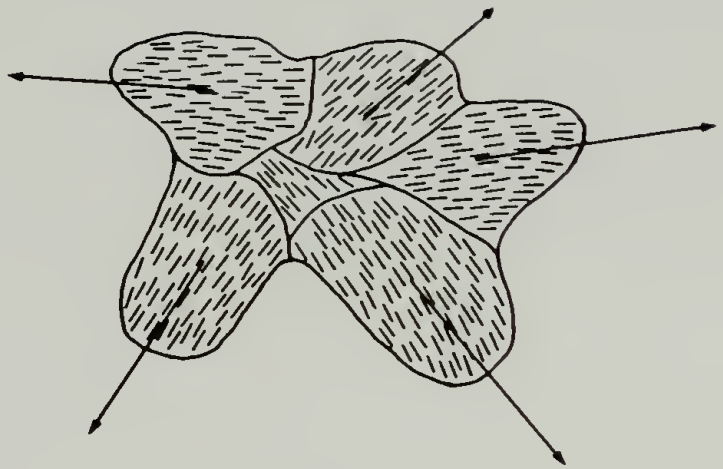

sharp-boundaried

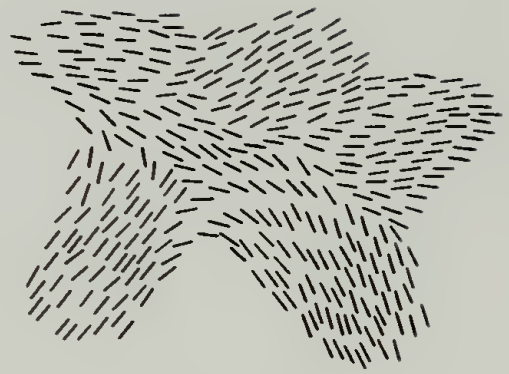

diffuse-boundaried

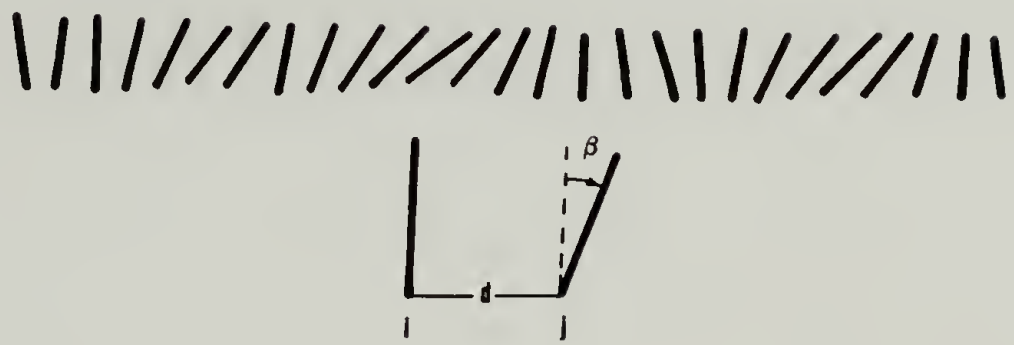

continuously changing orientation

Figure 6-2. Models of mesophase super-structural morphology which have been proposed.

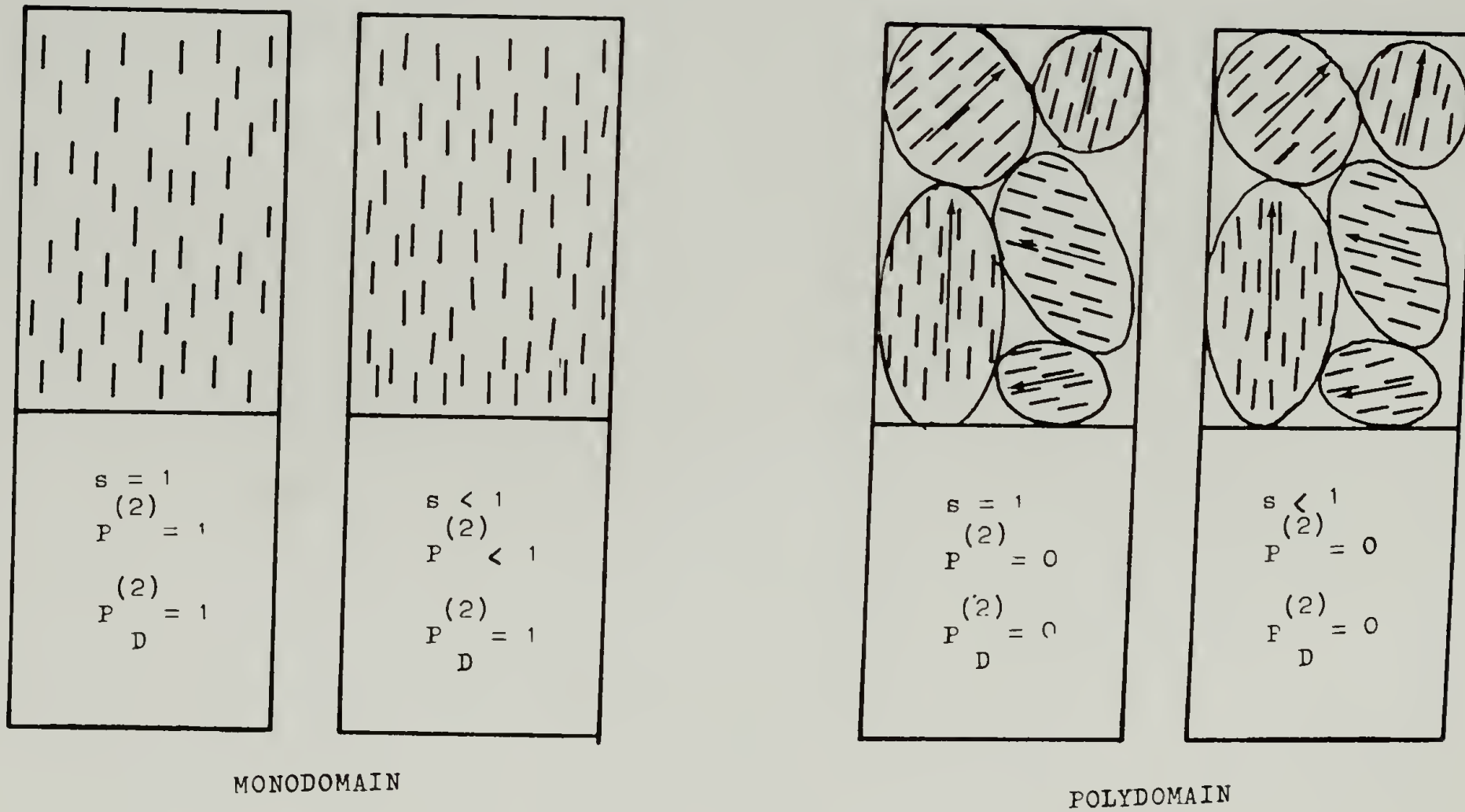

Figure 6-3. Schenarios for s, $P^{(2)}$ and $P_D{}^{(2)}$.

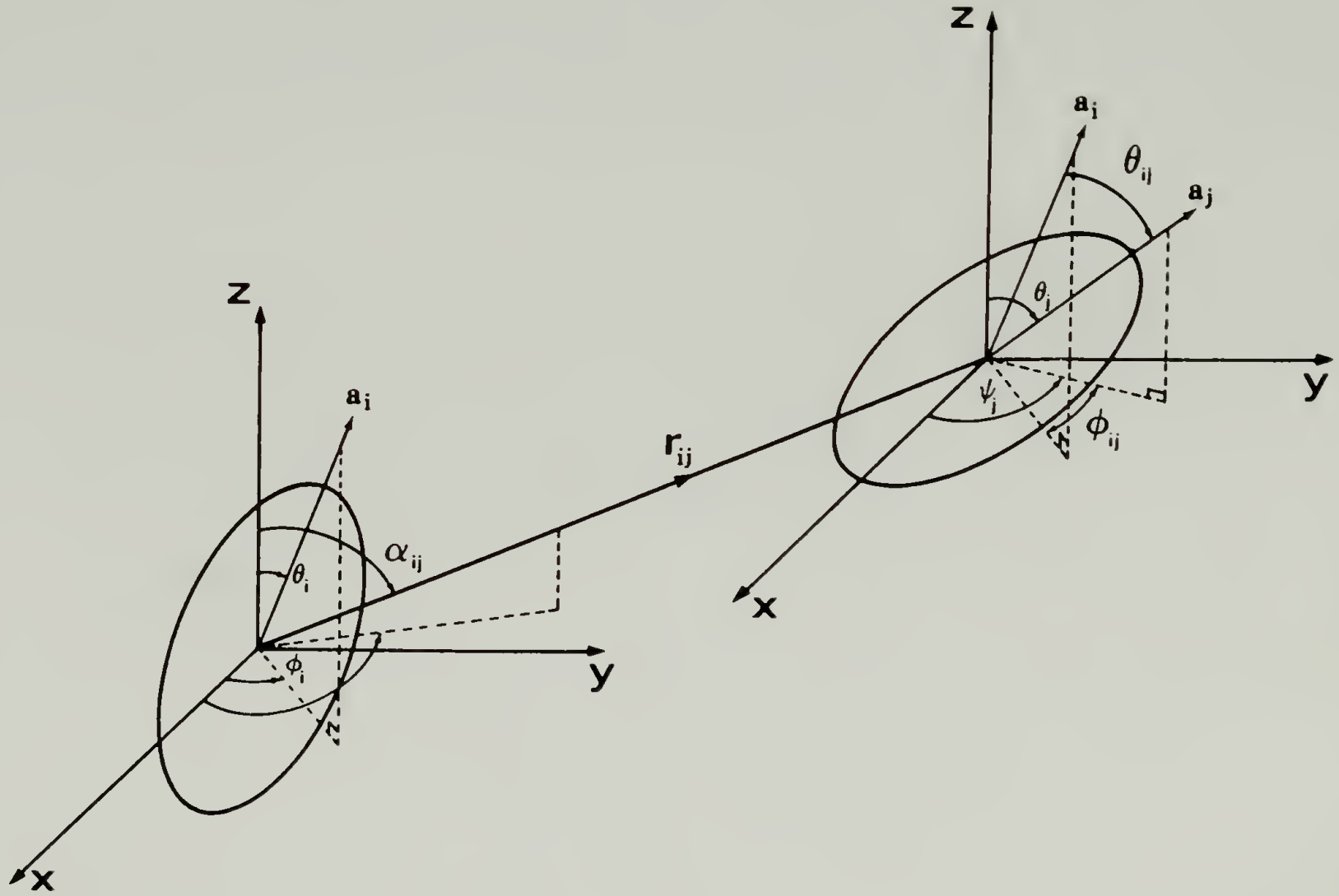

Figure 6-4. Definition of angles characterizing the optic axes of scattering elements and r_{ij}.

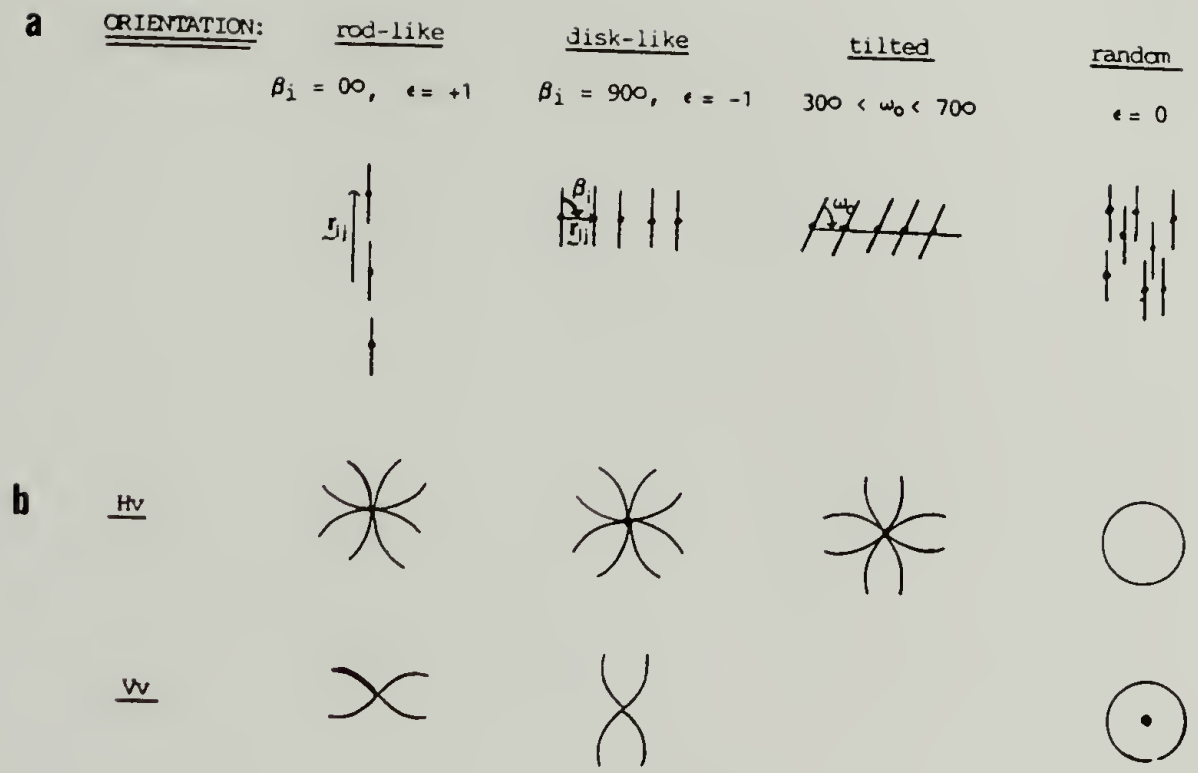

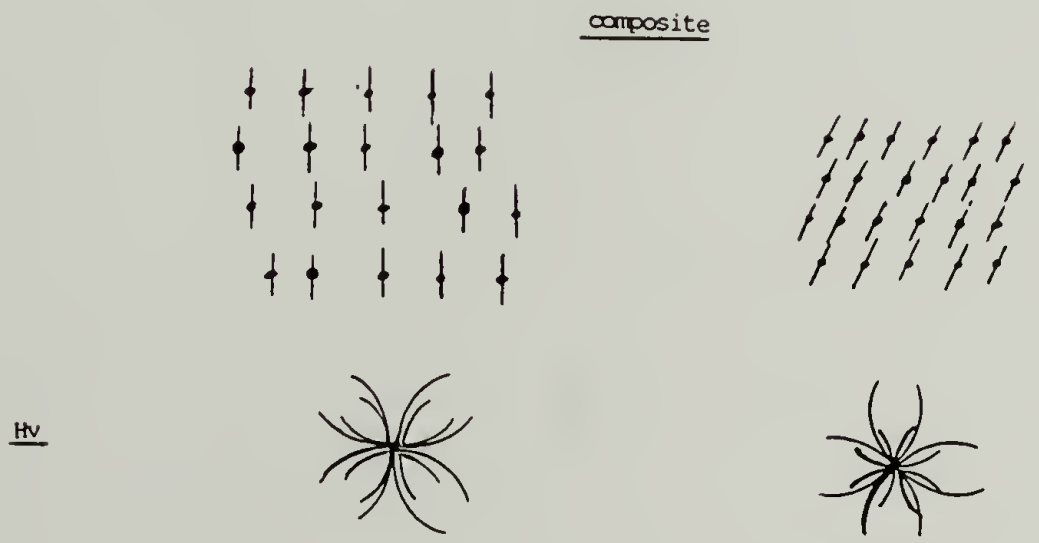

Figure 6-5. a) Rod- and disk-like anisotropic orientation and random orientation models. b) Schematic diagrams of predicted scattering patterns.

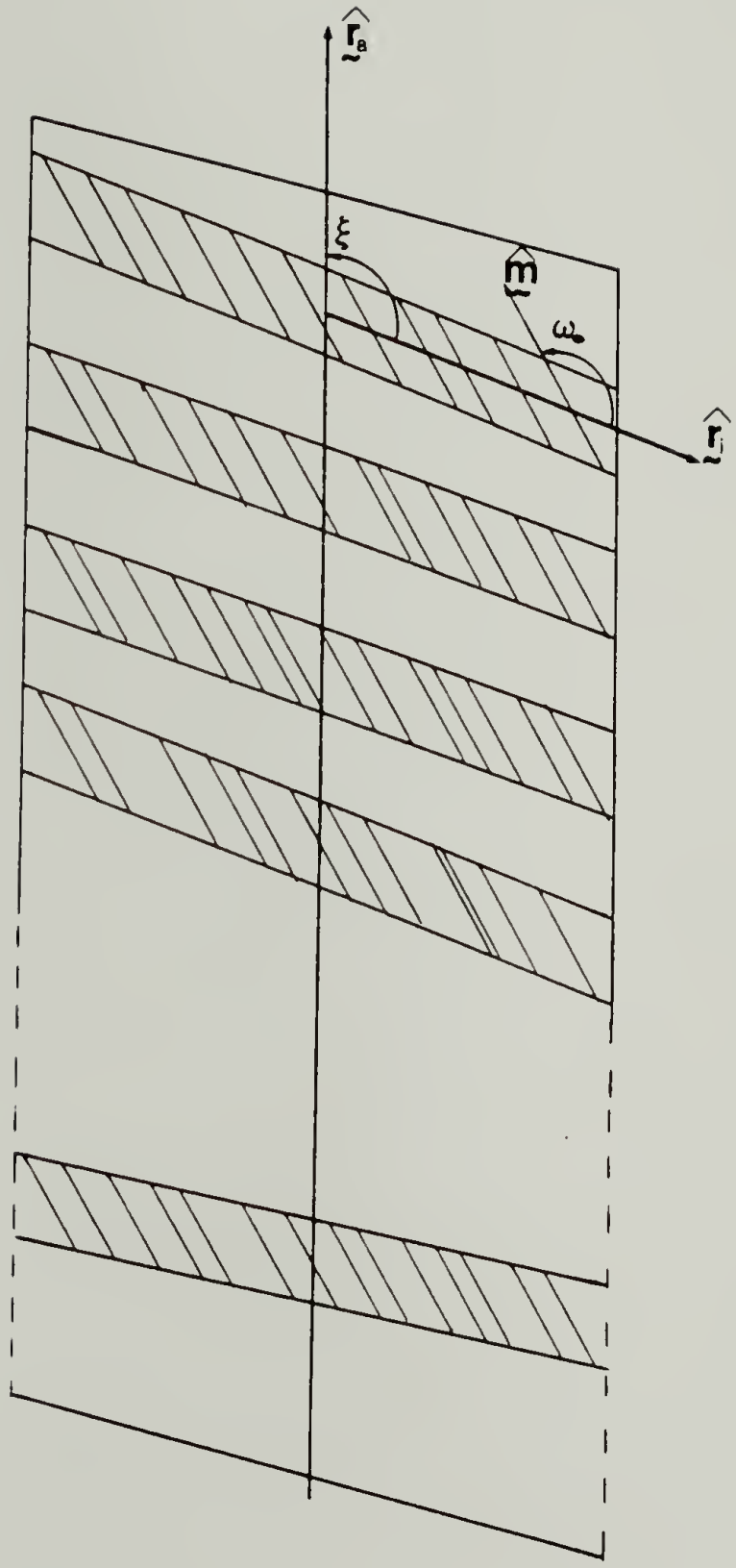

Figure 6-6. Hashimoto model of rod-like anisotropic scattering structure.

C H A P T E R VII

RESULTS OF SMALL ANGLE LIGHT SCATTERING EXPERIMENTS

Introduction

SALS patterns which are circularly symmetric about the incident beam have been observed for the mesophase of a number of main-chain thermotropic PLCs synthesized in this laboratory [101]. In the cases in which such an isotropic scattering pattern is obtained, we feel justified in applying the random orientation approximation. Such scattering behavior has been generally observed in, although is not limited to, selected members of the class of PLCs in which there are triad mesogenic units separated by flexible spacers. The central benzene ring of the triad may or may not contain a small substituent. As detailed in Chapter III, very thin films (<20 μm) which transmit >75% of the incident radiation are cast on microscope cover glasses. Thin samples are required to insure that multiple scattering and scrambling of the polarization with each scattering event can be neglected. This problem has been treated by Rojstaczer [102]. The mesophase is arrived at by heating the sandwiched polymer film at a controlled rate.

Occassionally, and frequently unreproducibly, an anisotropic rod-like pattern is observed at the edge of the

sample. Possible reasons may be sample thickness variation, enhanced mobility due to reduced surface restraints of the cover glass sandwich and annealing effects, degradation, fractionation of lower molecular weight components during the casting process, or orientation due to surface forces. This phenomena constitutes an area of future study.

Annealing of the sample in the mesophase temperature regime over the course of five hours is insufficient to effect a change from an isotropic to an anisotropic scattering pattern. By annealing for longer periods, even when the sample is blanketed by nitrogen, one runs the risk of degrading these high melting PLCs and changing the chemical composition. The potential for sample degradation was a major consideration when choosing members of the homologous series available for study by SALS.

The polymers chosen for study had the most easily accessibly mesophase range (i.e., lowest transition temperatures) yet demonstrated the mesophase behavior of interest: TQT(Br)-10 has a nematic mesophase and fairly simple thermal behavior while HTH-9 has a smectic mesophase and an additional thermal transition. The melting behavior of HTH-9 is not as complicated as that of HTH-12 as discussed in Chapter V, however, and the mesophase occurs at a lower temperature. The type of liquid crystallinity reported for these PLCs, that is, nematic or smectic, was identified by microscopic textural observations and

supported by x-ray diffraction patterns taken of the mesophase. An unoriented nematic LC has only a diffuse halo at wide angles due to liquid-like order between molecular centers of gravity. Smectics display, in addition, a sharper ring at a relatively small angle due to diffraction from the regularly spaced layers.

SALS from a Nematic PLC

TQT(Br)-10 exhibits nematic liquid crystallinity between 140^{o} and 200^{o}C (DSC scan given in Figure 7-1). It was shown by Wang et al. [101] that a circularly symmetric scattering pattern was obtained from thin films of the mesophase of this polymer over the temperature range of 140^{o} to 198^{o}C under both H_v and V_v SALS conditions of polarization. Figures 7-2a and 7-2b show photographic light scattering patterns at various temperatures during the first heating from room temperature to the isotropic state of the film cast from 1,1,2,2-tetrachloroethane and the subsequent cooling process. The scattering pattern of the solution cast film is spherulitic. As with HTH-12, the melting of the crystallites organized in a spherulitic super-structure can be followed by SALS by the change from the four-lobed pattern to the circularly symmetric pattern of the mesophase at 140^{o}C. Over a 58^{o}C temperature range the circularly symmetric scattering pattern is observed both during the

heating and cooling cycles. Azimuthally dependent patterns are evident from 198° to 200°C, immediately prior to isotropization and after deisotropization.

Since the scattered intensity is independent of azimuthal angle between 140° and 198°C, the one-dimensional scan of the scattering pattern available from the OMA-1 apparatus is sufficient. Figures 7-3a and 7-3b are plots of the scattered intensity under H_v and V_v conditions, I_{Hv} and I_{Vv}, versus q at three temperatures, 150°, 170° and 190°C, within this range. V_v scattering is close to the intense incident beam and, for this reason, a beamstop is required which cuts off the scan at small q. I_{Hv} and I_{Vv} are of comparable magnitudes indicating that fluctuations in orientation of anisotropic scattering elements are at least as important a contribution to the scattering by the mesophase as are density fluctuations. Each increment of 20°C in the mesophase region results in a significant decrease in I_{Hv}. Two effects may account for the decrease in intensity. First, there may be less anisotropic scattering material or, secondly, the anisotropy of the scattering structures may be decreasing with increasing temperature. Other experimental techniques must be called upon to differentiate these two effects. By PLOM the mesophase appears to be a single phase throughout most of the mesophase temperature range until the onset of the clearing transition at which point liquid crystalline

and isotropic melt may coexist in thermodynamic equilibrium. It is known from NMR studies that the order parameter in nematic LCs decreases with increasing temperature. Thus, although there may be some effect from the decrease in volume of anisotropic structures especially in the vicinity of the isotropization temperature, the decrease in I_{Hv} is largely due to decrease in the anisotropy of regions which are correlated in orientation.

It is obvious from the curvature in the plots of $(I_{Hv})^{-1/2}$ versus q^2 (Figure 7-4a) that the assumption of an orientation correlation function which is exponential in form (eq. 6-17a, 18a) is incorrect. By extrapolation to zero q in Figure 7-4b, density correlation distances, a_p, (eq. 6-17b, 18b) in the range of 1.4 to 2.0 μm are calculated from I′ versus q data. a_p appears to increase slightly with an increase in temperature.

By taking the Fourier inverse of the H_v scattered intensity versus scattering angle data, the entire orientation correlation function, $p_{12}(r)$, was obtained at the three temperatures (Figure 7-5). The decay in orientation correlation and the correlation distance (estimated by the width at half maximum to be of the order of 1.6 to 1.7 μm) are apparently insensitive to temperature increments throughout the temperature range of the mesophase.

The orientation correlation function differs visibly from the anticipated exponential correlation function by exhibiting slower decay in orientation correlation at small distances of separation. The shape of the function may be described as "pseudo-Gaussian". The significance of the shape of the orientation correlation function will be expanded upon later in this chapter.

Since reciprocal or scattering space and real space have an inverse relationship, the shape of the scattering curve at large q has a significant effect upon the correlation function at small r, the region of interest. The scattering curves obtained in this experiment were artificially truncated by considering fewer data points. This was done to see if the orientation correlation function obtained from such truncated data would differ considerably. Although the width of $p_{12}(r)$ versus r curve did change slightly, the "pseudo-Gaussian" shape was constant. In subsequent SALS experiments, wider angle lenses were employed to reach larger values of q.

The decrease in I_{Hv} as the isotropization temperature is approached is a general observation for all the PLCs studied. However, TQT(Br)-10 exhibits a transformation to non-random orientation when close to the clearing transition (198^{o} to $200^{o}C$) evidenced by the "rod-like" pattern observed at small q. This x-shaped, four-lobed, low intensity H_v pattern has no maxima. Upon cooling from the isotropic melt

which scatters no light under conditions of crossed polarization, the pattern redevelops but is +-shaped. Such a change in the azimuthal angle dependence of scattering signifies that there has been a change in the optic axis orientation from along the rod axis to an angle of 45^{o} from the rod axis. In the temperature region of isotropization, anisotropic fluid and isotropic melt coexist. The anisotropic pattern may result from rod-like structures in an isotropic medium which are analagous to the cybotactic nematic structure described by deVries [103]. The cybotactic nematic phase is essentially a nematic mesophase which contains limited regions of stable smectic-like, layered ordering. One may speculate that such cybotactic nematic structures may act as primary nuclei for the transformation to the liquid crystalline state.

SALS from a Smectic PLC

HTH-9 illustrates the integration of DSC, microscopic and SALS analyses for a smectic PLC. Casting method or thermal prehistory play important roles in the events observed in subsequent DSC scans of many of these polymeric liquid crystalline materials. Figure 7-6 shows the DSC scans of the first heating of solvent-recrystallized HTH-9 from the synthetic laboratory and of second heatings of the polymer slowly cooled at 10^{o}C/min and rapidly quenched at

320°C/min in addition to a cooling curve. A T_g is evident at ~37°C in the second heating curves. In the first heating curve, the T_g may overlap with a low melting endotherm at ~77°C or there may be a negligible amount of amorphous polymer in this semi-crystalline material (evidence: no crystallization exotherm as seen in the second heating curves at 127° and 147°C). An alternate explanation, according to Wunderlich [104], is that the T_g belongs to liquid crystalline, not amorphous, glass which is trapped in a thermodynamically non-equilibrium state. The transition at 140°C shows no super-structural changes by microscopy or SALS although slight sub-structural changes are noted by WAXS; some crystal⇒crystal or crystal⇒ordered smectic transition may account for this endotherm. The major melting peak, T_m, occurs at 150°-175°C and there is a broad isotropization transition, T_i, centered at ~230°C. A large amount of crystallization occurs at 70° undercooling, yet further recrystallization is observed in subsequent heating cycles; as expected, recrystallization during reheating is greater in the quenched sample which would have more amorphous or LC glass "frozen in" than in the slowly cooled sample.

Microscopic and SALS results correlate well with DSC. Figure 7-7a shows the imperfect, radial-growth spherulites, of 10-20 μm radii, that form during the solution casting process. The central portion of the cast film contains

smaller (Figure 7-7b - 5-10 μm) spherulites on which the SALS measurements were performed. The spherulitic superstructure remains constant under the microscope until 152°C at which point there is a slight amount of flow at the edge of the spherulite; the polymer appears to be a soft solid. At 170°C, true melting accompanied with fluidity occurs and the spherulitic boundaries merge and a threaded texture is observed. In the broad region of isotropization two phases, liquid crystalline and amorphous, co-exist; the last fragments of birefringent mesophase have disappeared by 235°C. On cooling, fairly uniformly dispersed regions of mesophase begin to nucleate at 231°C in a fine grained texture which becomes fan-like by 202°C. There is no change in the texture upon cooling below T_m; the spherulitic structure does not reform, but such morphology may be hampered by the strong orienting forces of the glass surfaces on thin films of PLCs.

Figures 7-8 and 7-9 show, photographically and photometrically, the effect of temperature increase on the H_v and V_v small angle light scattering patterns of solution cast HTH-9 films. Photometric data was recorded on the OMA2 apparatus. The four-lobed pattern is evidence of a spherulitic structure. The maxima in θ at $\mu = 45^o$ is not prominent because there is a large distribution of spherulite sizes but corresponds to an average spherulite radius of ~ 5 μm. This pattern remains unchanged until

150°C at which point its definition slowly fades as the pattern becomes more circularly symmetric; at 162° most remnants of the four-lobed pattern are gone. The scattered intensity achieves its highest value at 165°, probably due to perfection of orientational order and greater anisotropy with increasing mobility. Above 165°C there is a steady decrease in intensity with temperature as T_i is approached (Figure 7-10).

The first heating of the solution cast films is non-reproducible since a spherulitic super-structure does not reform on cooling. However, scans of intensity along q exhibit the same behavior during the second heating above T_m (Figure 7-11). The H_v scattered intensity is considerably higher in the second heating scan than in the first heating scan even though the shape of the scattering patterns are very similar above T_m. Formation of the mesophase from the low viscosity isotropic phase probably allows regions of higher orientational order and anisotropy, at a given temperature, than if approached from the high viscosity solid phase.

Although not exactly alike, the orientational correlation functions obtained from the H_v data of the first (Figure 7-12) and second heating (Figure 7-13) cycles show similar trends. At a value of $p_{12}(r) = 0.5$, the orientational correlation lengths increase slightly with increasing temperature up to 166°C. a_o ranges from 1.1 to

1.3 μm in the first heating and 1.3 to 1.6 μm in the second. It appears in the process of slowly cooling from the isotropic state, higher orientational order is achieved. This might be expected purely from annealing and perfection of crystalline regions considerations of a semi-crystalline solid between T_g and T_m. Above T_m, the correlation length for orientation fluctuations also increases with temperature until ~204^oC at which temperature it begins to decrease: as energy is added to the system in the biphasic region of isotropization, the parallel alignment of mesogenic units becomes less perfect and the region over which alignment persists becomes smaller until, at T_i, the orientational correlation should have the same form as any isotropic melt. The subsidiary maximum at approximately 4 μm in the orientation correlation function of the first heating shows that there is memory of structure from the precursor crystalline spherulites. In order for this residual structure to be dissipated in a short time interval, the sample must achieve the more fluid state of the isotropic melt; the maxima is not observed in the curves of the subsequent heatings or coolings.

Domain Model to Simulate the Orientation Correlation Function

An exponential and a Gaussian function given by

$$f_e(r) = \exp -(r/a_e) \qquad (7\text{-}1a)$$

$$f_g(r) = \exp -(r^2/a_g^2), \qquad (7\text{-}1b)$$

where a_e and a_g are the respective correlation distances differ in appearance at small values of r (Figure 7-14). The exponential function decays rapidly and is concave everywhere whereas the Gaussian function decay is slower, that is, more "flat-topped", and is convex from the start. The mathematical expressions for the slopes are given in Appendix A.

Stein and Stidham [100] have given an exact mathematical justification for exponential decay of the orientation correlation function in one-dimension. Consider a linear array of uniaxial, anisotropic scattering elements separated by a distance, d (Figure 7-15a). Let the scatterer located at the origin be oriented at 0^o with respect to the vertical direction. The principal axis of the adjacent scatterer tends to be parallel but is misaligned by a small angle of $+\beta$ or $-\beta$ with equivalent probabilities of 1/2. The correlation function obtained from such a model is exponential with a correlation distance of

$$a_e = \frac{1}{2}\left(\frac{d}{\beta^2}\right) \qquad (7\text{-}2a)$$

This first order Markov statistics problem in one dimension has been extended to three dimensions by allowing the adjacent scatterer to be misaligned with respect to the orientation of its first neighbor about a cone of apex angle, β, and where the azimuthal angle, ϕ, takes all values with equal probability. The correlation distance in this case becomes

$$a_e = \frac{2}{3}\left(\frac{d}{\beta^2}\right) \qquad (7\text{-}2b)$$

Consider the extreme of a system which exhibits long-range perfect orientation of the scatterers (Figure 7-15b). The value of $\theta_{12} = 0^o$ for all r and the orientation correlation function $p_{12}(r)$ will be linear with a constant value of 1 and a slope of 0 for all r. The correlation distance in this case is infinite. The other extreme is a system where there is no orientation correlation in which case the correlation distance is 0.

The "pseudo-Gaussian" shaped orientation correlation function curve obtained experimentally appears to represent fairly perfect correlation in orientation at small r with more rapid decay in correlation as the distance of separation of two scatterers increases. This is consistent with either the sharp-boundaried or diffuse boundaried models of the mesophase super-structural morphology but not with the continuously changing orientation of mesogens which would give rise to exponential decay (Figure 6-2). Thus, we

present a simple model to simulate the observed experimental orientation correlation function, $p_{12}(r)$. The theory has been generalized to take account of the preference for parallel alignment of neighboring scattering elements by considering, in one dimension, values of θ_{12} of $-\beta$, 0, $+\beta$ which occur with probabilities of $\alpha/2$, $(1 - \alpha)$, $\alpha/2$, respectively.

To illustrate the point, let us consider the simplest example of a sharp-boundaried domain model. Within one domain the mesogens have a fairly narrow distributions of orientations centered about $\theta_{12} = 0^{o}$ and the intra-domain orientation correlation function is $f(r)_{intra}$. The domains are all the same size and contain n mesogens, their centers separated by a distance d. Thus, the size of each domain is $D = nd$. Furthermore, D is the distance between the centers of two adjacent domains. The average orientation of a domain is represented by its director, $\hat{n}$, located at the center of the domain.

Allow the directors of neighboring domains to be misaligned by the angle $-\beta$, 0 or $+\beta$. Thus, the inter-domain correlation distance or correlation distance of the directors becomes

$$a_{inter} = \frac{D}{2\alpha\beta^2} \qquad (7\text{-}3a)$$

$$= \frac{nD}{2\alpha\beta^2} \qquad (7\text{-}3b)$$

When $r > D$, the two mesogens must reside in different domains and for these long-range correlations, the correlation of the mesogens becomes that of the directors of their respective domains. When $r \leq D$, two mesogens have a finite probability of being in the same domain. The probability for being in the same domain has been given by Vonk [105] as:

$$P(r) = \frac{D - r}{D} \quad \text{if } r \leq D \text{ and}$$

$$= 0 \quad \text{if } r > D. \qquad (7\text{-}4)$$

If mesogen 1 and mesogen 2 are in the same domain

$$p_{12}(r) = f(r)_{intra}, \qquad (7\text{-}5a)$$

while if in different domains

$$p_{12}(r) = f(r)_{inter} = \exp -(r/a_{inter}). \qquad (7\text{-}5b)$$

The general form for the composite orientation correlation function is

$$p_{12}(r) = [P(r)]\, f(r)_{intra} + [1 - P(r)]\, f(r)_{inter}. \qquad (7\text{-}6)$$

Substituting eq. 7-4 in eq 7-6, one obtains

$$p_{12}(r) = \left[\frac{D-r}{D}\right] f(r)_{intra} + \left[\frac{r}{D}\right] f(r)_{inter}. \qquad (7\text{-}7)$$

Assume, for the sake of simplicity, that within a domain the distribution of θ_{12}'s is a delta function (Figure 7-15c). In other words there is perfect order expressed as $f(r)_{intra} = 1$. Then, upon rearrangement

$$p_{12}(r) = \left[1 - \left(\frac{r}{D}\right)\right] \left[1 - f(r)_{inter}\right]. \qquad (7\text{-}8)$$

Substituting an exponentially decaying orientation correlation function of domain directors, eq. 7-8 becomes

$$p_{12}(r) = \left[1 - \left(\frac{r}{D}\right)\right] \left[1 - \exp -\left(\frac{r}{a_{inter}}\right)\right]. \qquad (7\text{-}9)$$

The synthesis of the linear and exponential functions resulting in a "pseudo-Gaussian" orientation correlation function is shown schematically in Figure 7-16. Observe that parallel alignment dominates at small distance of separation of two mesogens while at separations greater than the size of the domain exponential decay dominates the shape of the curve. Eq. 7-9 has the correct limiting value of $p_{12}(0) = 1$. Comparison of the slope of the composite curve with an exponentially decaying and a Gaussian decaying function is given in Appendix A.

A fit of eq. 7-9 to the experimentally obtained $p_{12}(r)$ may be made by choosing reasonable values for the domain size, D, and the correlation distance of domain directors a_{inter}. Figure 7-17 shows a series of curves in which the domain size is held constant at 1μm and the a_{inter} is varied from 1 μm to 10 μm. In Figure 7-18 a_{inter} was set at a value of 1 μm and D was varied from 0.1 μm to 1 μm. The best fit of the data is when D and a_{inter} are of the same order of magnitude and approximately 1 to 2 μm.

To extend the theory to three dimensions, we approximate the domains as spheres of equal size, radius R. The

probability that two scattering elements, a distance r apart, will be located in the same sphere is given as [106]

$$P(r) = 1 - (3/4)\,(r/R) + (1/16)(r/R)^3. \qquad (7\text{-}10)$$

The equation analogous to the one dimensional case (eq. 7-9) is

$$p_{12}(r) = 1 - \left[\left(\frac{3}{4}\right)\left(\frac{r}{D}\right) - \left(\frac{1}{16}\right)\left(\frac{r}{D}\right)^3\right]\left[1 - \exp -\left(\frac{r}{a_{inter}}\right)\right] \qquad (7\text{-}11)$$

which behaves similarly to the one dimensional function.

Certainly the assumptions of perfect orientation correlation among mesogens within a domain, a monodisperse distribution of domain sizes and the sharp-boundaried domain premise are severe simplifications. Distributions of orientations and domain sizes and the inclusion of a transition zone between domains would generalize the description. However, the point is made that to account for the shape of the experimentally observed $p_{12}(r)$, extended regions of roughly parallel orientation must exist, rather than a continuously changing orientation of mesogenic axes which would give rise to an exponentially decaying function.

Summary

Small angle light scattering techniques may be used to understand the morphology of the liquid crystalline state and to obtain a statistical description of the orientational order of the mesophase. By making the random orientation

approximation and obtaining correlation functions from the scattered intensity, one is able to compare the effect of temperature and mesophase order on density and orientation fluctuations. In the case of a nematic PLC the correlation length for orientation was smaller than that for density fluctuations and both correlation distances increased slightly with temperature. For the smectic PLC orientational correlation lengths increased over a temperature range at which annealing took place and throughout most of the mesophase range but decreased over the temperature range of very fluid mesophase as the clearing temperature was approached. The correlation lengths were of the order of 1 to 2 μm's and may be considered to be statistical approximations of the "domain" structure size.

By using a two-parameter model, based upon the sharp-boundaried domain description and in which intra-domain and inter-domain correlation distances between domain directors are taken into account, the "pseudo-Gaussian" shape of the experimental orientation correlation function may be simulated.

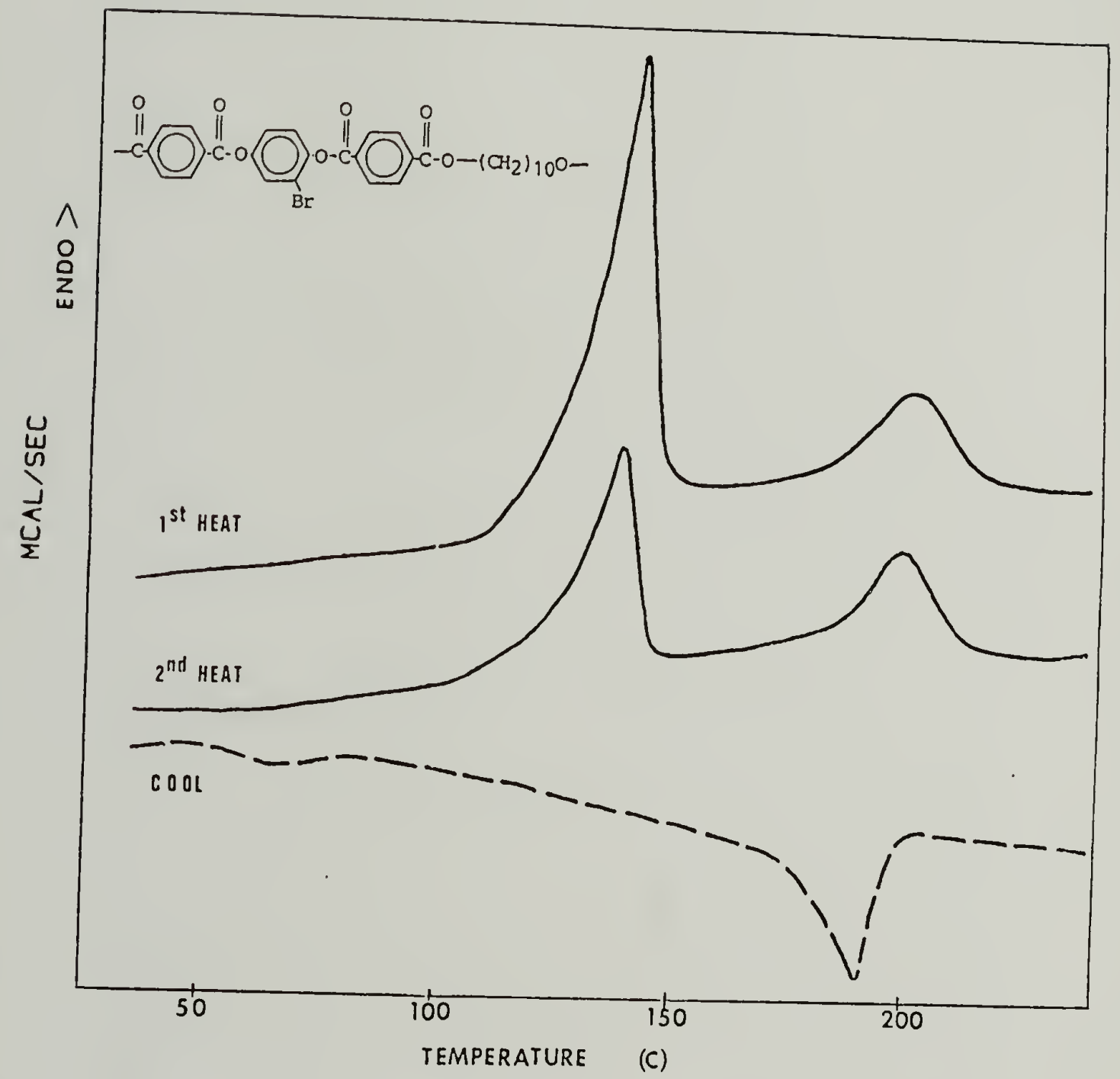

Figure 7-1. DSC scans of TQT(Br)-10.

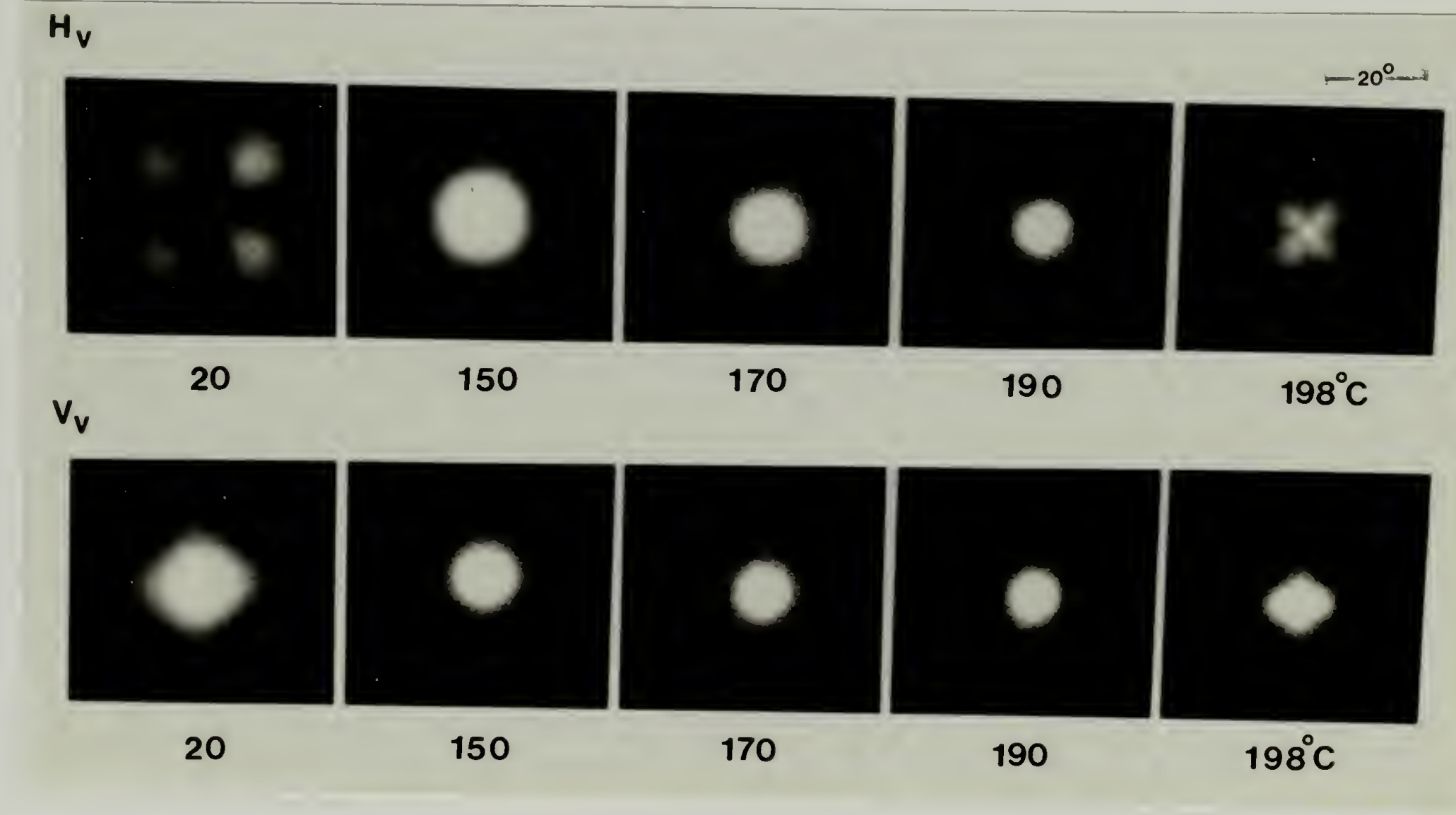

Figure 7-2. Photographic SALS pattern of TQT(Br)-10 a) heating cycle

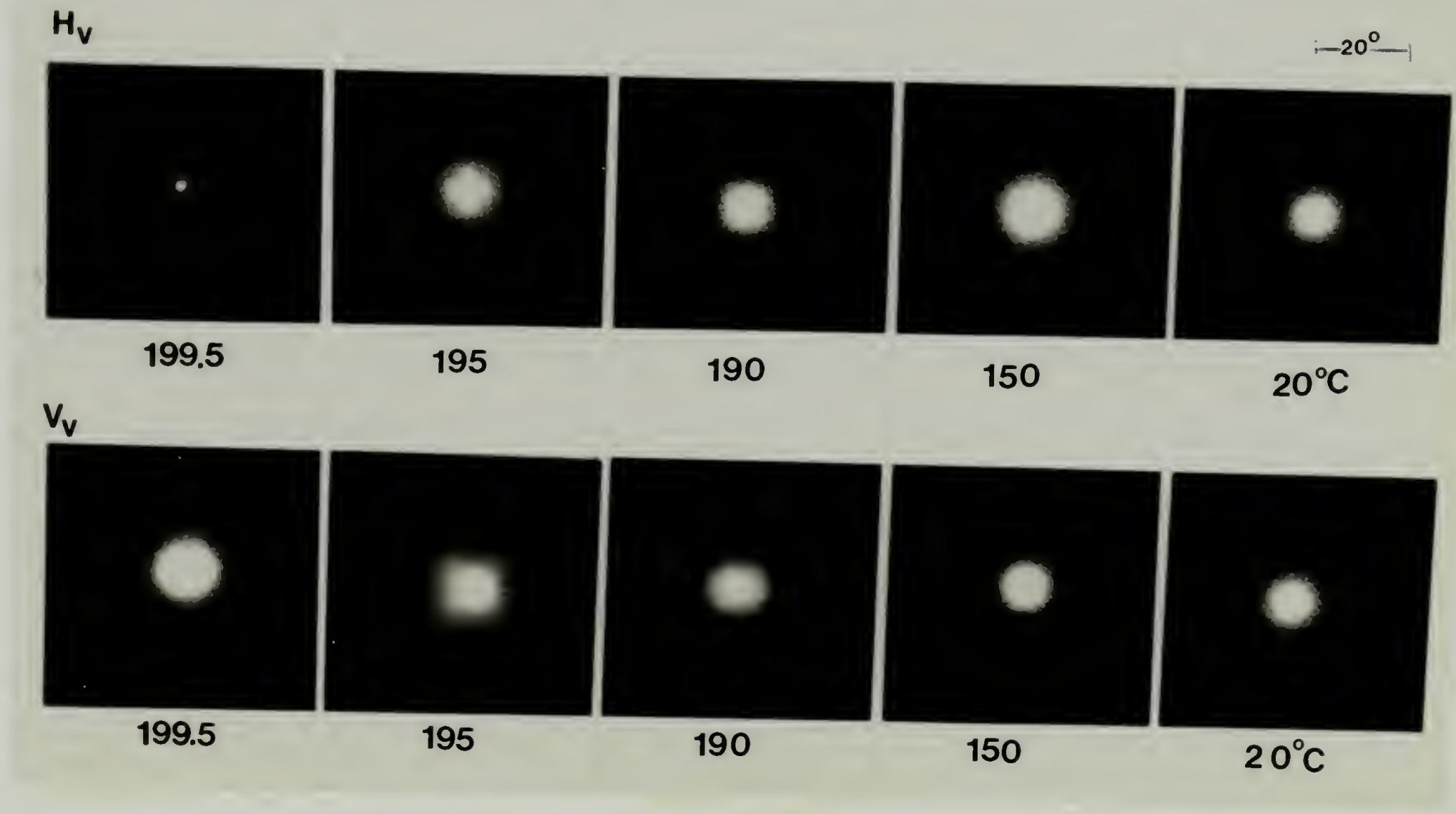

Figure 7-2. b) cooling cycle.

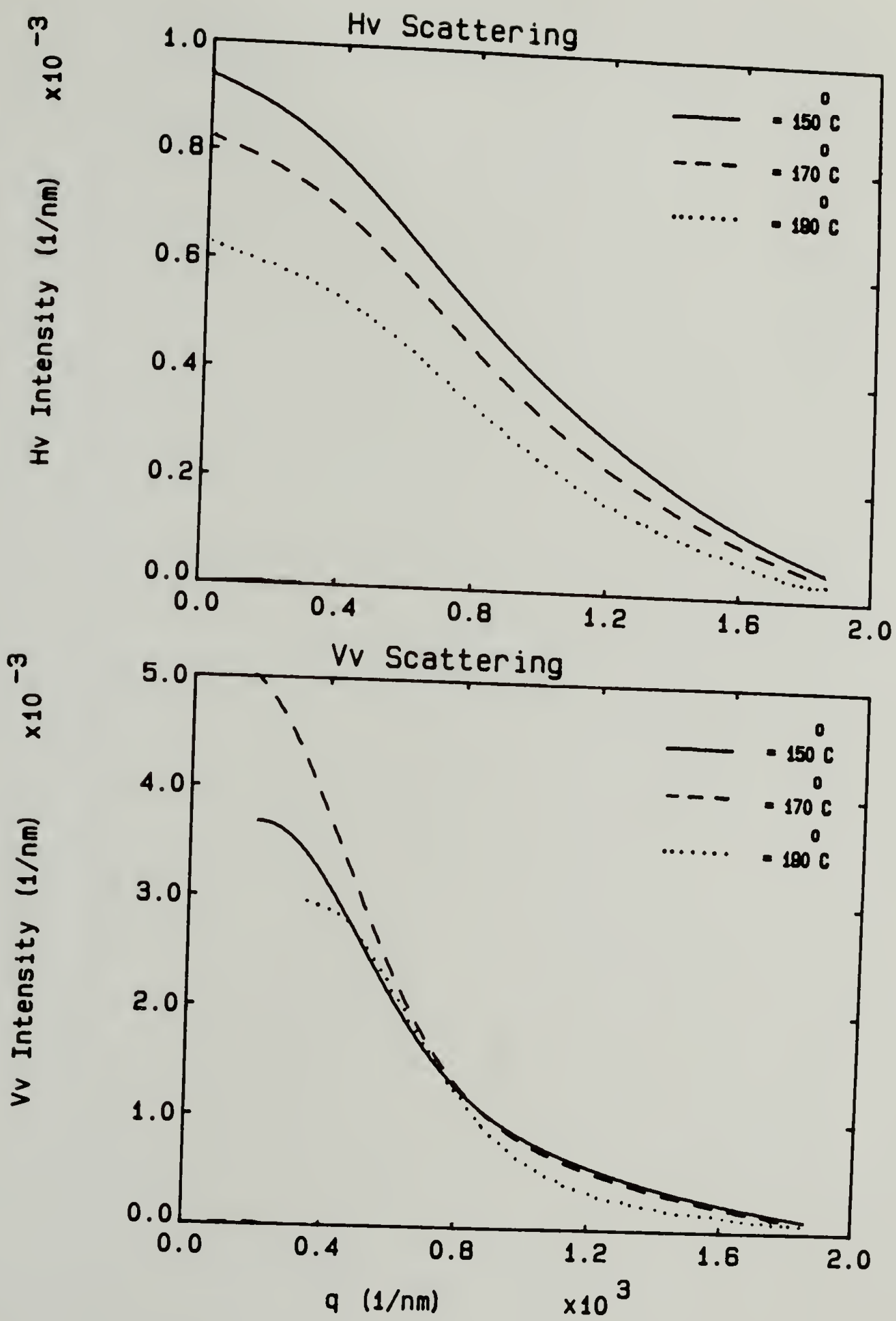

Figure 7-3. Intensity vs q at three temperatures under H_v and V_v conditions.

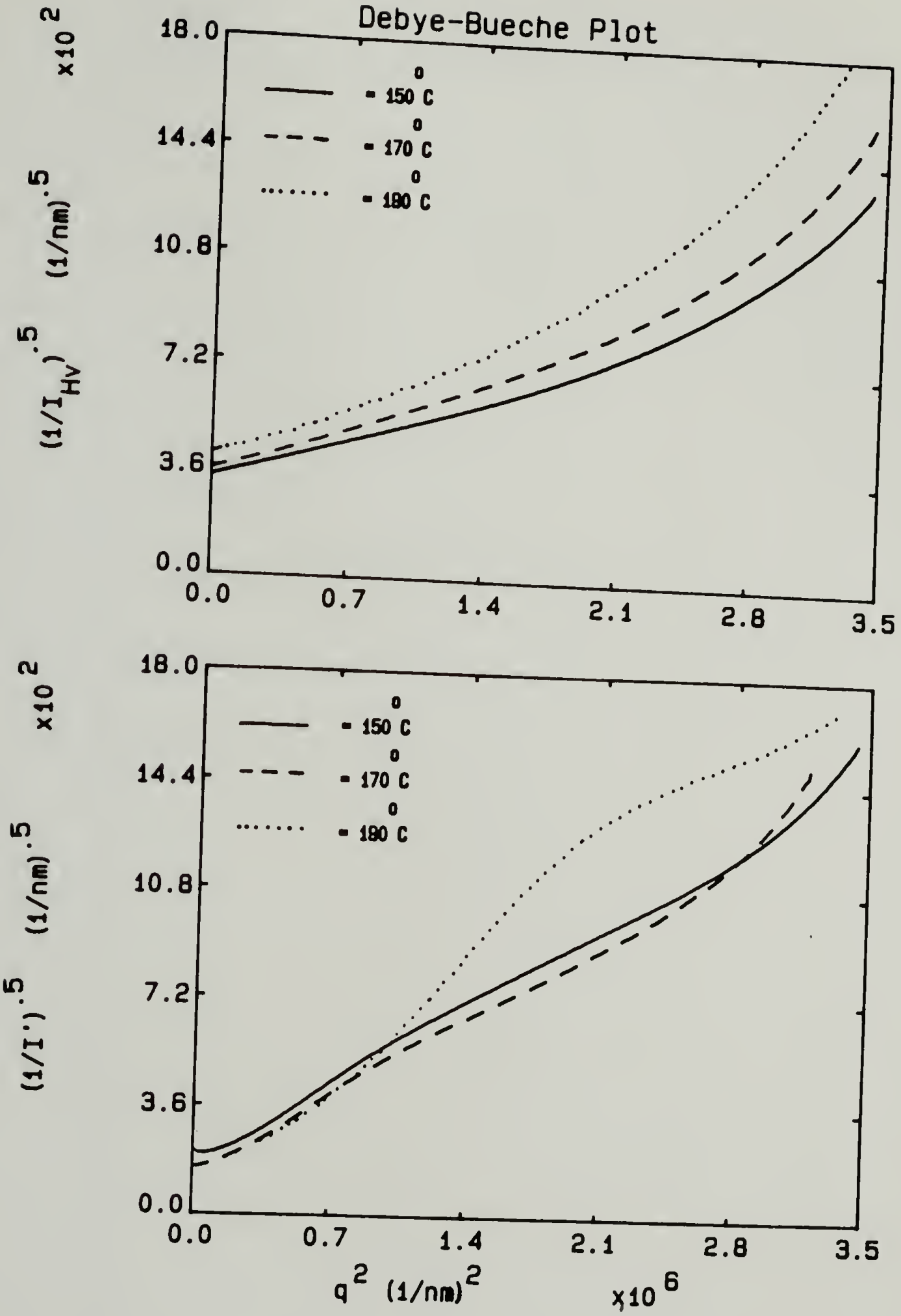

Figure 7-4. Debye-Bueche plots:
a) $(I_{Hv})^{-1/2}$ vs q^2 and b) $(I')^{-1/2}$ vs q^2.

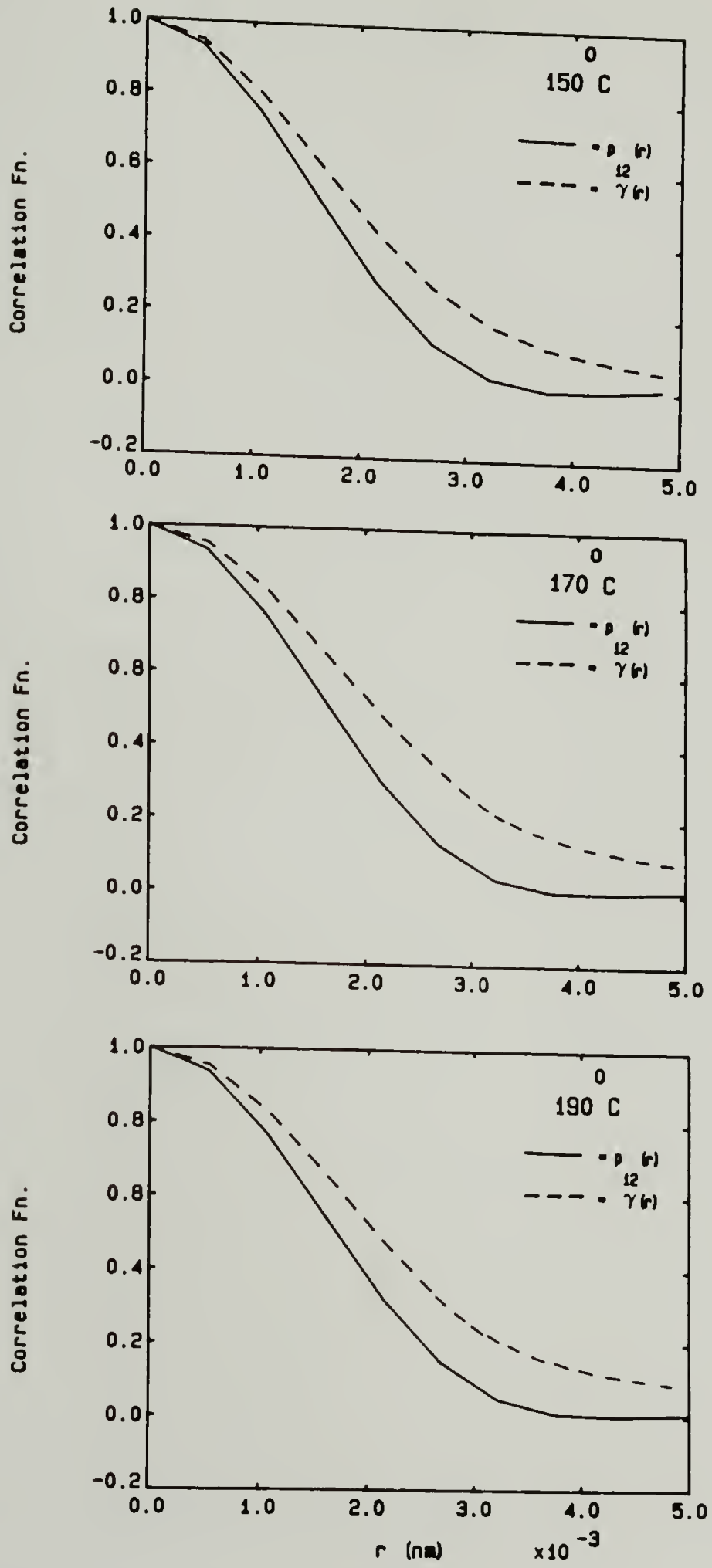

Figure 7-5. Average polarizability $\gamma(r)$ (dash) and orientational $p_{12}(r)$ (solid) correlation function curves for mesophase of TQT(Br)-10 at 150^{o}, 170^{o} and $190^{o}C$.

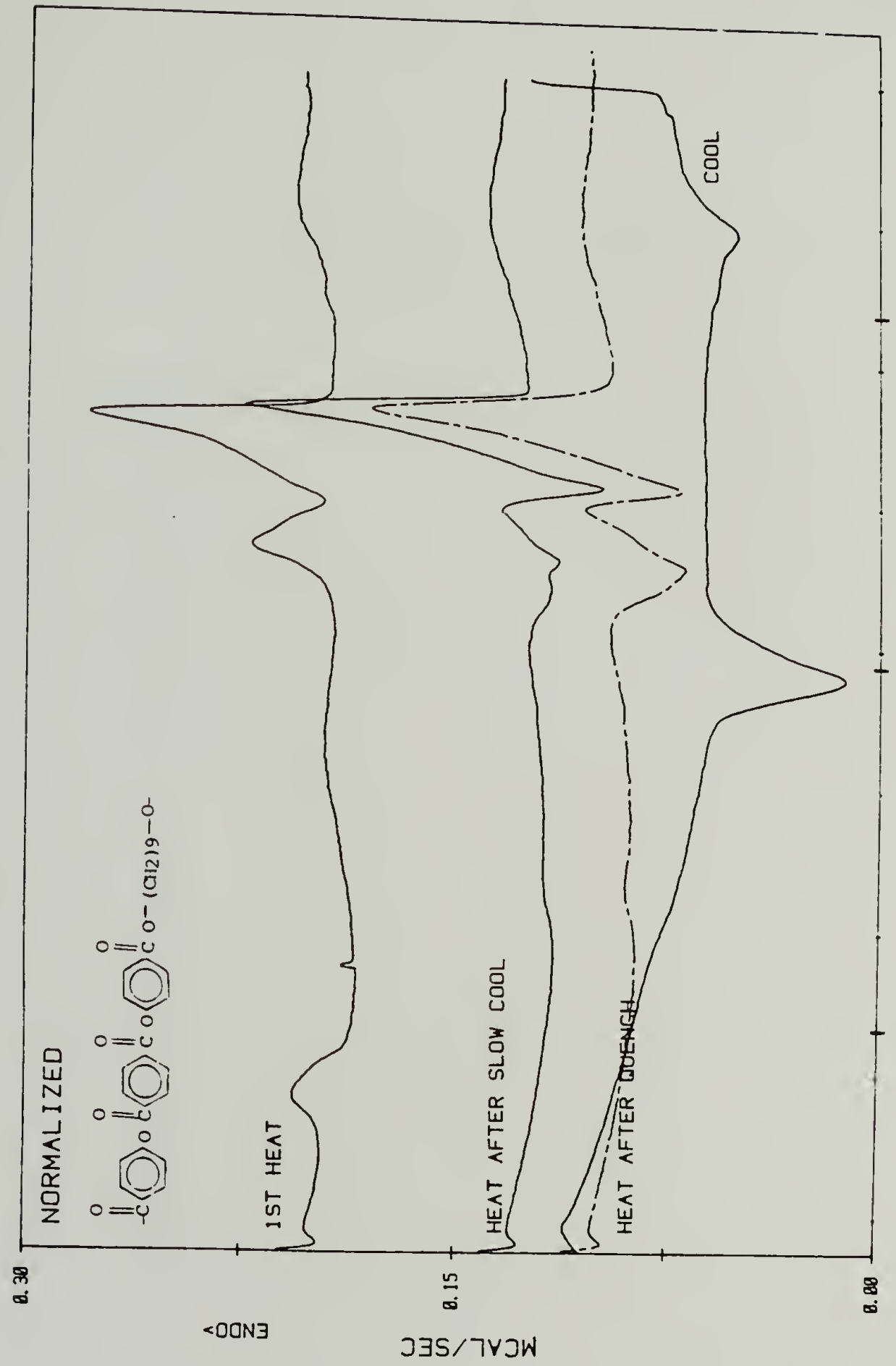

Figure 7-6. DSC scans of HTH-9.

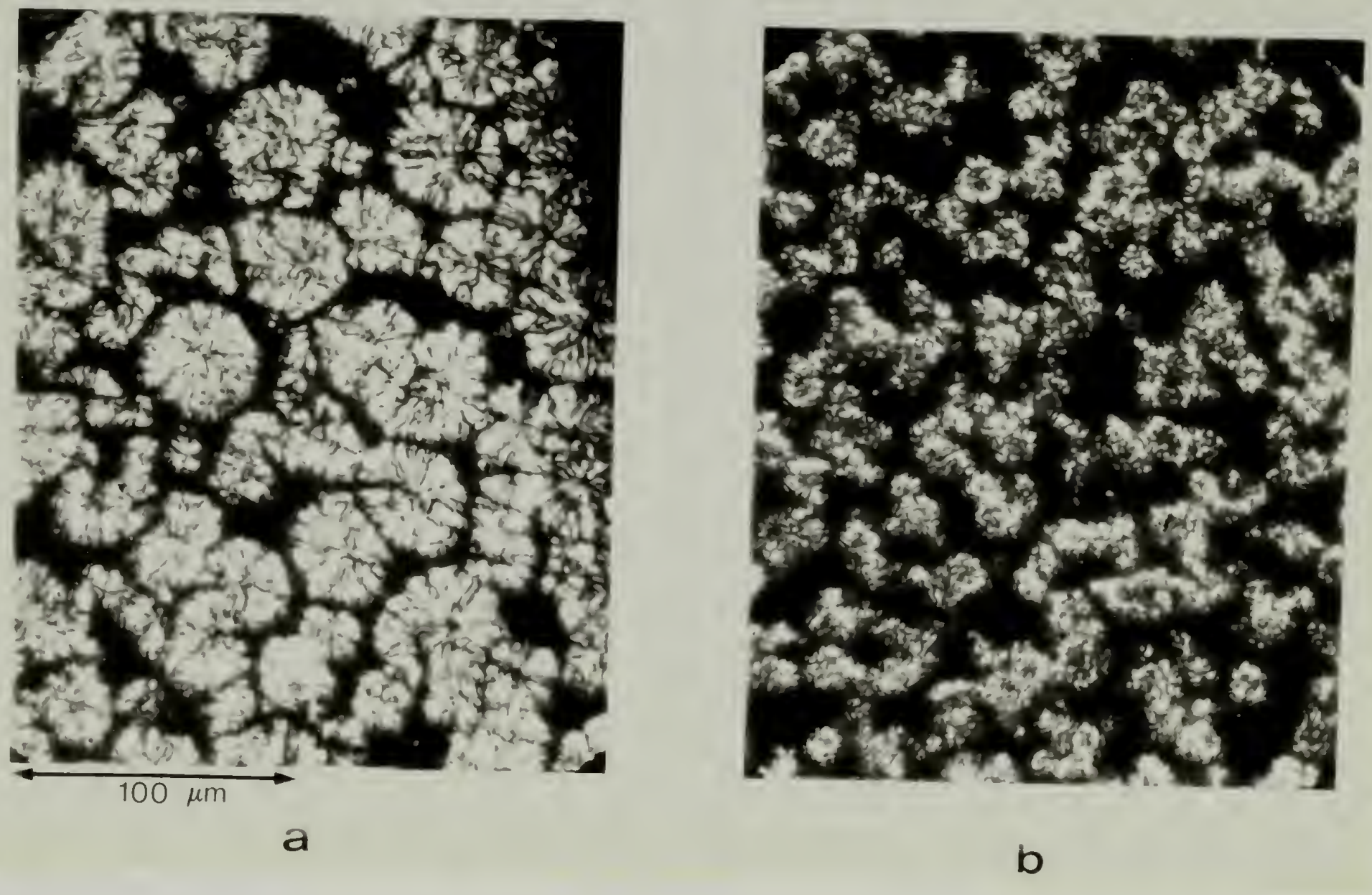

Figure 7-7. Micrographs under crossed polars of solution cast HTH-9 films at a) 30°, large spherulites toward edge of film, b) 30°, small spherulites from center of film,

c

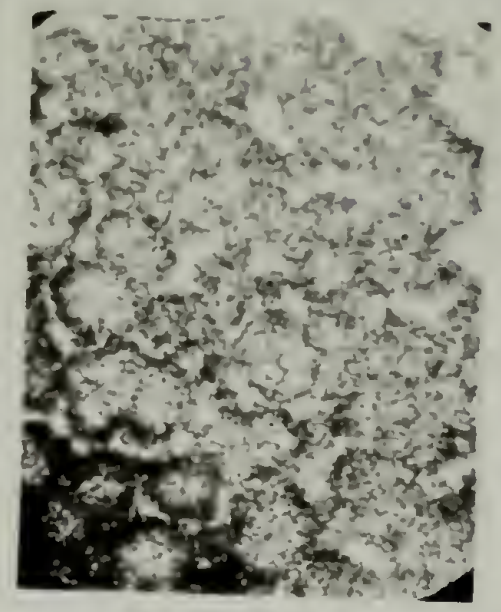

d

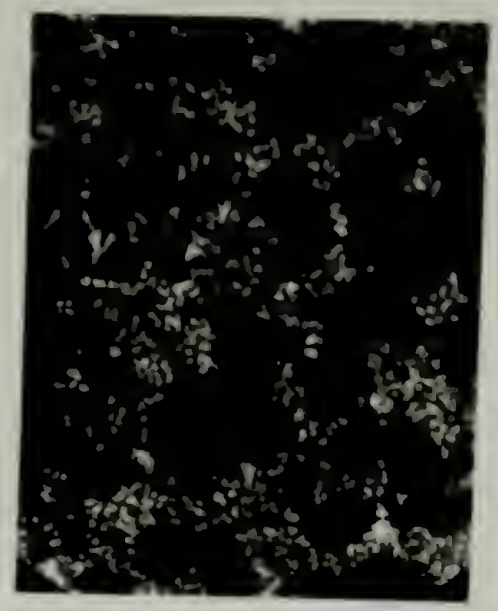

e

g

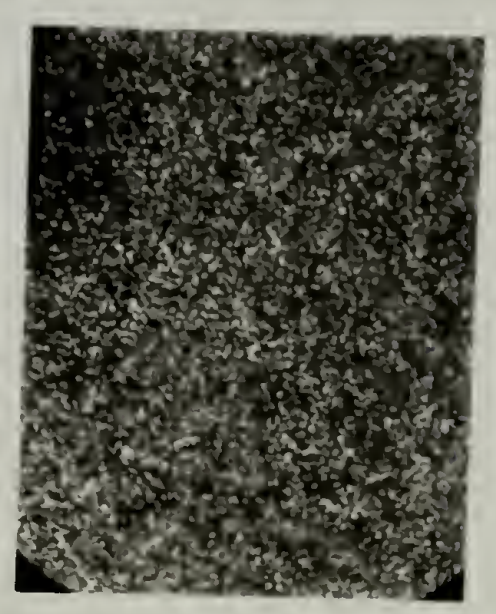

f

Figure 7-7. c) 140^{o}, d) 177^{o}, e) 220^{o}, f) 220^{o} (upon cooling) and g) 205^{o} C (upon cooling).

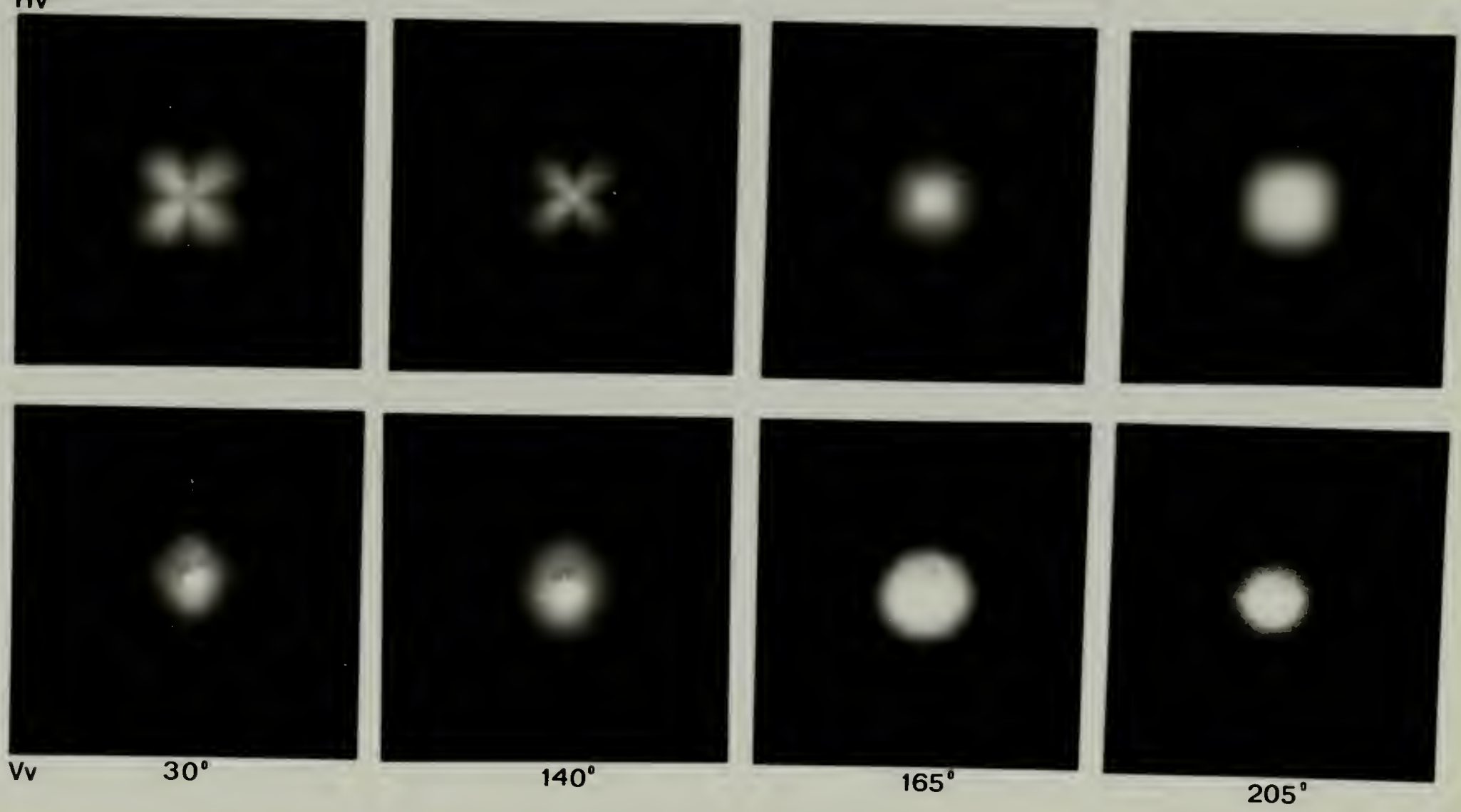

Figure 7-8. Photographic H_v and V_v SALS patterns of HTH-9 at various temperatures in the first heating cycle.

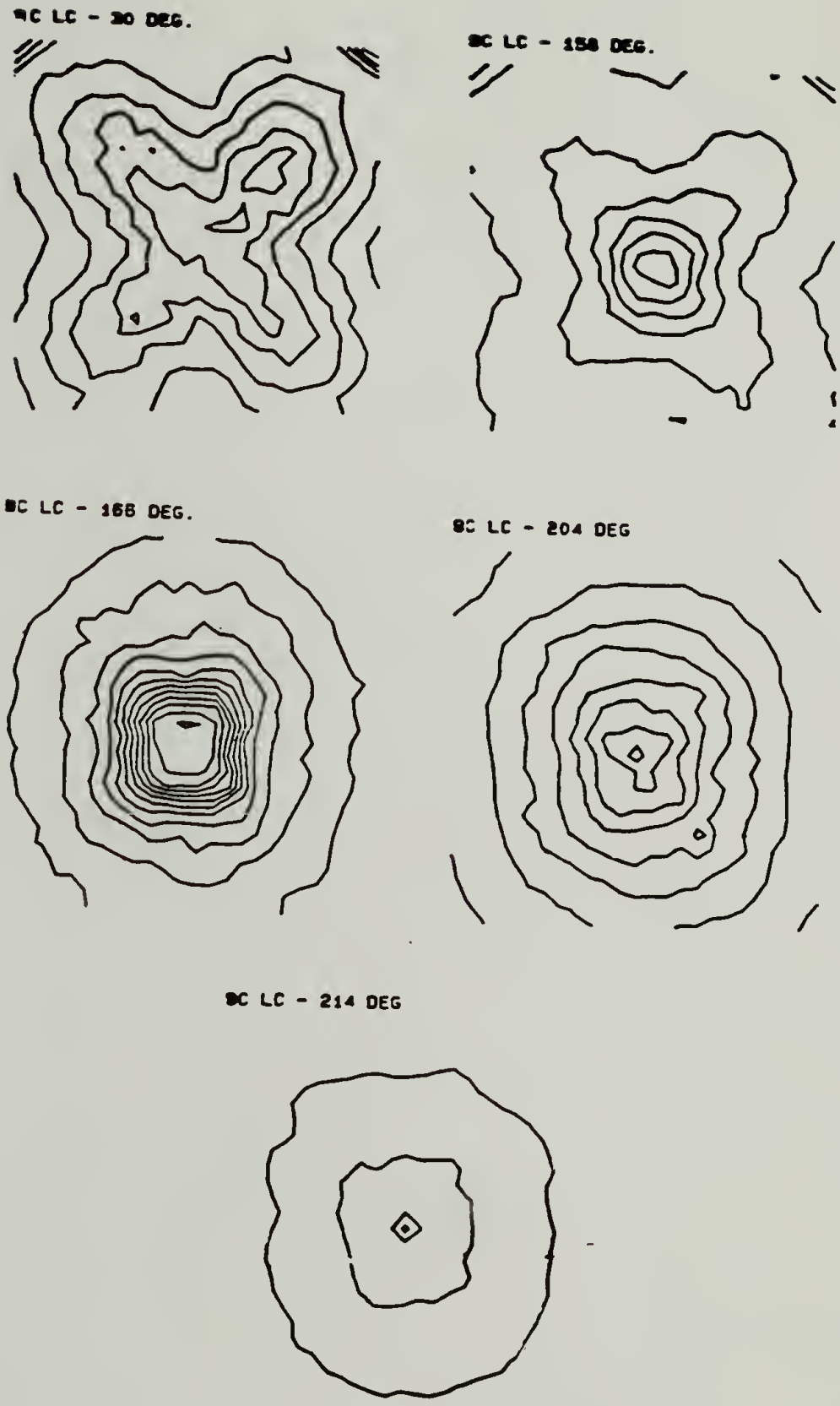

Figure 7-9. H_V isointensity contour plots of SALS data of HTH-9 at various temperatures during the first and second heating cycles.

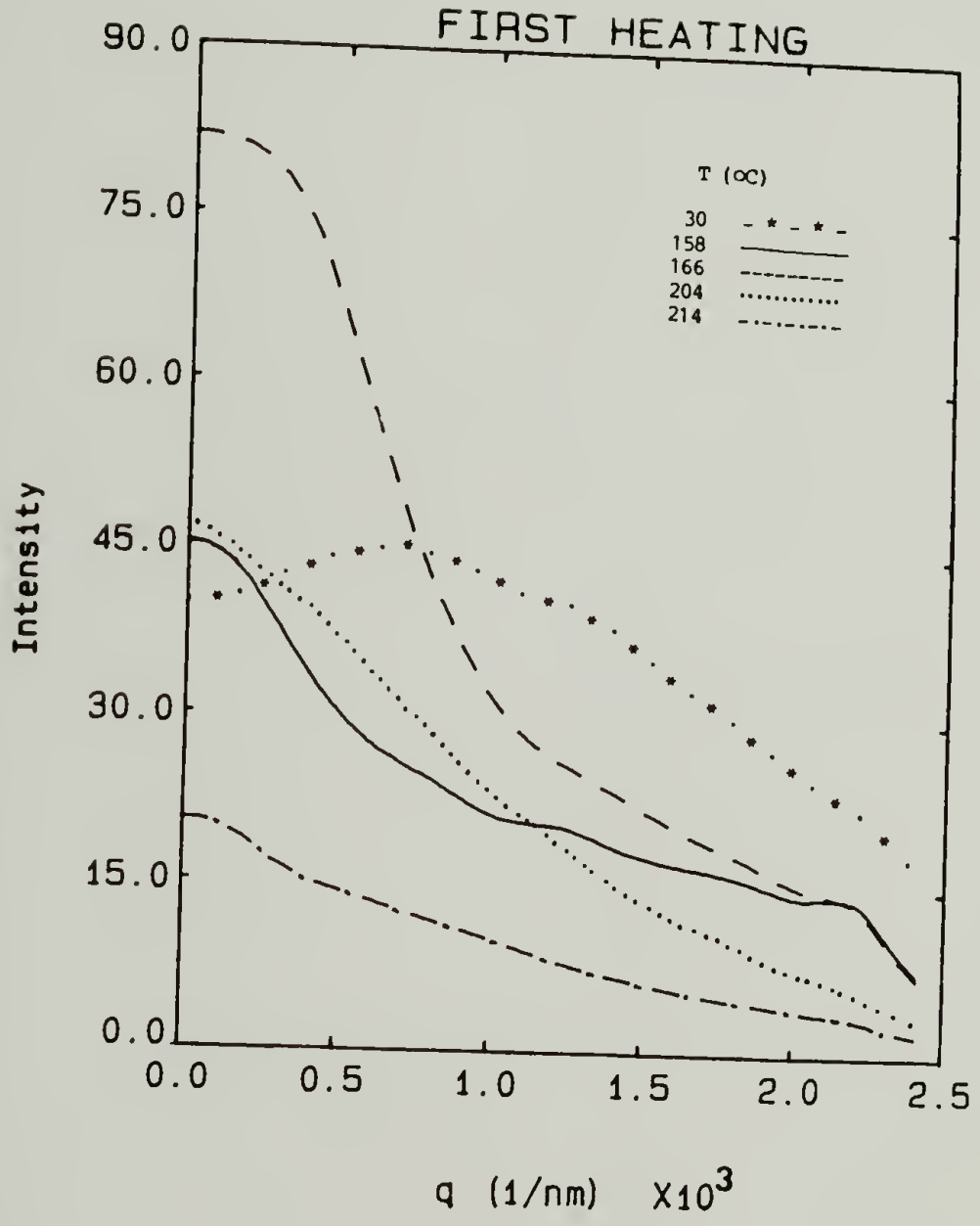

Figure 7-10. Intensity as a function of q at $\mu=45^{o}$ for first heating of HTH-9.

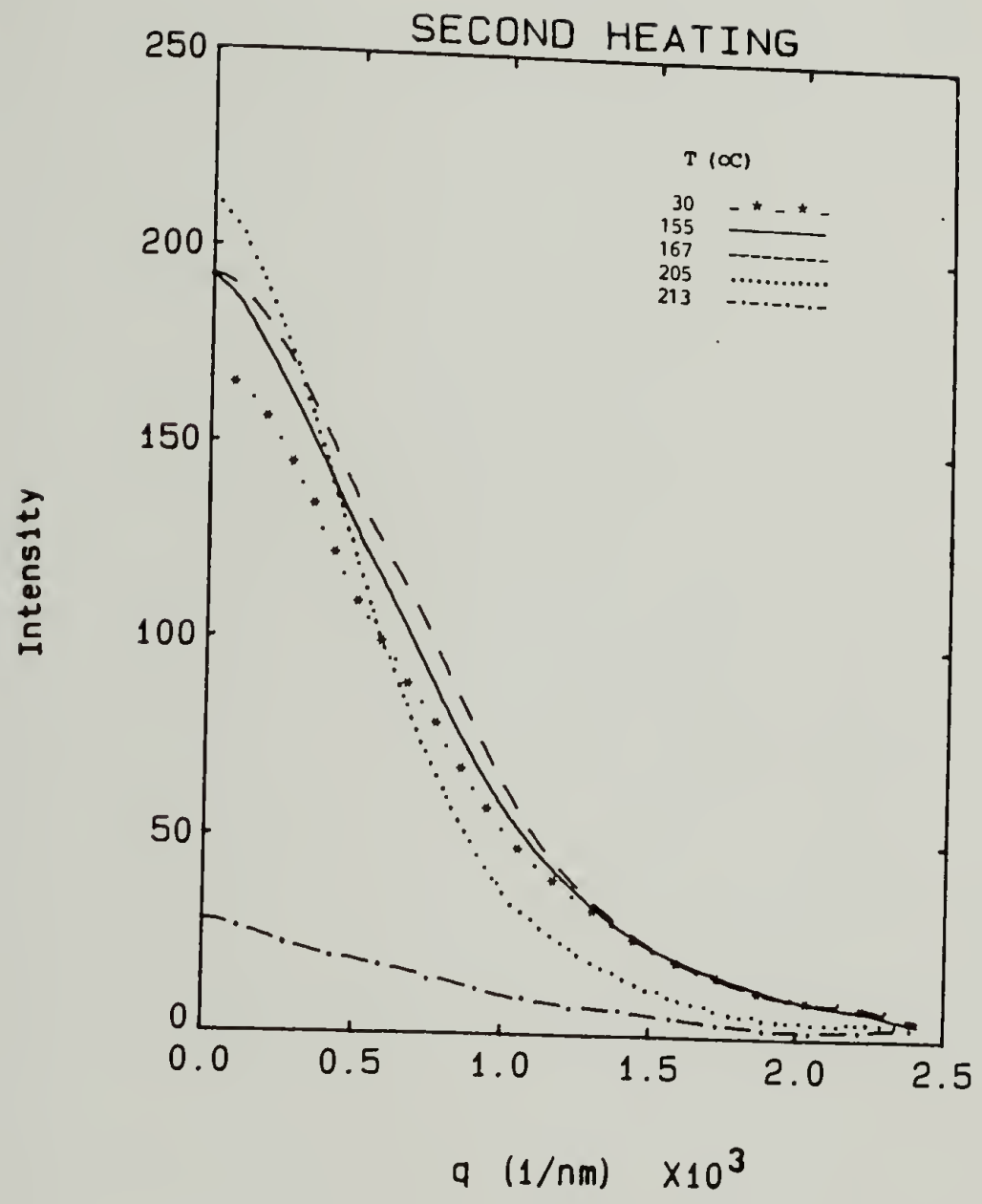

Figure 7-11. Intensity as a function of q at $\mu=45^{o}$ for the second heating of HTH-9.

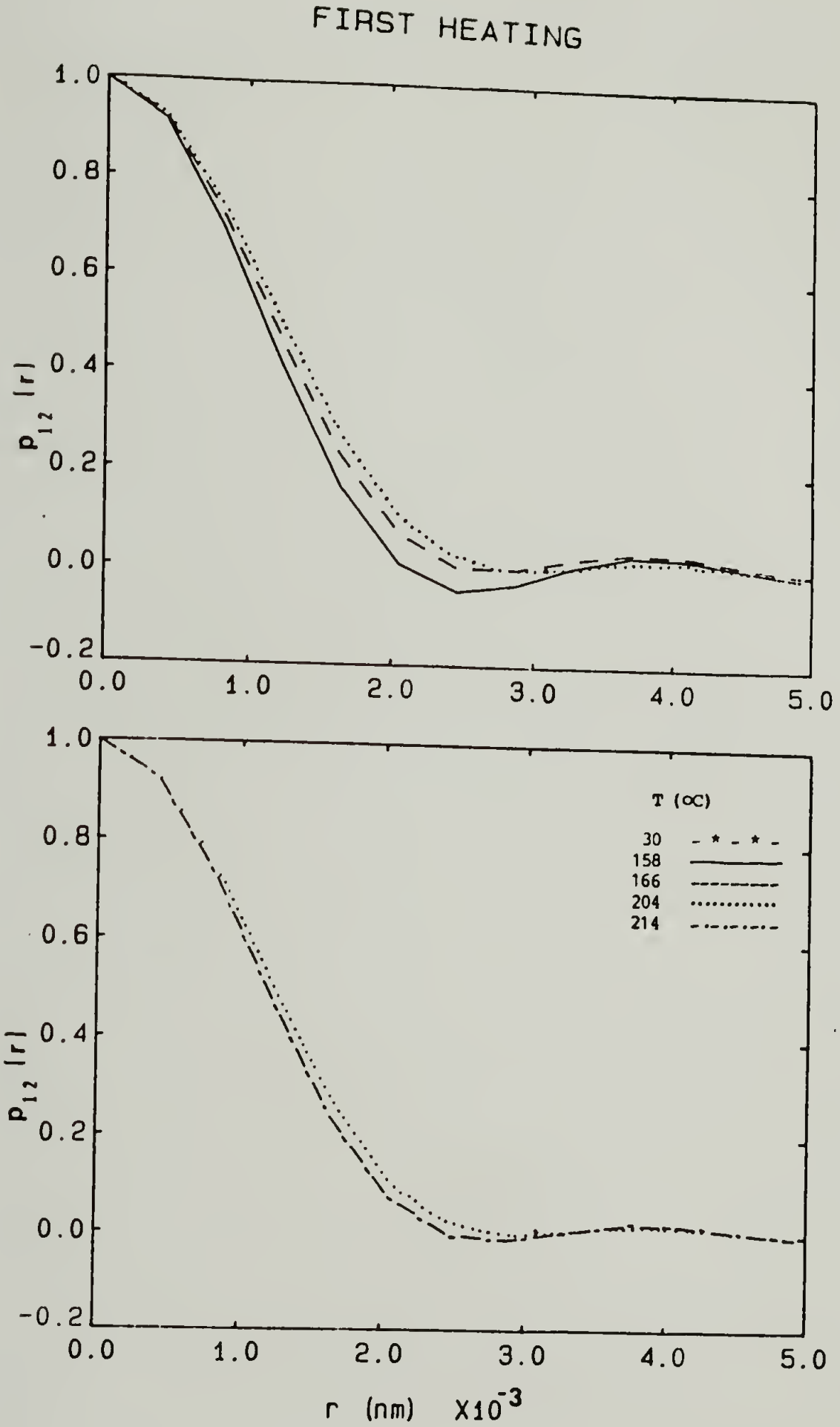

Figure 7-12. Orientational correlation function at various temperatures during first heating.

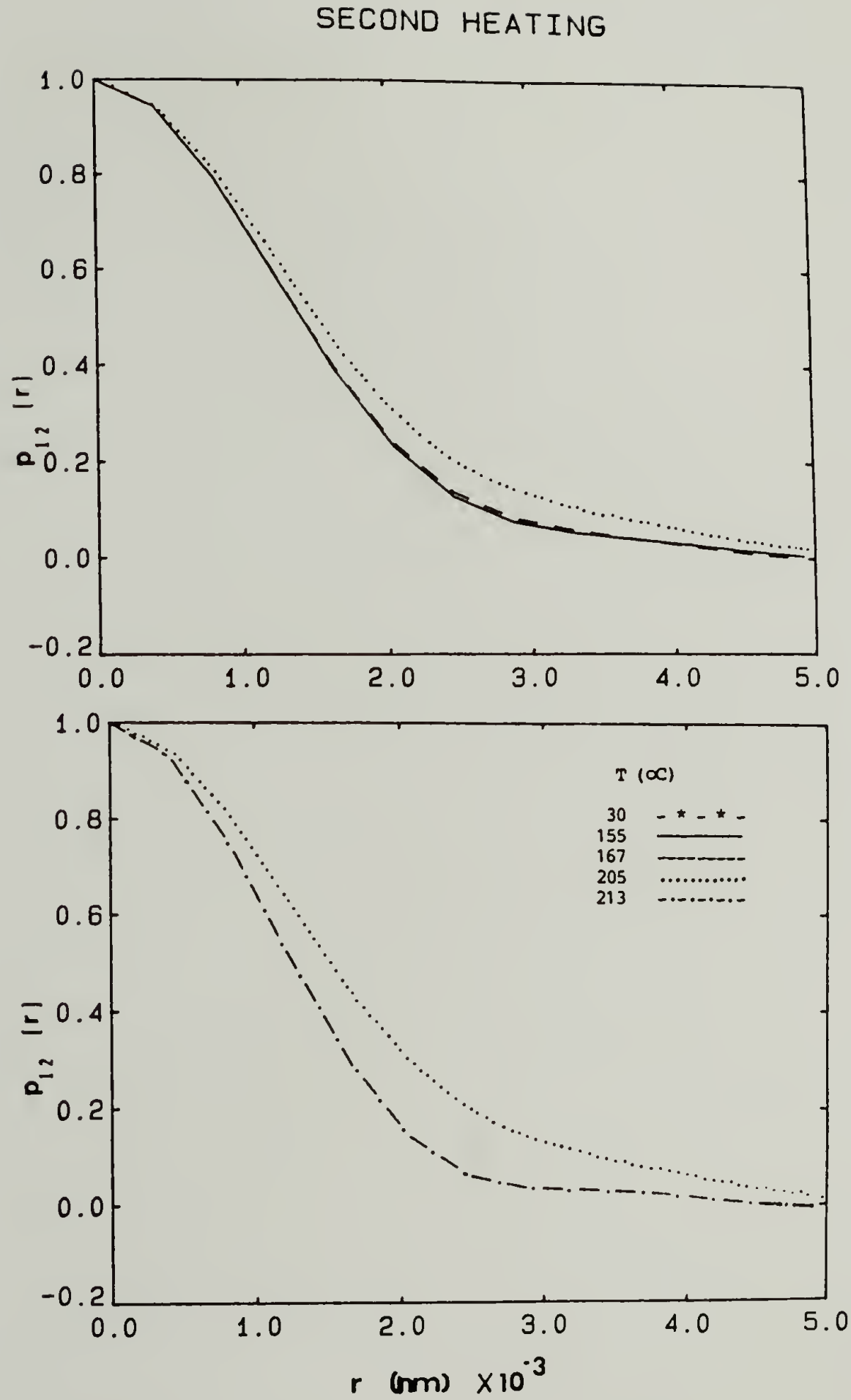

Figure 7-13. Orientational correlation function at various temperatures during second heating.

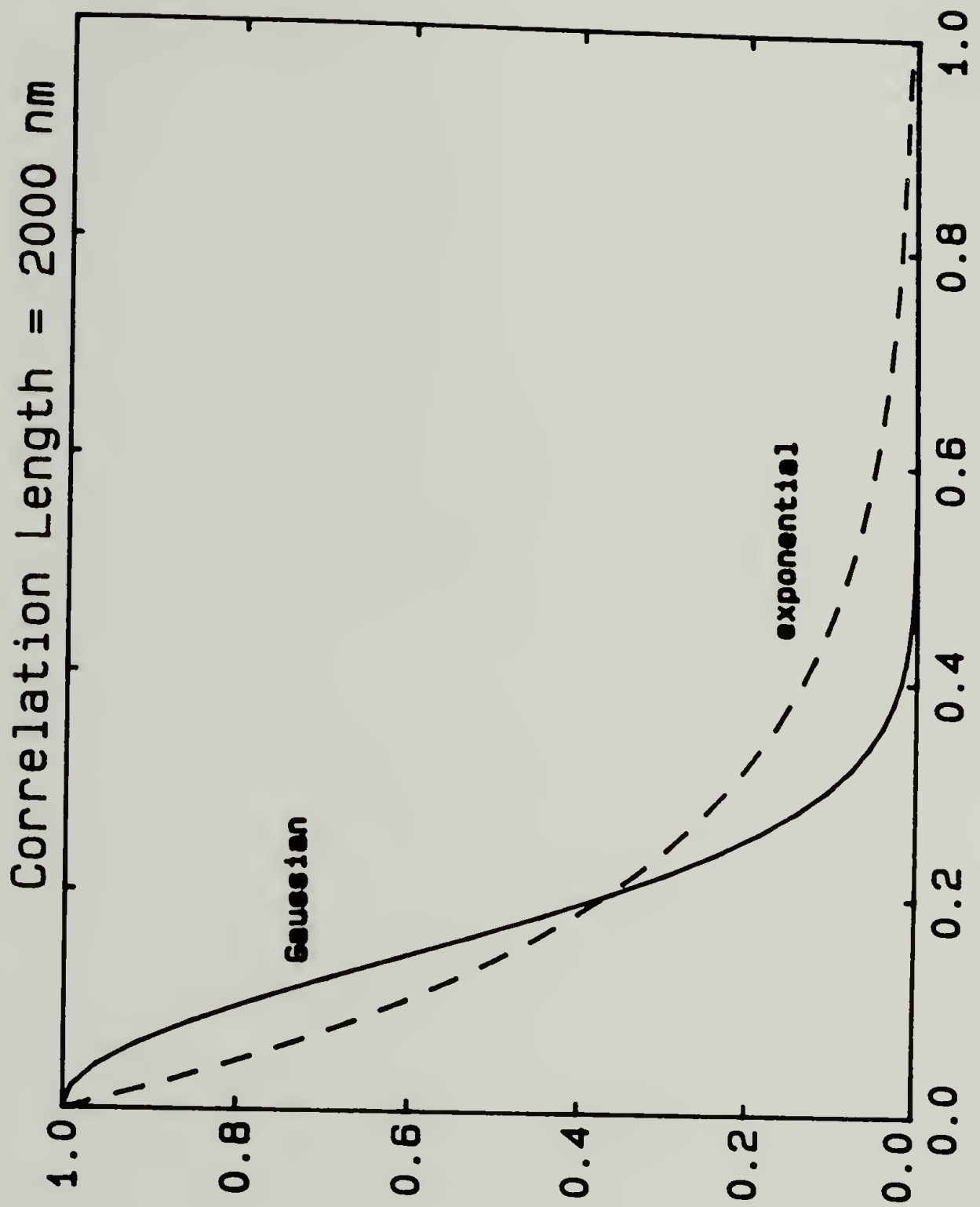

Figure 7-14. Difference in shape between an exponential and a Gaussian function.

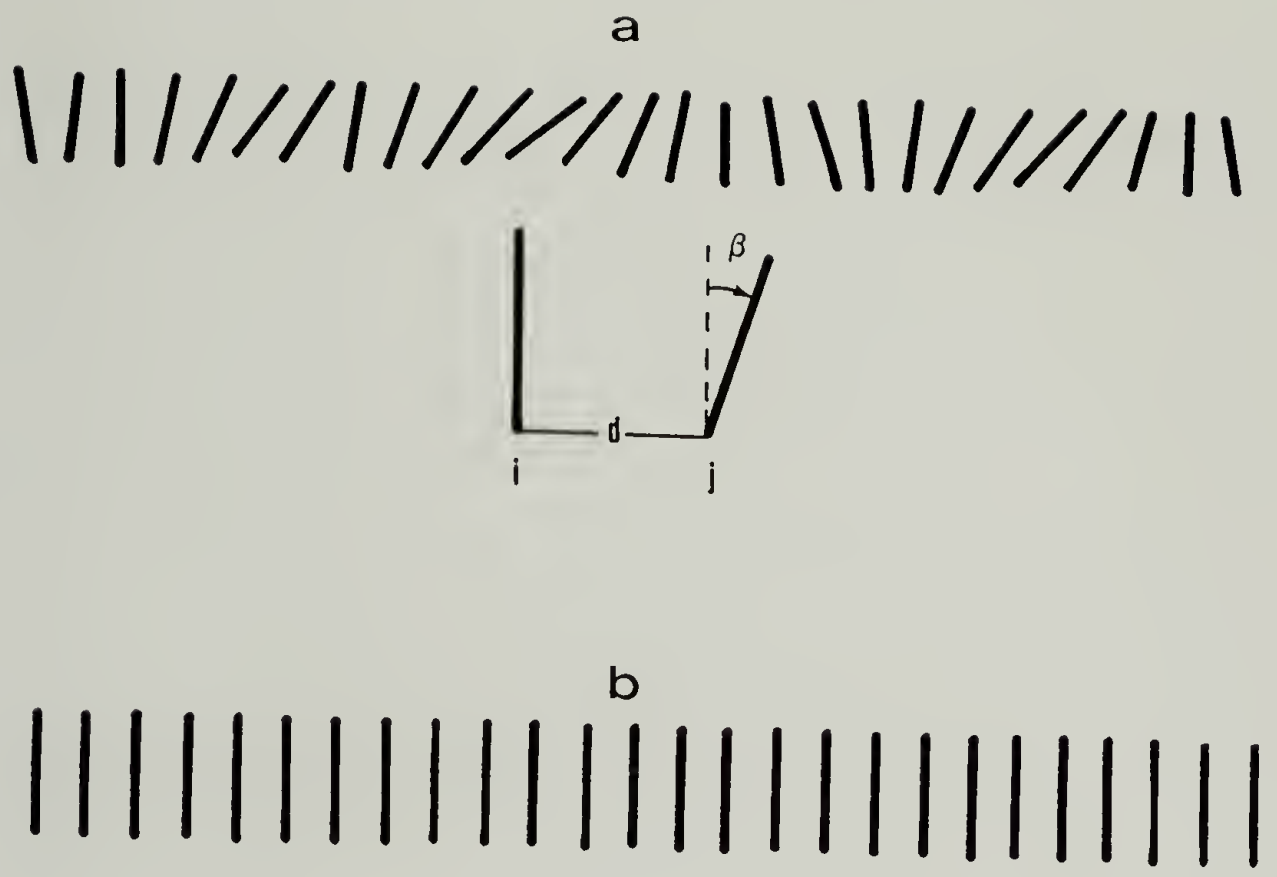

Figure 7-15. Schematic diagram of mesogens:
a) misaligned by an angle of $\pm \beta$,
b) displaying long-range orientational order and
c) with perfect order within a one-dimensional domain where directors are misaligned by angle of $\pm \beta$.

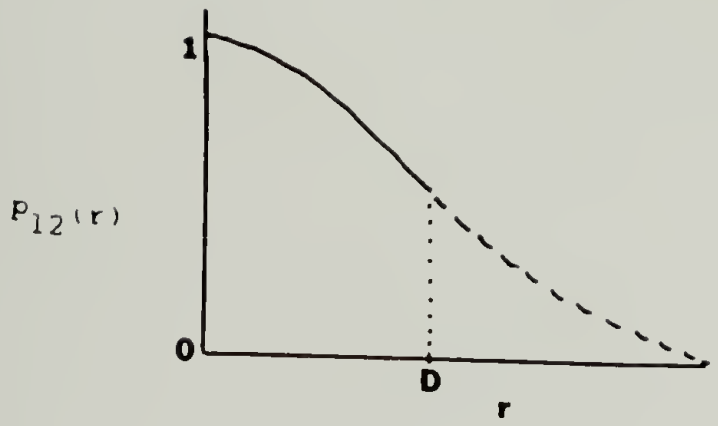

$P_{12}(r)$

$$f(r) = (P)\, f(r)_{intra} + (1 - P)\, f(r)_{inter}$$

where D = "domain" size

$$P = \frac{D - r}{D} \qquad \text{if } r \leq D$$

$$= 0 \qquad \text{if } r > D$$

Let $f(r)_{intra} = 1$

$$P_{12}(r) = P + (1 - P)\, f(r)_{inter}$$

$$= P + (1 - P) \exp -\left(\frac{2\beta^2 r}{D}\right)$$

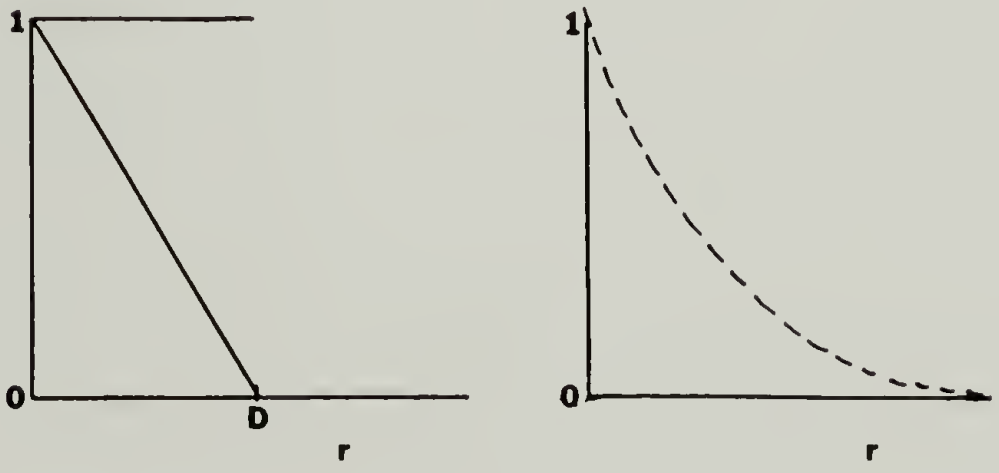

$$P_{12}(r) = 1 \times P + (1 - P) \times \exp -\left(\frac{2\beta^2 r}{D}\right)$$

Figure 7-16. Synthesis of "pseudo-Gaussian" function.

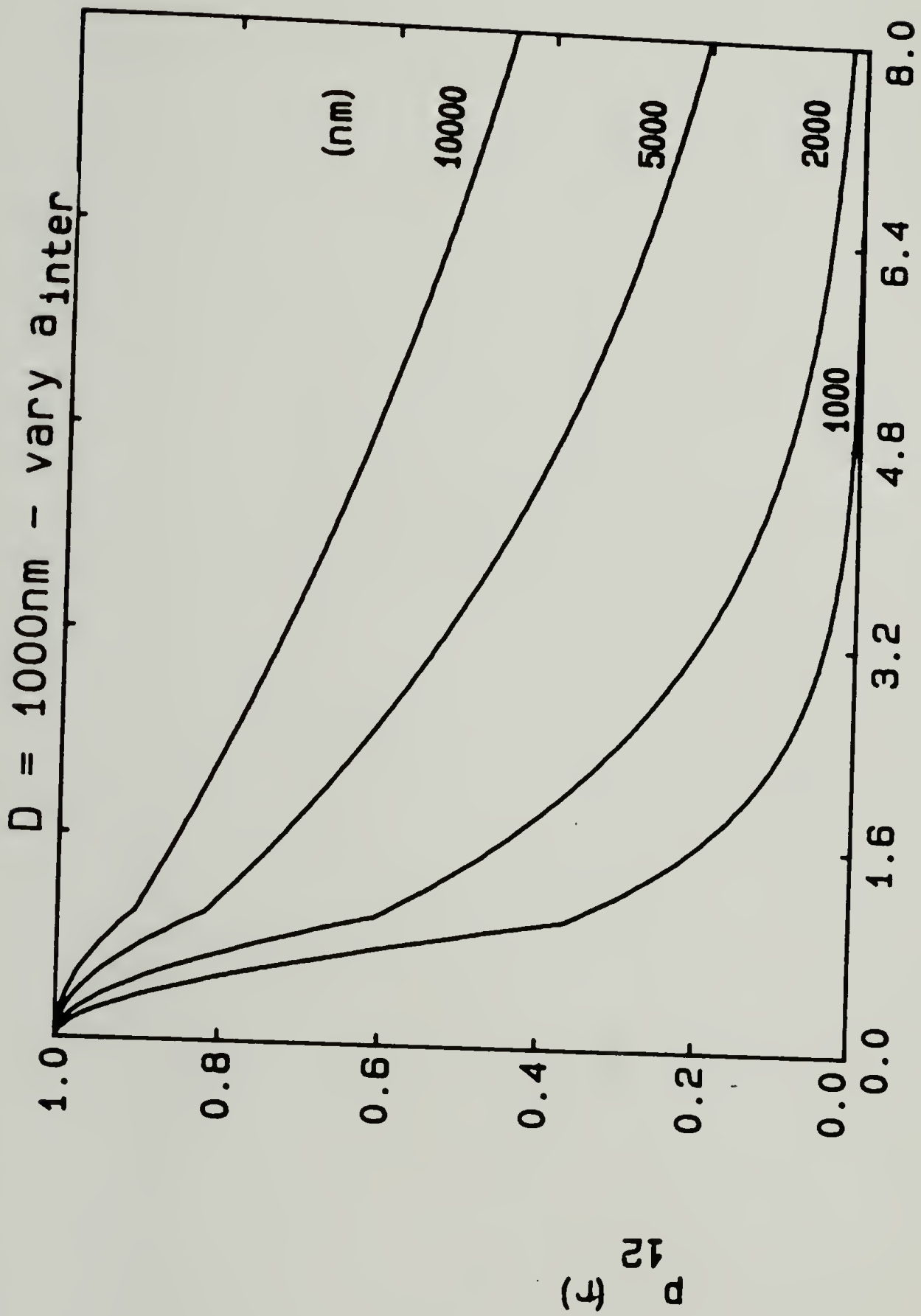

Figure 7-17. Plot of $p_{12}(r)$ versus r where D is held constant and a_{inter} is varied.

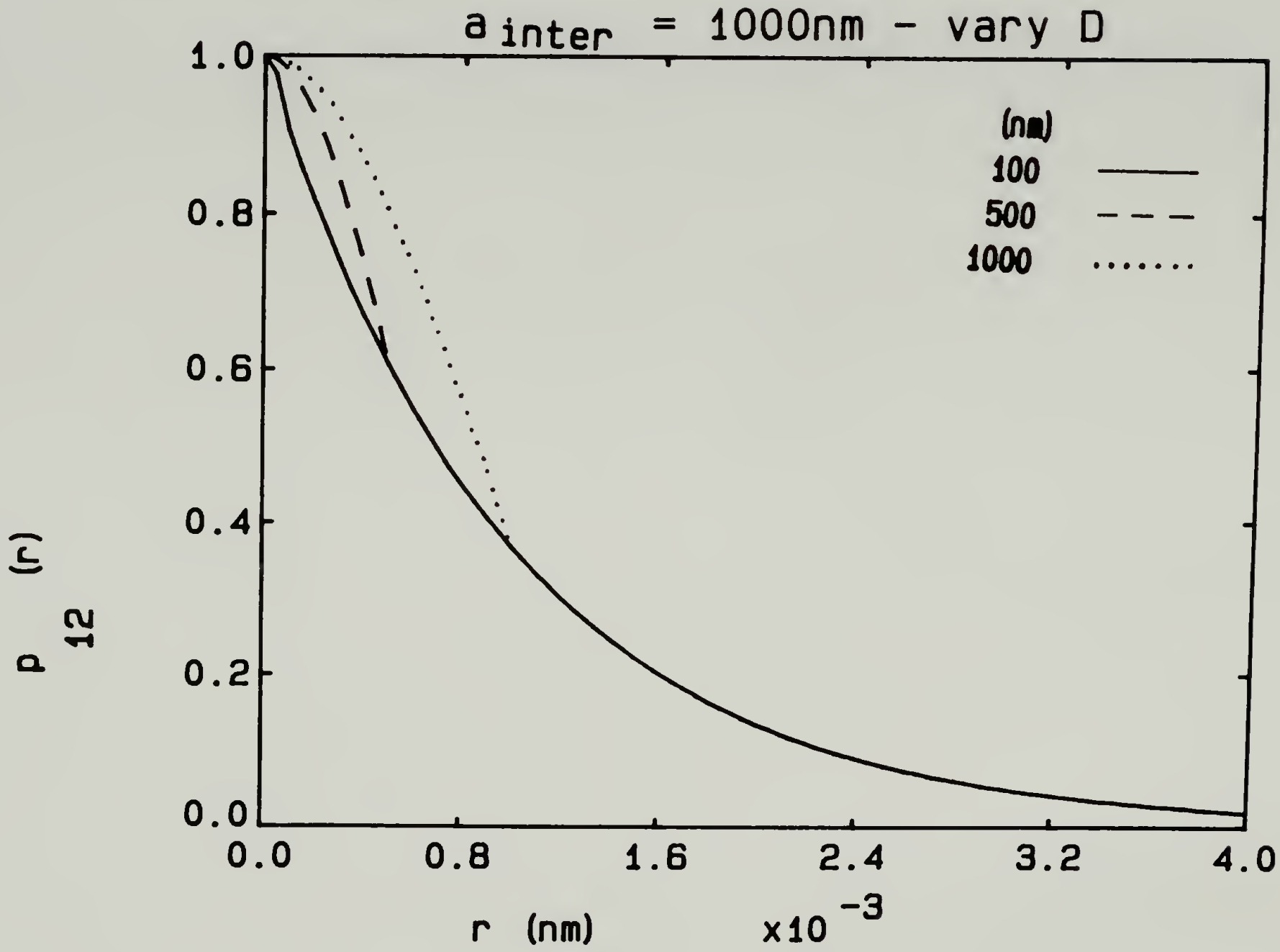

Figure 7-18. Plot of $p_{12}(r)$ versus r where a_{inter} is held constant and D is varied.

C H A P T E R VIII

CONCLUSIONS

Mesophase Morphology

In the decade or so that thermotropic PLCs have been researched, the synthetic polymer chemist has provided much insight into the relationship between the variables of chemical structure and the way in which they affect mesophase type and stability of the mesophase. Yet, other than the general classification of mesophase, for the most part determined by texture, that is, nematic or smectic liquid crystallinity, the complete picture of the mesophase was in its infancy. There is currently substantial activity in the fields of x-ray scattering, nuclear magnetic resonance spectroscopy, infrared spectroscopy and electron microscopy and diffraction to fill this gap in understanding the state of order.

Several questions concerning the total structural picture of the mesophase of PLCs were addressed during the course of this dissertation. Major emphasis was placed on utilizing scattering techniques to probe the morphological state. However, in many instances other experimental techniques were necessary to provide complementary

information on aspects of thermal and structural behavior.

In several systems studied, scattering techniques gave insight into the complicated thermal behavior of the PLCs. The step-wise disordering of the highly ordered crystalline state to one more closely resembling the mesophase was observed. In the PLCs with flexible spacers this was manifested by a crystal $\rightarrow$ crystal transition while in the rod-like PLCs a biaxial nematic $\longrightarrow$ uniaxial nematic transition was detected by x-ray techniques. With the inclusion of the technique of small angle light scattering, the extent of orientational order on the μm level is obtainable. The orientation correlation distance was found to be in the range of 1 to 2 μm for both a nematic and a smectic PLC studied; the distance increased slightly upon annealing. A general model for correlations in orientation of mesogenic units which considers both intra-domain and inter-domain correlations can be used to describe both the discrete domain picture and that of continuous variation in mesogen orientation.

The biaxial to uniaxial nematic transition accounts for the dual DSC endotherms observed in the alkyl-substituted poly(phenylene terephthalate) series. This phenomena may be driven by alkyl/aromatic phase segregation on the molecular level and may be related to similar explanations for the appearance of smectic order in a homologous series as the

flexible spacer length is increased. Orienting the specimen by fiber formation allowed one to separate intermolecular and intramolecular interference effects in the x-ray scattering. In this particular case, thwarting crystallization by quenching in biaxial nematic order was successful; this is not generally true of PLCs. Therefore, a major thrust of this research was to study the mesophase at elevated temperatures, a task hampered by high melting temperatures in proximity to the degradation temperature.

In conclusion, mesophase morphology on the local level is largely determined by chemical structure (size, shape and specific interactions of the mesogens and a particular spacer or substituent), whereas, on the larger scale, approximate parallel orientation persists over several microns and can be affected by external forces.

Suggestions for Future Research

The technique of solution casting the PLCs to obtain the more ordered semi-crystalline state, proved to be a clever method to understand the process of "liquid crystallization" with the application of heat. It would be of interest to cast slowly from very dilute solution in order to obtain single crystals. SMLCs easily form monodomain mesophases by application of electrical or magnetic fields or surface

orientation; PLCs do so reluctantly. However, it is likely that a polymeric single crystal would melt to a polymeric single liquid crystal. A study by x-ray and small angle light scattering on a single liquid crystal or monodomain would provide information on the change in the local and global states of order of the mesophase with temperature in the absence of the complication of overall random orientation. An understanding of the total morphological structure of the mesophase and its control will be of importance in the many proposed applications for liquid crystalline polymers a few of which are high strength fibers, molded parts, perm/selective membranes and barrier films.

REFERENCES

1. G. Friedel, Ann. Phys., 18, 273 (1922).

2. F. Reinitzer, Monatsch. Chem., 9, 421 (1888).

3. O. Lehmann, Z. Phys. Chem., Stoechiom. Verwandschaftsl., 4, 462 (1889).

4. D. Vorlander, Chemische Kristallographie der Flussigkeiten, Akad. Verlagsges, Leipzig (1924).

5. J. D. Litster and R. J. Birgeneau, Physics Today, 35, 26 (1982).

6a. G. Friedel and L. Royer, Comp. rend., 174, 1523 and 1607 (1922).

6b. G. Friedel, Compt. rend., 180, 269 (1925).

6c. G. Friedel, Compt. rend., 182, 425 (1926).

7. P. J. Flory, Proc. Royal Soc. (London), A234, 73 (1956).

8. S. L. Kwolek, US Patent 3,600,350 (1971).

9. S. G. Cottis, J. Economy and L. C. Wohrer, Ger. Patent 2,248,127 (1973).

10. V. Frosini, G. Levita, J. Landis and E. A. Woodward, J. Polym. Sci., Polym. Phys. Ed., 15, 239 (1977).

11. S. G. Cottis, J. Economy and B. E. Novak, US Patent 3,637,595 (1972).

12. G. Calundann, US Patents 4,067,852 (1978), 4,161,470 (1979), 4,185,996 (1980) and 4,256,624 (1981).

13. H. T. Kuhfuss and W. J. Jackson, US Patent 3,778,410 (1973).

14. T. E. Helminiak, T. E. Arnold and C. L. Benner, ACS Polym. Prepr., 16, 659 (1975).

15. Christopher K. Ober, Jung-Il Jin and Robert W. Lenz, Advances in Polymer Science, 59, 103 (1984).

16. A. Ciferri in Polymer Liquid Crystals, A. Ciferri, W. R. Krigbaum and Robert B. Meyer, eds., Academic Press, New York (1982).

17. A. Blumstein, J. Asrar and R. B. Blumstein in Liquid Crystals and Ordered Fluids, vol. 4, A. C. Griffin and J. H. Johnson, eds., Plenum Press, New York (1984).

18. J. Hermans, Jr., J. Colloid Sci., 17, 638 (1962).

19. W. G. Miller, C. C. Wu, E. L. Wee, G. L. Santee, J. H. Rai and K. G. Goebel, Pure Appl. Chem., 38, 25 (1974).

20. S. de Teressa, Ph.D. dissertation, University of Massachusetts (January, 1986).

21. D. C. Prevorsek in Polymer Liquid Crystals, A. Ciferri, W. R. Krigbaum and Robert B. Meyer, eds., Academic Press, New York (1982).

22. R. W. K. Honeycombe, The Plastic Deformation of Metals, 2nd ed., Edward Arnold, London (1984).

23. P. G. de Gennes, The Physics of Liquid Crystals, Oxford University Press, Oxford (1974).

24. Hans Kelker and Rolf Hatz, Handbook of Liquid Crystals, Verlag Chemie, Weinheim (1980).

25. S. Chandrasekhar, Liquid Crystals, Cambridge University Press, Cambridge (1977).

26. The Molecular Physics of Liquid Crystals, G. R. Luckhurst and G. W. Gray, eds., Academic Press, New York (1979).

27. William M. Gelbart, J. Phys. Chem., 86, 4298 (1982).

28. M. A. Cotter, J. Chem. Phys. Rev., A10, 625 (1974).

29. S. Marcelja, J. Chem. Phys., 60, 3599 (1974).

30. Do Y. Yoon and Sergio Bruckner, Configurational Characteristics of Thermotropic Polymers Comprising Rigid Groups Connected by Polymethylene Spacers, IBM Research Report (1984).

31. T. C. Lubensky and A. J. McKane, J. Phys. Lett. (Paris), 43, L-217 (1982). ().

32. Mario Liu, Phys. Rev., A24, 2720 (1981).

33a. M. J. Freiser, Mol. Cryst. Liq. Cryst, 14, 165 (1971).

33b. M. J. Freiser, Phys. Rev. Lett., 24, 1041 (1970).

34. Richard Alben, Phys. Rev. Lett., 30 778 (1973).

35. F. Dowell and D. E. Matire, J. Chem. Phys., 68, 1088 (1978).

36. F. Dowell and D. E. Matire, J. Chem. Phys., 68, 1094 (1978).

37. M. Born, Sitz d. Phys. Math., 25, 614 (1916).

38a. W. Maier and A. Saupe, Z. Naturforschg., 13a, 564 (1958).

38b. W. Maier and A. Saupe, Z. Naturforschg., 14a, 882 (1959).

38c. W. Maier and A. Saupe, Z. Naturforschg., 15a, 287 (1960).

39. P. Weiss, Compt. rend., 143, 1136 (1906).

40. Joseph O. Hirschfelder, Charles F. Curtiss and R. Byron Bird, Molecular Theory of Gases and Liquids, John Wiley & Sons, New York (1954).

41. John M. Prausnitz, Ruediger N. Lichtenthaler and Edmundo Gomes de Azevedo, Molecular Thermodynamics of Fluid-Phase Equilibria, 2nd ed., Prentice-Hall, Englewood Cliffs, NJ (1986).

42. Donald A. McQuarrie, Statistical Mechanics Harper & Roe, New York (1976).

43. L. D. Landau and E. M. Lifshitz, Statistical Physics, Part 1, 3rd ed., Pergamon Press, Oxford (1980).

44. G. Sigaud, D. Y. Yoon and A. C. Griffin, Macromolecules, 16, 875 (1983).

45. L. Onsager, Ann. NY Acad. Sci., 51, 627 (1949).

46. P. G. de Gennes, Mol. Cryst. Liq. Cryst,. 12, 193 (1971).

47. L. D. Landau, Collected Papers, Gordon and Breach, New York (1965).

48a. J. D. Litster and T. W. Stinson, J. Appl. Phys., 41, 966 (1970).

48b. T. W. Stinson and J. D. Litster, Phys. Rev. Lett., 25, 503 (1970).

48c. T. W. Stinson, J. D. Litster and N. A. Clark, J. Phys. (Paris), Suppl. 33, C1-169 (1972).

48d. T. W. Stinson and J. D. Litster, Phys. Rev. Lett., 30, 688 (1973).

49. B. Chu, C. S. Bak and F. L. Lin, Phys. Rev. Lett., 28, 1111 (1972).

50. C. W. Oseen, Trans. Far. Soc., 29, 883 (1933).

51. H. Zocher, Trans. Far. Soc., 29, 945 (1933).

52. J. L. Ericksen, Appl. Mech. Rev., 20, 1029 (1967).

53. F. M. Leslie, Mol. Cryst. Liq. Cryst., 7, 407 (1969).

54. F. C. Frank, Disc. Far. Soc., 25, 19 (1958).

55. D. Demus and L. Richter, Textures of Liquid Crystals, Verlag Chemie, Weinheim (1978).

56. J. A. Pople and F. E. Karasz, J. Phys. Chem. Solids, 20, 294 (1961).

57. J. E. Lennard-Jones and A. F. Devonshire, Proc. Roy. Soc. (London), A170, 464 (1939).

58. Hans-Rudolf Dicke and Robert W. Lenz, J. Polym. Sci, Polym. Chem. Ed., 21, 2581 (1983).

59. J. Majnusz, J. M. Catala and R. W. Lenz, Eur. Polym. J., 10/11, 19, 1043 (1983).

60. Juric Majnusz, private communication.

61. Paolo Nieri and Robert W. Lenz, to be published.

62. J.-I. Jin, S. Antoun, C. Ober and R. W. Lenz, Brit. Polym. J., 12, 132 (1980).

63. C. Ober, J.-I. Jin and R. W. Lenz, Polym. J., 14, 9 (1982).

64. Christopher K. Ober, Jung-Il Jin and Robert W. Lenz, Makromol. Chem., Rapid Commun., 4, 49 (1983).

65. Christopher K. Ober, The Synthesis and Characterization of Some Liquid Crystalline Polyesters Based upon the Oxybenzoate-Terephthalate Mesogenic Unit, Ph.D. dissertation, University of Massachusetts (May, 1982).

66. Paoli Nieri and Robert W. Lenz, to be published.

67. Q.-F. Zhou, J.-I. Jin and R. W. Lenz, Can. J. Chem., 63, 181 (1985).

68. Qi-Feng Zhou, The Synthesis and Characterization of Thermotropic Polyesters with Substituents on the Mesogenic Units, Ph.D dissertation, University of Massachusetts (February, 1983).

69. Christopher Ober, Robert W. Lenz, Giancarlo Galli and Emmo Chiellini, Macromolecules, 16, 1034 (1983).

70. S. Antoun, R. W. Lenz and J.-I. Jin, J. Polym. Sci., Polym. Phys. Ed., 19, 1901 (1981).

71. R. S. Stein, Structure and Properties of Polymeric Films, R. W. Lenz and R. S. Stein, eds., New York, (1973).

72. A. Wasiak D. Peiffer and R. S. Stein, J. Polym. Sci., Polym Lett. Ed., 14, 381 (1976).

73. R. J. Tabar, R. S. Stein and M. B. Long, J. Polym. Sci., Polym. Phys. Ed., 20, 2041 (1982).

74. Ronald J. Tabar, Quantitative Small Angle Light Scattering Studies of Semi-Crystalline Polymers, Ph.D. dissertation, University of Massachusetts (February, 1983).

75. Mattias Ballauff, Makromol. Chem., Rapid Commun., 7, 407 (1986).

76. P. Meurisse, C. Noël, L. Monnerie and B. Fayolle, Br. Polym. J., 13, 55 (1981).

77. P. Corradini, R. Napolitano, L. Oliva, V. Petraccone, B. Pirozzi and G. Guerra, Makromol. Chem., Rapid Commun., 3, 753 (1982).

78. L. Azároff, a review in press.

79. A. I. Kitaigorodsky, Molecular Crystals and Molecules, Academic Press, New York (1973).

80. Barbara A. Wood, Ultrastructural Studies of Thermotropic Liquid Crystalline Polymers, Ph.D. dissertation, University of Massachusetts, (September, 1985).

81. C. Viney, G. R. Mitchell and A. H. Windle, Mol. Cryst. Liq. Cryst., 129, 75 (1985).

82. Leroy E. Alexander, X-Ray Diffraction Methods in Polymer Science, Krieger, New York (1979).

83. J. D. Bernal and D. Crowfoot, Trans. Far. Soc., 29, 1032 (1933).

84. Fraser P. Price and Joachim H. Wendorff, J. Phys. Chem., 75, 2839 (1971).

85. S. K. Bhattacharya, A. Misra, R. S. Stein, R. W. Lenz and P. E. Hahn, submitted to Polymer Bulletin.

86. A. Blumstein, Liquid Crystal Polymers, Gordon Conference (1986).

87. Tadahiro Asada in Polymer Liquid Crystals, A. Ciferri, W. R. Krigbaum and Robert B. Meyer, eds., Academic Press, New York (1982).

88. G. Marrucci, presentation at Int. Congr. Rheology, Acapulco (1984).

89. G. R. Mitchell and A. H. Windle, Polym., 24, 1513 (1983).

90. V. N. Tsvetkov, Acta Physicochim., USSR, 16, 132 (1942).

91. R. S. Stein, P. Erhard, S. Clough, J.J. van Aartsen and M. B. Rhodes, in Electromagnetic Scattering, Gorden and Breach, New York (1967).

92. S. Clough, J. J. van Aartsen and R. S. Stein, J. Appl. Phys., 36, 3072 (1965).

93. Stuart B. Clough and R. S. Stein, J. Polym. Sci., A2, 6, 783 (1968).

94. M. B. Rhodes and R. S. Stein, J. Polym. Sci., A2, 7, 1539 (1969).

95. Takeji Hashimoto, Satoshi Ebisu and Hiramichi Kawai, J. Polym. Sci., Polym. Phys. Ed., 19, 59 (1981).

96. P. Debye and A. M. Bueche, J. Appl. Phys., 20, 518 (1949).

97. Martin Goldstein and E. R. Michalik, J. Appl. Phys., 26, 518 (1955).

98. Richard S. Stein and Philip R. Wilson, J. Appl. Phys., 33, 1914 (1962).

99. P. Debye, H. Anderson and R. Brumberger, J. Appl. Phys., 28, 679 (1957).

100. R. S. Stein and S. N. Stidham, J. Appl. Phys., 35, 42 (1964).

101. X. Wang, P. E. Hahn, R. W. Lenz and R. S. Stein, J. Polym. Sci., Polym. Phys. Ed., in press.

102. Sergio Rojstaczer, personal communication, University of Massachusetts (October, 1986).

103. A. deVries, Mol. Cryst. Liq. Cryst., 10, 31 (1970).

104. B. Wunderlich and J. Grebowicz, Advances in Polymer Science, 60/61, 1 (1984).

105. C. G. Vonk, J. Appl. Cryst., 11, 541 (1978).

106. R. S. Stein, P. R. Wilson and S. N. Stidham, J. Appl. Phys., 34, 46 (1963).

APPENDIX A

Comparison of Shapes of Exponential, Gaussian and "Pseudo-Gaussian Functions

Given an exponential and a Gaussian function,

$$f_e(r) = \exp -(r/a_e) \qquad \text{(A-1a)}$$

$$f_g(r) = \exp -(r^2/a_g^2), \qquad \text{(A-1b)}$$

their respective series expansions are

$$f_e(r) = 1 - (r/a_e) + (r^2/2a_e^2) - \ldots \qquad \text{(A-2a)}$$

$$f_g(r) = 1 - (r^2/a_g^2) + (r^4/2a_g^4) - \ldots \qquad \text{(A-2b)}$$

Note that the expansion of the Gaussian function contains only terms which are even powers of r. This results in a striking difference in the appearance of the two curves at small values of r. Mathematically, this may be demonstrated by examining the slope of the curves by taking the first derivative of their respective expansions:

$$\frac{df_e(r)}{dr} = -\left(\frac{1}{a_e}\right) + \left(\frac{r^2}{2a_e^2}\right) - \ldots. \qquad \text{(A-3a)}$$

$$\frac{df_g(r)}{dr} = -\left(\frac{2r}{a_g^2}\right) + \left(\frac{2r^3}{a_g^4}\right) - \ldots. \qquad \text{(A-3b)}$$

The slope of the exponential curve has a value of $-(1/a_e)$ at $r = 0$, whereas the initial slope of the Gaussian curve is 0.

The series expansion of the function, eq. 7-9, which is a composite of linear and exponential terms

$$f_c(r) = \left[1 - \frac{r}{D}\right] \left[1 - \exp -\left(\frac{r}{a_c}\right)\right] \qquad \text{(A-1c)}$$

is

$$f_c(r) = 1 - \left(\frac{r^2}{a_c D}\right) + \left(\frac{r^3}{2a_c^2 D}\right) - \ldots . \qquad \text{(A-2c)}$$

The first derivative is

$$\frac{df_c(r)}{dr} = - \left(\frac{2r}{a_c D}\right) + \left(\frac{3r}{2a_c^2 D}\right)^2 - \ldots . \qquad \text{(A-3c)}$$

It is evident that, similar to the Gaussian, the initial slope of the curve is 0 and that the curve decays with increasing r. The rate of decay is dependent upon $(a_c D)^{-1}$, thus, for larger D, the rate of decay is slower. Also, eqs. A-2b and A-2c are similar with respect to the power of r of the first and second terms. Thus, Gaussian-like behavior dominates at small r, whereas exponential-like behavior does at larger r.

By comparing the coefficients of the second term,

$$a_g^2 = a_c D.$$

Upon substitution of eq. 7-2a, we obtain

$$a_g^2 = \frac{D^2}{2\beta^2}$$

$$= \frac{n^2 d^2}{2\beta^2}$$

or $$a_g = \sqrt{2}\left(\frac{nd}{\beta}\right) . \qquad \text{(A-4)}$$

Thus, the correlation distance of the composite function is dependent upon domain size and misalignment of domain directors.

APPENDIX B

Fast Fourier Inverse Program

```
      PROGRAM FORINV
C-----------------------------------------------------------------
C
C     PURPOSE :
C     THIS PROGRAM IS USED TO OBTAIN THE SINE-FAST FOURIER
C     TRANSFORM.THE INPUT DATA IS INTENSITY I(Q) VS
C     SCATTERING VECTOR Q.
C           THE FUNCTION Q*I(Q) VS Q IS TRANSFORMED BY A
C     SINE-FAST FOURIER TRANSFORMATION TO GIVE R*GAMMA(R)
C     VS R.THE OUTPUT IS GAMMA(R) VS R.
C
C     THE PROGRAM FLIPS THE DATA ABOUT THE LAST POINT TO
C     INPUT AN ODD FUNCTION TO THE FFT SUBROUTINE.
C-----------------------------------------------------------------
      DIMENSION SV(1024),XINT(1024),GR(1024),R(1024)
      DOUBLE PRECISION SV2,QR,SQR,GR, QINV
      BYTE INFIL(27),OUTFL(27)
      REAL FMT(30)
C-----------------------------------------------------------------
C     Read in the I(q) vs q data
C-----------------------------------------------------------------
C
      TYPE *,' Input data file name '
      ACCEPT 2,LEN,(INFIL(K),K=1,LEN)
      INFIL(LEN+1)=0
2     FORMAT(Q,80A1)
C
      OPEN(UNIT=1,NAME=INFIL,TYPE='OLD')
      TYPE *,'Input the number of data points'
      ACCEPT *,NPTS
C
      TYPE 4
4     FORMAT(' Enter the number of lines to skip in the file: ')
      ACCEPT *, NLINE
C
      TYPE *, ' Enter the format of the x,y data : '
      ACCEPT 5, FMT
5     FORMAT( 30A1)
C
      IF(NLINE.EQ.0) GO TO 45
      DO 40, L=1,NLINE
      READ(1,23)ALINE
23    FORMAT( A2)
40    CONTINUE
C
45    DO 50 K=1,NPTS
          READ(1,FMT) SV(K),XINT(K)
      IF(K.LT.3)TYPE *,SV(K),XINT(K)
50     CONTINUE
       CLOSE(UNIT=1)
      DQ = SV(2)-SV(1)
C
```

```
C-------------------------------------------------------------
C       Delta R should be 1/gmax, and R steps * delta R
C       should equal 1/gmin
C-------------------------------------------------------------
C
        TYPE *,' Input delta R and number of R steps: '
        ACCEPT *, DELR,IRFIN
        DR=DELR
C
C--- SET UP INTEGRATION LOOP

        T1 = SECNDS(0.)
        DO 200 J=2,IRFIN
        GR(J) = 0.0
        DO 100 I=2,NPTS
C-------------------------------------------------------------
C       The J loop is for the various gamma(rJ)
C       the i loop is the q integration
C-------------------------------------------------------------
C
        SV2 = SV(I)*SV(I)
        QR = SV(I)*DR
        SQR = SIN(QR)
C
        GR(J) = GR(J) + XINT(I)*SV2*(SQR/QR)
C
100     CONTINUE
        R(J) = DR
        DR = DR + DELR
200     CONTINUE
        DELTA = SECNDS(T1)
        TYPE *, 'Time to transform = ',DELTA,' seconds'
        DTIM = DELTA/(FLOAT(IRFIN)*FLOAT(NPTS))
        TYPE *, ' Time for each computation = ',DTIM,' seconds'
C
        GR(1) = 1.0
        R(1) = 0.0
C
C-------------------------------------------------------------
C       Calculate the invariant in seperate loop
C-------------------------------------------------------------
C
        QINV = 0.
        DO 220 I=2,NPTS
        SV2 = SV(I)*SV(I)
        QINV = QINV + XINT(I)*SV2
220     CONTINUE
        TYPE *, 'INVARIANT = ',QINV
C
```

```
C-----------------------------------------------------------------------
C       Open the output file
C-----------------------------------------------------------------------
C
         TYPE *,'Output file name for correlation function file : '
         ACCEPT 2,LEN,(OUTFL(K),K=1,LEN)
         OUTFL(LEN+1)=0
         OPEN(UNIT=2,NAME=OUTFL,TYPE='NEW')
C
         WRITE(2,400)
400      FORMAT(5X,'R VS GAMMA(R) PROJECTED')
         WRITE(2,440)
440      FORMAT(5X,' R(I) ',11X,'NORMALIZED GAMMA(R)')
C
510      FORMAT(3X,E14.7,3X,E18.11)
        WRITE(2,510) R(1), GR(1)
C
C-----------------------------------------------------------------------
C       Write out the calculated data, GR(I)/QINV is the invariant
C       normalized correlation function
C-----------------------------------------------------------------------
C
         DO 90 I=2,IRFIN
         WRITE(2,510) R(I), GR(I)/QINV
90       CONTINUE
C
         CLOSE(UNIT=2)
         STOP ' FORINV COMPLETE'
         END
```